Final Report

Project No. 20651

Innovative Vibration Isolation Unit with Quasi-Zero Dynamic Stiffness

Jinchen(JC) Ji, Terry Brown

Email: jin.ji@uts.edu.au; terry.brown@uts.edu.au

School of Mechanical and Mechatronic Engineering

University of Technology Sydney (UTS)

28 December 2019

Report Summary

This is the third report (and the final report) on the project entitled “Innovative Vibration Isolation Unit with Quasi-Zero Dynamic Stiffness”. In this report, research work conducted at Stages 1 and 2 is summarized and the investigations at Stage 3 from 1st October to 20th December 2019 are presented. At Stage 1, using negative stiffness structures to design nonlinear quasi-zero stiffness (QZS) vibration isolation systems was studied and then two types of QZS vibration isolation systems based on multi-cam-roller and limb-like oblique springs were designed. At Stage 2, we have: 1) fabricated two proof of concept designs of QZS vibration isolation units; 2) carried out extensive laboratory tests on the two QZS systems to validate the theoretical results; 3) improved the designs to maximise the isolation performance. Both static behaviour and dynamic response measured in the laboratory test for the two types of QZS isolation systems are in excellent agreement with those of the innovative theoretical predictions which were obtained at Stage 1. The experimental results show: 1) static behaviour and dynamic response measured in the tests correlate well with those predicted by theoretical analyses of the two QZS systems; 2) the transmissibility of the QZS isolation systems is much less than that of the corresponding linear isolation system; and 3) the transmissibility at the excitation frequency of 4 Hz is less than 0.4 for the two QZS isolation systems whereas it is larger than 1.0 for the corresponding linear isolation systems. At Stage 3, a practical multi-cam-roller QZS isolation system with the loading capacity of 60~100 kilograms was designed, fabricated and tested. The experimental results demonstrate the abilities and great potentials of the present design as practical applications to significantly attenuate the vibration in low frequency range for mobile mining equipment.

Acknowledgements

We would like to thank CS Health & Safety Trust for supporting this project. We would also like to thank the Trust Secretary Bruce Grimshaw and Project Liaison Officer Lynne Magee for their time in overseeing and liaising this project, and also to thank Rochelle Kramer for her correspondence. Furthermore, we are thankful to the technical staffs at UTS for their support on conducting the laboratory tests.

Table of Contents

Report Summary ii
Acknowledgements iii
Table of Contents iv
List of Tables vii
List of Figures viii
Abbreviations and Nomenclature xii
1 Project Objectives and Summary of Progress Report 1
1.1 Project Objectives 1
1.2 Project Summary of Each Stage 1
1.2.1 Stage One 2
1.2.2 Stage Two 2
1.2.3 Stage Three 2
1.3 Organization of this Progress Report 3
2 Project Background 3
2.1 Quasi-Zero-Stiffness Vibration Isolation Theory 3
2.2 ISO Standards about Vibration-Induced Health Issues 5
3 Theoretical Analysis 8
3.1 Limb-like QZS Structure using Two Pairs of Oblique Springs 8
3.1.1 Static Analysis of the Limb-like QZS Structure 8
3.1.2 Dynamic Response of the Limb-like QZS Structure 10
3.2 Multi-Cam-Roller QZS Isolation System 12
3.2.1 Static Analysis of the Cam-Roller QZS Structure 13
3.2.2 Dynamic Response of the Multi-Cam-Roller QZS Structure 17
4 Proof of Concept (POC) Design, Fabrication and Test 20
4.1 Detailed Mechanical Design and Optimization 20
4.1.1 Multi-Cam-Roller QZS Structure 20
4.1.1.1 Cam Structure Design 20
4.1.1.2 Roller Structure 23
4.1.1.3 Spring Stiffness 24
4.1.2 Limb-like Structure using Two Pairs of Oblique Springs 24
4.1.2.1 Oblique Springs 24
4.1.2.2 Vertical Rod-Spring Structure 25
4.2 Fabrication 25

4.2.1 Multi-Cam-Roller QZS Isolation System 25
4.2.2 Limb-like Isolation System using Oblique Springs 26
4.3 Test Rig Set-Up and Instrument 26
4.3.1 Test Machine and Experimental Set-up 26
4.3.2 Equipment for Data Acquisition 27
4.3.3 Test Set-up 29
4.4 POC prototype test results 31
4.4.1 Limb-Like QZS Structure 31
4.4.1.1 Limb-like QZS Design and its Assembly 31
4.4.1.2 Static Tests on Stiffness Characteristics 32
4.4.1.3 Dynamic Tests on Isolation Performance 33
4.4.2 Multi-Cam-Roller QZS System 37
4.4.2.1 Multi-Cam-Roller Structure and its Assembly 37
4.4.2.2 Static Tests on the Multi-Cam-Roller QZS Structure 38
4.4.2.2.1 Friction Analysis 38
4.4.2.2.2 Optimized Structure Performance 41
4.4.2.3 Dynamic Tests on Multi-Cam-Roller QZS Structure 42
5 Prototype Design, Fabrication and Test 47
5.1 Prototype Design 47
5.1.1 Main Springs 47
5.1.2 Horizontal Spring Set and Adjustment 47
5.1.3 Design of Multiple Cams 48
5.1.4 Prototype Assembly 49
5.2 Test Instrument 49
5.2.1 Static Test Machine 49
5.2.2 Dynamic Test Machine 50
5.2.3 Equipment for Data Acquisition 51
5.3 Test Set-up 51
5.4 Prototype Test Results 53
5.4.1 Static Tests 53
5.4.2 Dynamic Tests 57
5.4.2.1 Linear system with vertical springs only 57
5.4.2.2 The QZS system 59
5.5 Result Analysis and Discussion 61
5.5.1 Excitation and Response Analysis 61
5.5.2 The corresponding linear System 62
5.5.3 The QZS System 64

5.6 The Improved Design for Practical Applications 64
5.6.1 Cam Structure for Accurate Weight Response 64
5.6.2 Friction (Damping) and Rotation Issue 65
5.6.3 Integration with a Standard Vehicle Seat 66
6 Conclusion and the Further Work beyond this Project 66
6.1 Concluding Remarks 67
6.2 Tangible Outputs of this Project 68
6.3 Further Work beyond this Project 68
7 References 70
8 Appendix 72
8.1 Prototype Springs 72
8.2 Raw Data of the Dynamic Tests 73

List of Tables

Table 1. ISO-2631-1 guideline for an 8 hour per day exposure of vibrations..... 6

Table 2. ISO-2631-4 symptoms of vibration exposure at frequencies of 1-20 Hz..... 7

Table 3. Key system parameters of the limb-like POC prototype 32

Table 4. Key system parameters of the cam-roller QZS prototype for different cases.....40

Table 5. Parameters of the sinusoidal displacement excitations 43

Table 6. Summary of the vibration transmissibility 46

Table 7. Detailed weight levels and their equivalent forces applied on the system 53

List of Figures

Fig. 1. Linear isolation system: (a) linear force-displacement relationship, (b) transmissibility curve for the damping coefficients of 0.1 and 0.3. 4

Fig. 2. Force-displacement curve of a nonlinear quasi-zero-stiffness isolation system. 5

Fig. 3. Effects of the WBV exposure at different vibration frequencies on the different parts of human body. 7

Fig. 4. Limb-like QZS system using two pairs of oblique springs: (a) the initial position, (b) the static equilibrium position under the supporting weight. 8

Fig. 5. Stiffness-displacement curves under different sets of system parameters: (a) $a = 0.96$, $\alpha = 1.45$, $\delta = 0.71$, $\beta = 2.81$, $\gamma = 2$; (b) $a = 0.96$, $\alpha = 0.9$, $\delta = 0.81$, $\beta = 1.01$, $\gamma = 2.1$. . 9

Fig. 6. Comparison of performance of the isolation systems with one or two pairs of oblique springs: (a) force-displacement curves, (b) stiffness-displacement curves. 11

Fig. 7. Amplitude-frequency curves of the isolation systems under 0.025 damping: (a) with two pairs of oblique springs, (b) with one pair of oblique springs. 12

Fig. 8. Mechanism of cam-roller QZS system with multi-weight capacity: (a) roller-spring structure, (b) multi-cam structure and roller positions. 13

Fig. 9. The operating zones of the cam-roller QZS system. *IN* indicates the ineffective zone, and *E* represents the effective zone. 13

Fig. 10. Relationship of the non-dimensional pre-compression and the spring stiffness ratio. 15

Fig. 11. Relationship of non-dimensional force and displacement response. 16

Fig. 12. Variation of the non-dimensional stiffness in the cam zone. 16

Fig. 13. Variation of the non-dimensional stiffness in the system. 17

Fig. 14. Vibration transmissibility under displacement excitations (dashed line is for the corresponding linear system). 19

Fig. 15. Non-dimensional force-displacement response and the system stiffness in full cam zone condition: (a) force-displacement curve, (b) stiffness. 21

Fig. 16. Operating zones of multi-cam-roller: (a) cam-roller with ineffective zone, (b) cam-roller without ineffective zone. 22

Fig. 17. Force-displacement response of the multi-cam-roller structure after removing the ineffective zone. 22

Fig. 18. Three types of cam structures: (a) $\delta = -0.2$, (b) $\delta = -0.5$, (c) $\delta = -0.8$. 23

Fig. 19. Two roller head designs: (a) bearing head, (b) hemisphere head. 23

Fig. 20. Design of limb-like oblique spring system: (a) oblique spring structure, (b) vertical rod and spring structure. 24

Fig. 21. The innovative cam-roller isolation system: (a) the schematic of the right half of the system, (b) 3D model. 25

Fig. 22. The limb-like isolation system: (a) the schematic of the right half of the system, (b) 3D model. 26

Fig. 23. Experimental set-up for the dynamic response test: (1) INSTRON E10000 machine, (2) Steel frame to hold the QZS isolation system, (3) QZS isolation system, (4) accelerometer to measure machine excitation, (5) two accelerometers to measure the response of the QZS isolation system, (6) NI cDAQ 9174/9234 data acquisition system to interface with accelerometers, (7) computer to control Instron E10000 via Bluehill3 or WaveMatrix software, (8) computer for data acquisition. 27

Fig. 24. Block diagram of LabVIEW program to control accelerometers and data acquisition: (1) DAQ assistant to interface with NI cDAQ 9174/9234, (2) Filter to filter noises with certain frequency range, (3) Spectral measurement for the FFT transformation, (4) Measurement file to record data in hard drive, (5) Waveform graph to display graphs in the front panel of LabVIEW platform. 28

Fig. 25. Front panel of the LabVIEW code interface to real-time display excitation and response: (1) excitation acceleration, (2) acceleration response, (3) displacement response, (4) acceleration response within 1 second, (5) frequency spectrum of acceleration excitation, and (6) frequency spectrum of acceleration response. 29

Fig. 26. POC prototype test set-ups: (a) static behaviour test, (b) dynamic response test. ...30

Fig. 27. POC design of the limb-like isolation system: (a) schematic of the right half of the structure, (b) physical model of the design. 31

Fig. 28. Force-displacement relationship acquired by experiment: (a) negative stiffness generated by two pairs of oblique springs, (b) positive stiffness produced by the vertical spring. 32

Fig. 29. Force displacement relationship acquired from experiments under QZS condition: (a) synthesis with positive and negative stiffness, (b) negative, positive and synthesis curves compared between experiments and theoretical analysis. 33

Fig. 30. Vibration response under the excitation of frequency 4Hz and amplitude 3mm: (a) linear response, (b) excitation and linear response, (c) QZS response, (d) excitation and QZS response. 34

Fig. 31. Vibration response under the excitation of frequency 5Hz and amplitude 3mm: (a) linear response, (b) excitation and linear response, (c) QZS response, (d) excitation and QZS response. 35

Fig. 32 Absolute displacement transmissibility: (a) comparison of the linear system and the QZS system, (b) comparison of the theoretical prediction and experimental measurement.....36

Fig. 33.The innovative multi-cam-roller QZS system: (a) the CAD drawing of the right section, (b) fabricated prototype.....37

Fig. 34. Force-displacement relationship in a full cam zone with different frictional coefficients.....39

Fig. 35. System stiffness in a full cam zone with different frictional coefficients. 39

Fig. 36. Static force-displacement response of a full cam zone. 40

Fig. 37. Force-displacement response of using the bearing roller and the hemisphere roller with a per-compression QZS condition of $\delta = -0.8$.....41

Fig. 38. Full range of force-displacement response of the multi-cam QZS system for Case 1 with optimized structure. 42

Fig. 39. Full range of force-displacement response of the multi-cam QZS system for Case 2 with optimized structure. 42

Fig. 40. Acceleration and displacement of time history response of the corresponding linear system at 4 Hz and 5 Hz.....44

Fig. 41. Displacement transmissibility of the corresponding linear isolation system. 44

Fig. 42. Acceleration and displacement of time-history response of the QZS system at 4 Hz. 45

Fig. 43. Comparison of the time-history of the linear system and the QZS system at 4 Hz. ..45

Fig. 44. Displacement transmissibility of the linear system and the QZS system. 46

Fig. 45. Horizontal roller set with different pre-compression conditions: (a) QZS condition with δ≈-7mm, (b) designed zero stiffness condition with δ≈0mm. 48

Fig. 46: The mechanical design and the photo of a fabricated part of the cam structure.....48

Fig. 47. Configuration design of the prototype. 49

Fig. 48. MAST and data acquisition system for prototype test at UTS TechLab.....50

Fig. 49. Interface of the controller and data acquisition system.....51

Fig. 50. The location of the sensors.....52

Fig. 51. Dynamic test of vehicle seat with weight (simulating the driver's weight). 53

Fig. 52. Force-compression response in static test with pre-compression $\delta \approx 0mm$. 54

Fig. 53. Force-compression response in static test with different pre-compressions. 55

Fig. 54. Cam structure: (a) with 2 sets of washers, (b) with 0, 1 or 2 sets of washers. 56

Fig. 55. Static performance of the QZS system with 0 (black lines), 1 (red lines) and 2 (green lines) sets of washer under QZS conditions (V1-V4 indicate the repeated tests). 56

Fig. 56. Raw test data of the corresponding linear system with a mass of 74 kg.....57

Fig. 57. Time-history of the response (Sensor 1) and the excitation (MAST platform) at 1.5Hz. 58

Fig. 58. Time-history of the response (Sensor 1) and the excitation (MAST platform) at 4Hz. 58

Fig. 59. Transmissibility of the linear system with a mass of 74 kg. 59

Fig. 60. Time-history response of the linear system and QZS system under 1.5Hz excitation. 60

Fig. 61. Transmissibility of the linear system and QZS system under different weight conditions. 60

Fig. 62. FFT of the excitation for QZS system with a mass of 75 kg (1-10Hz and enlarged 1-2Hz).....61

Fig. 63. FFT of Sensor 1 response for QZS system with a mass of 75 kg (at 6, 7.5 and 9 Hz). 62

Fig. 64. Transmissibility of the corresponding linear system with different weight conditions. 63

Fig. 65. Transmissibility of sensors for the corresponding linear system with Seat 52 VA1 (with a 0.2 Hz increase of the frequency from 2Hz to 5.4Hz). 63

Fig. 66. Transmissibility of the QZS system with different weight conditions.....64

Fig. 67. The improved cam structure. 65

Fig. 68. Integration with a vehicle seat.....66

Abbreviations and Nomenclature

Term	Definition
CSHST	Coal Services Health & Safety Trust
UTS	University of Technology Sydney
QZS	Quasi-Zero Stiffness
ISO	International Organization for Standardization
WBV	Whole-Body Vibration
NSS	Negative Stiffness Structure
DOF	Degree-of-Freedom
AF	The (response) Amplitude-(excitation) Frequency equation
POC	Proof of Concept
f_i	Force applied by the springs
$F(x), f(x)$	Reaction force from the system
ω_n	Natural frequency
ω, Ω	Excitation frequency
A_i ,Z_i	Amplitudes of the excitation or response
T, Ta	Vibration transmissibility
K	Total stiffness of the system
k_i	Stiffness of the spring
M, m	Weight (mass) applied on the system
d, u	Deformation or displacement
δ	Pre-compressed length of the spring
N	Number of the horizontal spring sets
θ	Angle between a line connecting cam and roller centres and a horizontal line
φ	Phase change between the excitation and the response
α	Stiffness ratio between the horizontal and vertical springs
R, r	Radius of the cam and roller
ξ	Damping ratio
a, d, h	Structure parameters for the oblique spring QZS system
$\hat{\imath}, \bar{\imath}$	Non-dimensional form of the parameters

1 Project Objectives and Summary of Progress Report

This project aims to design innovative quasi-zero-stiffness (QZS) vibration isolation systems which can effectively minimise the transfer of environmental vibrations to those working with mining equipment.

1.1 Project Objectives

Objectives of this project (Project No. 20651) are to develop a mechanism that can significantly reduce the transfer of hazardous vibration from mining equipment such as longwall excavators and trucks to drivers and operators and to design innovative and effective vibration isolation systems to greatly isolate vibrations with relatively low frequencies in mining operation environments. In this project, innovative nonlinear QZS systems will be originally developed. Modelling and theoretical analysis are performed and the practical designs are implemented. The designed nonlinear QZS vibration isolation systems are fabricated and experimentally verified.

The project is divided into six research tasks: 1) mathematical modelling of QZS structures; 2) design of bio-inspired limb-like and multi-cam-roller vibration isolation structures; 3) theoretical analysis of static and dynamic characteristics; 4) mechanical design of novel vibration isolation systems; 5) proof of concept development and experimental study; and 6) prototype design, fabrication and test for a practical application.

1.2 Project Summary of Each Stage

This final report summarizes the research work conducted for the duration of the project (covering the work for 3 stages). Stage 1 was to investigate the mechanism of innovative vibration isolation using QZS structures and to develop theoretical models of limb-like and cam-roller QZS vibration isolation systems. In Stage 2, innovatively designed two types of QZS isolation systems were fabricated and tested to verify their formulations and theoretical predictions conducted in Stage 1. A practical prototype design of the multi-cam-roller QZS isolation system was fabricated and tested in Stage 3 for evaluating its vibration isolation performance.

1.2.1 Stage One

In the first progress report for Stage 1 (submitted at the end of June 2019), the theory using negative stiffness structures to design nonlinear quasi-zero stiffness (QZS) vibration isolation systems was first discussed and then the design objectives for addressing the vibration-related health issues for those working in mining environments were presented. Innovations of the present QZS designs based on cam-roller mechanism and oblique springs are: 1) they have wide ranges of QZS characteristics; 2) the proposed cam-roller structure has the capacity of supporting multi-weight to isolate vibrations; 3) the developed limb-like structure has a wide working zone; and 4) two proof of concept designs of vibration isolation systems were proposed in this stage.

1.2.2 Stage Two

In Stage 2, we have 1) fabricated two POCs of QZS vibration isolation units based on the designs and analyses highlighted in the *First Progress Report*; 2) carried out extensive laboratory tests on the POCs to validate the theoretical results; 3) improved structure designs to maximise the isolation performance; and 4) initiated preliminary designs to implement the QZS vibration isolation structures on the driver's seats of heavy duty trucks. The two POCs are: 1) the oblique spring based limb-like quasi-zero stiffness structure, which has a large region of the quasi-zero stiffness; and 2) the multi-cam-roller structure to produce QZS characteristic and to have multi-weight capacity (one structure can provide vibration isolation for different drivers having different weights). Both static behaviour and dynamic response measured in the laboratory tests for both POC prototypes are in excellent agreement with those of the innovative theoretical predictions.

1.2.3 Stage Three

In Stage 3, the prototype using the multi-cam-roller structure was designed, fabricated and tested with a loading capacity of 60~100kg. The design specifications and test methods were discussed first. Then the structure configurations of the fabricated prototype were examined in the static tests and the system performances were evaluated from the dynamic tests. As an innovative design and the first prototype for practical application, the initial experimental results confirmed the vibration isolation ability of the proposed QZS system and its capacity to

respond to multi-weight levels (different loads applied). Further improvement of the design for a better performance is also proposed for practical applications.

1.3 Organization of this Progress Report

This final progress report is organized into six sections. Section 1 provides the project objectives and summary. Background is introduced in Section 2. Theory and design of two types of QZS vibration isolation systems are presented in Section 3. Proof of concept design, fabrication and experimental verification are given in Section 4. Practical prototype design and test for the multi-cam-roller QZS isolation structure are discussed in Section 5. The summary of the project work and the further work beyond this project are presented in Section 6.

2 Project Background

Vehicles and mobile equipment operated at mining sites are subjected to severe ground excitations while in operation or traveling over uneven terrain. Drivers, operators, and passengers of mobile plants, equipment or vehicles are frequently exposed to unpleasant vibrations transmitted through the seat, platform or operating unit. These unavoidable vibrations are the main risk factors for lumbago or backache, and can seriously affect the mental and physical health of the workers. Exposure to hazardous levels of whole-body vibrations (WBV) has been recognised by mining industry as a significant issue. However, the commonly used linear passive isolation system has unsatisfactory performance on such vibration in the low frequency range of 1-10Hz. This project aims to develop innovative and effective nonlinear QZS vibration isolation systems to greatly isolate these unwanted vibrations.

2.1 Quasi-Zero-Stiffness Vibration Isolation Theory

To isolate or eliminate vibrations transmitted from ground excitations to drivers and operators, linear passive isolation methods are commonly used to suppress the undesirable vibrations in many engineering applications. A simplest linear passive isolation system is modelled as a mass-spring-damping unit. In this unit, vibration suppression is effective only when $(\omega/\omega_n) > \sqrt{2}$, where ω and ω_n are the excitation frequency and the natural frequency of the unit, as shown in Fig. 1.

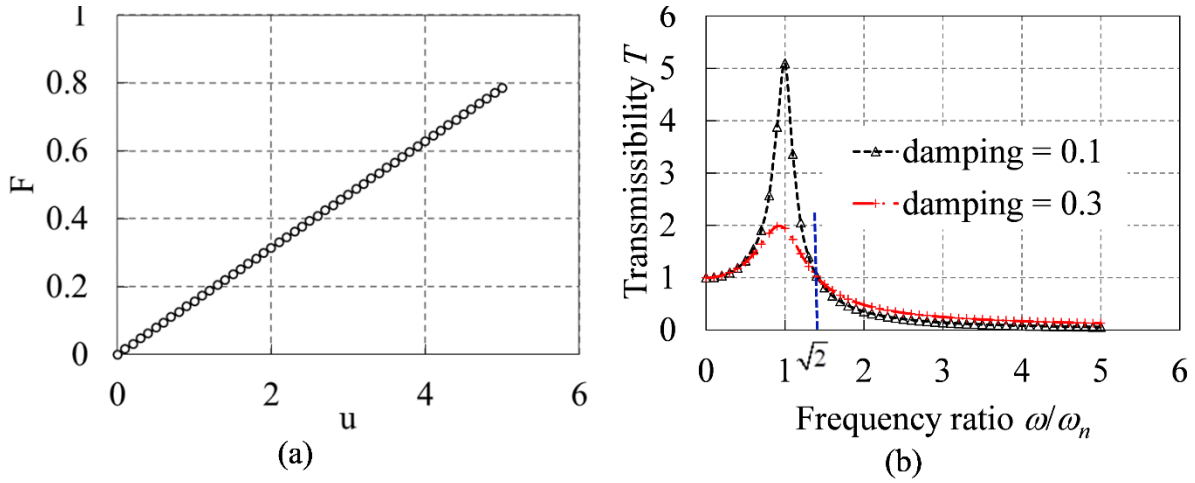

Fig. 1. Linear isolation system: (a) linear force-displacement relationship, (b) transmissibility curve for the damping coefficients of 0.1 and 0.3.

The transmissibility, the ratio of output to input, is widely used to indicate the isolation performance in the context of vibrations. In Fig. 1(b), the transmissibility T is defined as:

$$T = \frac{A_{isolator}}{A_{excitation}} \qquad (1)$$

where $A_{isolator}$ and $A_{excitation}$ are the amplitudes of the isolator output and the excitation. Some vibration isolation systems use low stiffness springs to reduce the natural frequency, however this will result in a large displacement, and reduce the load-bearing capacity [1, 2].

Nonlinear vibration isolation systems offer performance advantages over their linear counterpart by producing high-static-stiffness and low-dynamic-stiffness [3-8]. The high-static-stiffness implies the high load-bearing capacity and the low-dynamic-stiffness provides the vibration isolation around the operating points. One typical nonlinear isolation system is the nonlinear quasi-zero-stiffness (QZS) vibration system.

Force-displacement relationship of a quasi-zero-stiffness (QZS) structure shown in Fig. 2 can be obtained by using oblique springs [3, 9], buckled beams [10, 11], magnetic springs [7, 12] and cam-roller structures [13, 14], in combination with vertical linear springs.

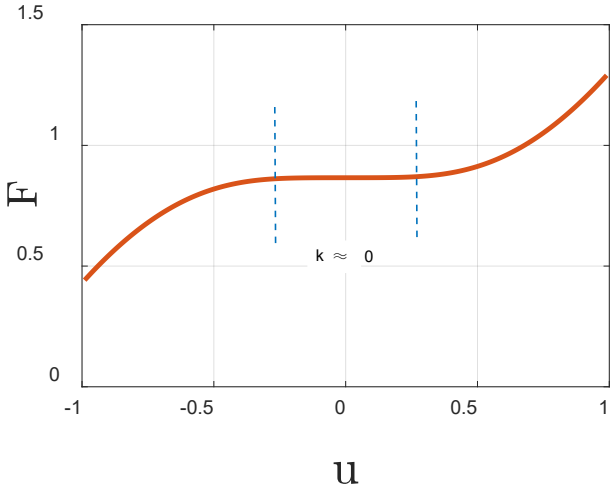

Fig. 2. Force-displacement curve of a nonlinear quasi-zero-stiffness isolation system.

When the nonlinear QZS isolation system operates in the range of $k \approx 0$ in Fig. 2, the transmitted vibrations can be greatly attenuated as the external vibrations would not excite the nonlinear QZS structure due to the QZS characteristics. The larger the range of $k \approx 0$, the better its isolation performance. In this project, novel nonlinear QZS structures meeting the requirement of the ISO standard for vibration-induced health issues will be designed for vehicles and mobile equipment operating in mining environments.

2.2 ISO Standards about Vibration-Induced Health Issues

The International Organization for Standardization (ISO) has developed three standards for vibration-induced health issues, which will be briefly discussed below.

ISO 2631-1 (1997): Mechanical vibration and shock - Evaluation of human exposure to whole-body vibration - Part 1: General requirements.
Part 1 of the ISO 2631 is a general guide on the influence of mechanical vibration and shock on the health of drivers operating mobile vehicles and equipment, and defines the types of whole-body vibrations (WBV) such as transient, periodic and random vibrations that operators are exposed. It gives the effects of the acceleration levels for an eight hour per day exposure to vibrations on the comfort levels, as summarized in Table 1. The acceleration threshold is 0.315 m/s^2 and the acceleration greater than 2 m/s^2 is classified as an extremely uncomfortable level for operators exposed for 8 hours.

Table 1. ISO-2631-1 guideline for an 8 hour per day exposure of vibrations

Acceleration (m/s^2)	Comfort level
< 0.315	Not uncomfortable
0.315-0.63	A little uncomfortable
0.5-1.0	Fairly uncomfortable
0.8-1.6	Uncomfortable
1.25-2.5	Very uncomfortable
>2.0	Extremely uncomfortable

ISO 2631-4 (2001): Mechanical vibration and shock- Evaluation of human exposure to whole-body vibration-Part 4: Guidelines for the evaluation of the effects of vibration and rotational motion on passenger and crew comfort in fixed-guideway transport systems. Part 4 of the ISO 2631 focuses on evaluating human exposure to WBVs as a result of interacting with fixed-gateway transport systems. This part analyses how these vibrations affect the comfort levels of the passengers and crew members that use fixed-gateway transportation system.

ISO 2631-5 (2018): Mechanical vibration and shock - Evaluation of human exposure to whole-body vibration - Part 5: Method for evaluation of vibration containing multiple shocks. Part 5 of ISO 2631 deals with the evaluation of mechanical systems with emphasis on the human exposure to WBVs and provides methods of studying vibrations that undergo multiple shocks. It is also used to evaluate vibration levels that have multiple shocks at the seat pads of seated persons.

Symptoms for vibration exposure frequencies in the range 1 Hz to 20 Hz are shown in Table 2. Vibration with frequencies of 4-8 Hz affects breathing and vibration with frequencies of 4-9 Hz causes a general feeling of discomfort and muscle contractions. As shown in Table 2, a person exposing to vibration with the frequencies between 4 and 10 Hz experiences abdominal pains, and chest pains between 5 and 7 Hz frequency exposures. Lower jaw symptoms can appear between 6 and 8 Hz. Head symptoms, increased muscle tone, and influence on speech symptoms can occur at frequencies of 13-20 Hz.

Table 2. ISO-2631-4 symptoms of vibration exposure at frequencies of 1-20 Hz

Symptoms	Frequency (Hz)
Influence on breathing movement	4-8
General feeling of discomfort	4-9
Muscle contraction	4-9
Abdominal pain	4-10
Chest pain	5-7
Lower jaw symptoms	6-8
Urge to urinate	10-18
Lump symptoms	12-16
Head symptoms	13-20
Influence on speech	13-20
Increased muscle tone	13-20

Fig. 3 indicates the perceived effects of the WBV exposure to various vibration frequencies [15, 16], which shows similar results to those of Table 2. This project will use the data given in Tables 1 and 2 specified by the ISO standards as the benchmark data.

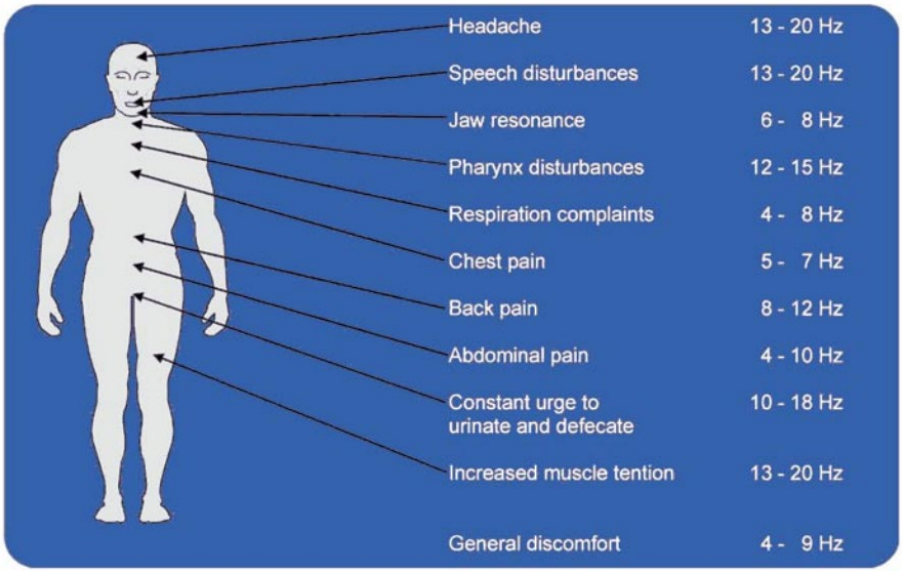

Fig. 3. Effects of the WBV exposure at different vibration frequencies on the different parts of human body.

3 Theoretical Analysis

Two types of nonlinear QZS vibration isolation systems are proposed in this section to focus on different issues. The first design uses two pairs of oblique springs forming a limb–like structure to provide an exceptional performance of the nonlinear isolation. The second design employs a multi-cam-roller mechanism to respond to the multi-weight (of the drivers) issue. The separable mechanism of the cam and the roller makes the system be able to respond to multiple weight conditions. Both designs are able to work individually or be combined to make the best use of their characteristics. The two designs will be referred to as limb-like QZS structure and cam-roller QZS isolation system, respectively, which will be subsequently discussed in detail.

3.1 Limb-like QZS Structure using Two Pairs of Oblique Springs

3.1.1 Static Analysis of the Limb-like QZS Structure

The limb-like QZS system comprised of two pairs of oblique springs is shown in Fig. 4. This design is bio-inspired by limb structures, which can significantly increase the operating zone of quasi-zero stiffness as compared to the conventional oblique spring isolation systems. As two pairs of oblique springs symmetrically placed in inclined direction produce negative stiffness in vertical direction, the quasi-zero stiffness (QZS) can be obtained by combining with the vertical spring with positive stiffness. As compared to the conventional QZS structure with one pair of oblique springs, the present design can significantly increase the operating zone and improve the isolation performance.

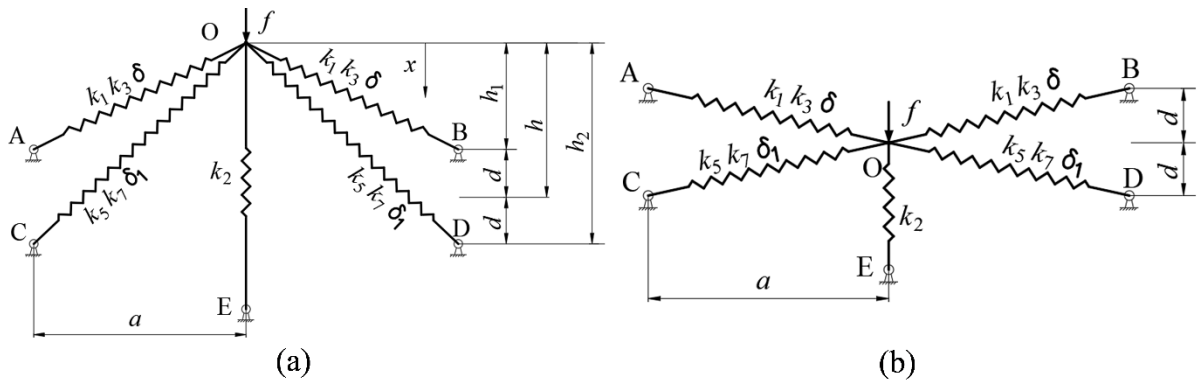

Fig. 4. Limb-like QZS system using two pairs of oblique springs: (a) the initial position, (b) the static equilibrium position under the supporting weight.

The spring stiffness and other parameters are defined in Fig. 4. The resultant vertical force *f* can be formulated by using the principle of the virtual work:

$$(f + 2f_{1x} + 2f_{3x} + f_2)\delta x = 0 \qquad (2)$$

where δx is the virtual displacement, f_{1x} and f_{3x} denote the vertical components of forces generated by the upper and lower pairs of oblique springs, f_2 is the force produced from the vertical spring. The non-dimensional force expression $\hat{f}$ can be derived from Eq. (2) as:

$$\hat{f} = \hat{x} + N_1 + N_2 + N_3 + N_4 \qquad (3)$$

where $\hat{x}$ is the non-dimensional displacement, N_i (i = 1, 2, 3, 4) represent the non-dimensional force components.

The non-dimensional stiffness of the limb-like structure formed by two pairs of oblique springs can be determined by:

$$\widehat{K} = \frac{d\hat{f}}{d\hat{x}} = 1 + \frac{dN_1}{d\hat{x}} + \frac{dN_2}{d\hat{x}} + \frac{dN_3}{d\hat{x}} + \frac{dN_4}{d\hat{x}} \qquad (4)$$

The stiffness-displacement curves for two combined sets of parameters are plotted in Fig. 5, where $\hat{y}$ denotes the relative displacement, the parameters $\hat{a}$, α, $\hat{\delta}$, β and γ depend on the spring stiffness and geometry of the limb-like structure.

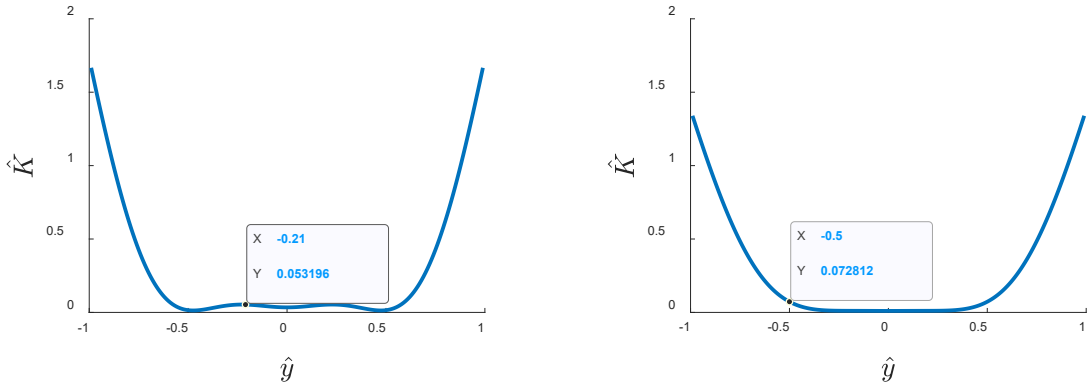

(a) (b)

Fig. 5. Stiffness-displacement curves under different sets of system parameters: (a) $\hat{a} = 0.96$, $\alpha = 1.45$, $\hat{\delta} = 0.71$, $\beta = 2.81$, $\gamma = 2$; (b) $\hat{a} = 0.96$, $\alpha = 0.9$, $\hat{\delta} = 0.81$, $\beta = 1.01$, $\gamma = 2.1$.

The dynamic stiffness $\widehat{K}$ < 0.055 is in the range of $\hat{y}$ ∈[-0.5 0.5] as shown in Fig. 5(a), and $\widehat{K}$ < 0.075 is in the range of $\hat{y}$ ∈[-0.5 0.5] as shown in Fig. 5(b). In an early study on the optimized deign with one pair of oblique springs [9], $\widehat{K}$ < 0.1 holds in the range of $\hat{y}$ ∈[-0.2 0.2] only. Therefore, the QZS effective zone of the proposed limb-link structure with two pairs of oblique springs is significantly larger than that of the existing design with one pair of oblique springs.

3.1.2 Dynamic Response of the Limb-like QZS Structure

When an external harmonic force or displacement excitation is applied to a vibration isolation system, the equation of motion can be respectively expressed as [5]:

$$m\ddot{y} + c\dot{y} + f(y) = Fcos(\omega t) \quad (5)$$

$$m\ddot{y} + c\dot{y} + f(y) = -m\ddot{y}_e \quad (6)$$

Under the operating condition, the force-displacement relation of the limb-like QZS isolation system can be expanded in a Taylor series. The expanded results include constant, linear and third-order terms where the higher order terms are ignored. The constant term refers to the static load capacity, while the linear term and third-order nonlinear term contribute to vibration isolation. In dynamic analysis, the dynamic force can be expressed as:

$$\hat{f} = \mu_1\hat{y} + \mu_2\hat{y}^3 \quad (7)$$

The non-dimensional equation of motion of the supporting mass in the QZS isolation system with two pairs of oblique springs can be written by combining Eq. (5) and (7) as:

$$\ddot{\hat{y}} + 2\xi\dot{\hat{y}} + \mu_1\hat{y} + \mu_2\hat{y}^3 = \hat{F}cos\Omega\tau \quad (8)$$

where μ_1 and μ_2 are the coefficients of linear and nonlinear stiffness, which can be obtained by using the specific values of the five independent parameters under the QZS condition. The linear term of the stiffness is very small, leading to the quasi-zero stiffness characteristics of the proposed isolation system in a wider frequency range. However, the third-order nonlinear term may affects the effective frequency range.

Eq. (8) can be solved by using the harmonic balance method. Under principal resonances, the lowest harmonics dominates and the higher harmonics is relatively small so as to be omitted. Hence, the response at an excitation frequency, or a *T*-periodic solution, can be expressed as:

$$\hat{y}_0(\tau) = \hat{y}_0(\tau + T) = Acos(\Omega\tau + \varphi) \quad (9)$$

where $T = \frac{2\pi}{\Omega}$, $\Omega = \frac{\omega}{\omega_n}$, and ω_n is the natural frequency determined from the mass supported and the vertical spring of the QZS isolation system.

By substituting $\hat{y}_0$ into Eq. (8), performing some algebraic manipulations and ignoring the higher order terms, the relationship between the excitation frequency and response amplitude (AF) can be obtained as:

$$\frac{9}{16}{\mu_2}^2A^6 + \left(\frac{3}{2}\mu_1\mu_2 - \frac{3}{2}\mu_2\Omega^2\right)A^4 + \left(\Omega^4 - 2\mu_1\Omega^2 + {\mu_1}^2 + 4\xi^2\Omega^2\right)A^2 - \hat{F}^2 = 0 \quad (10)$$

Dynamic performance of the proposed limb-like isolation system also depends on the parameters given in Fig. 6. By performing the optimization using MATLAB, the optimized parameters are obtained as: $\hat{a} = 0.96,\ \alpha = 0.9,\ \hat{\delta} = 0.81,\ \beta = 1.01,\ \gamma = 2.1$. By using these parameter values, the dynamic response of the proposed QZS isolation system with two pairs of oblique springs is illustrated in Fig. 7, where the optimized results for the corresponding QZS isolation system with one pair of oblique springs [9] are also given for comparison. As shown in Fig. 7(a), the dynamic force (0.535) of the present design is 38.2% less than that (0.866) of the corresponding isolation system with one pair of oblique springs.

It is also observed from Fig. 7(b) that the QZS effective zone of the proposed design is considerably larger than that for the one pair of oblique springs. Also as shown in Fig. 7, the peak frequency (0.8382) of the proposed QZS isolation system is much lower than that (1.2456) for the corresponding isolation system with one pair of oblique springs. Fig. 6 and Fig. 7 demonstrate that superior dynamic performance of the proposed limb-like design with two pairs of oblique springs to the conventional system with one pair of oblique springs.

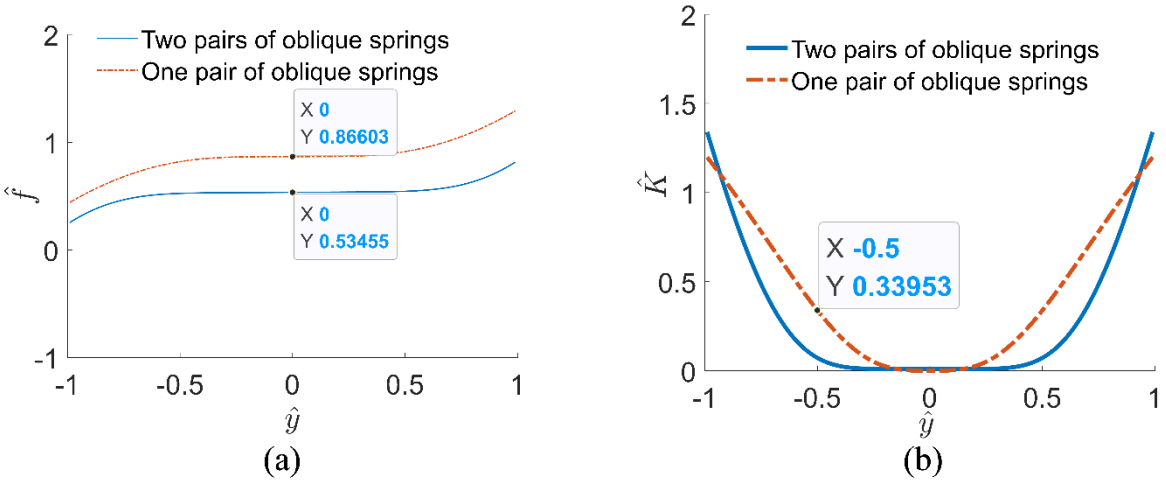

Fig. 6. Comparison of performance of the isolation systems with one or two pairs of oblique springs: (a) force-displacement curves, (b) stiffness-displacement curves.

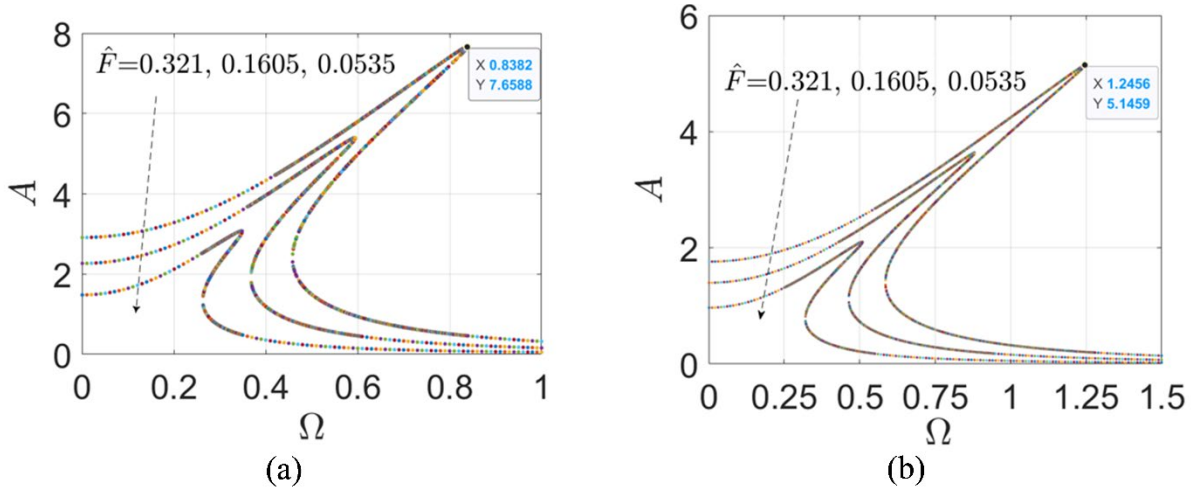

Fig. 7. Amplitude-frequency curves of the isolation systems under 0.025 damping: (a) with two pairs of oblique springs, (b) with one pair of oblique springs.

3.2 Multi-Cam-Roller QZS Isolation System

The nonlinear vibration isolation system is designed for dealing with low frequency excitations and should be able to respond to different weights of operators.

The proposed multi-cam-roller QZS isolation system includes a normal spring-damping-mass unit for supporting static load capability and a cam-roller structure used to form QZS characteristics. The cam-roller system consists of two individual structures, namely, cam structure and roller structure. The multi-cam design makes the isolation system be able to effectively respond to multiple weight situations. The cam structure can be attached or combined to one end of the main spring-damping system, meanwhile the roller structure joins the other end. The QZS mechanism is activated hen the roller contacts the cams.

Multiple cams are placed in a row along the axial direction in the proposed innovative design. Each cam can respond to one weight at its centre as in Fig. 8. The supported weight can be determined by distance d_i from the cam centre to the designed reference plane and the vertical spring stiffness k_v. The designed reference plane is the initial vertical position of the roller when no weight is applied. The roller structure is configured by a roller head and a spring in the horizontal direction. When the roller comes to contact the cam, the horizontal spring will be compressed and a force in the vertical direction will be generated due to cam-roller

interaction. Such a force then applies to the spring-damping-mass unit to achieve a QZS mechanism.

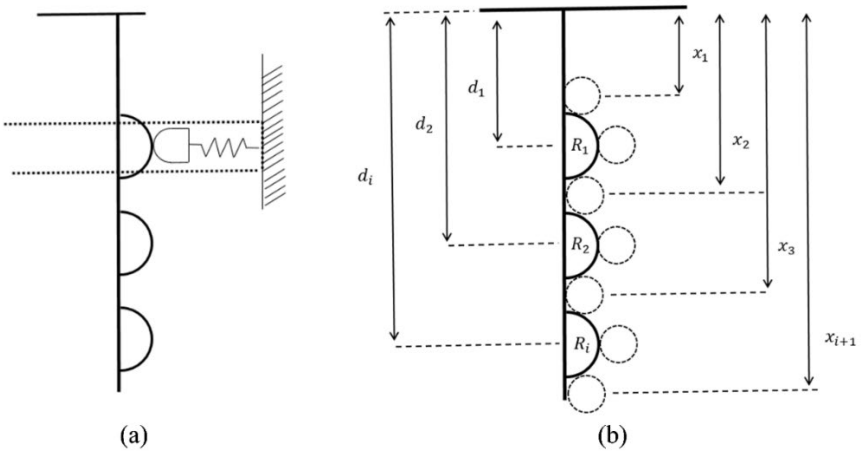

Fig. 8. Mechanism of cam-roller QZS system with multi-weight capacity: (a) roller-spring structure, (b) multi-cam structure and roller positions.

3.2.1 Static Analysis of the Cam-Roller QZS Structure

Fig. 9 shows the operating zones of a cam-roller system. In a full zone of a cam, there exist effective and ineffective zones. The QZS mechanism can be achieved in the effective zones but the system will return to a linear isolation system once in the ineffective zones. The size of effective zone is determined by cam radius *R*, roller radius *r* and pre-compressed length of horizontal spring δ. The effective range for each zone is $d_i \pm x_d$, where x_d is given by

$$x_d = \sqrt{(R+r)^2 - \delta^2} \tag{11}$$

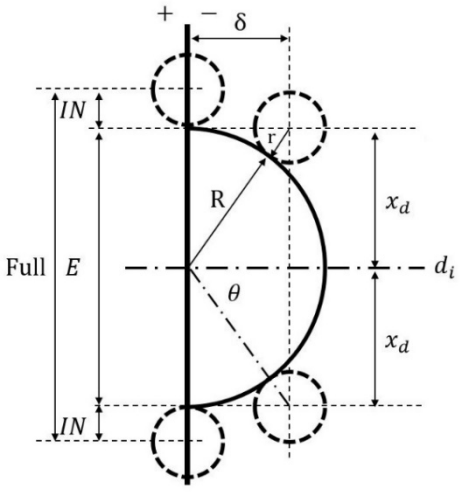

Fig. 9. The operating zones of the cam-roller QZS system. *IN* indicates the ineffective zone, and *E* represents the effective zone.

In the effective zone, the applied force to the cam can be calculated as:

$$f(x) = f_v - \mathrm{N}f_h\tan(\theta) = k_v x - Nk_h[\delta + (R+r)\cos(\theta)]\tan(\theta) \qquad (12)$$

where f_v is the force applied by the vertical spring, f_h is the force applied by the horizontal spring, N is the number of the horizontal spring sets, θ is the angle between a line connecting cam and roller centres and a horizontal line, and its geometrically-trigonometric relationships are:

$$\cos(\theta) = \frac{\sqrt{(R+r)^2-(x-d_i)^2}}{(R+r)}; \qquad \tan(\theta) = \frac{(x-d_i)}{\sqrt{(R+r)^2-(x-d_i)^2}} \qquad (13)$$

Substituting Eq. (13) into Eq. (12) yields:

$$f(x) = k_v x - \mathrm{N}k_h(x-d_i)\left(\frac{\delta}{\sqrt{(R+r)^2-(x-d_i)^2}} + 1\right) \qquad (14)$$

Eq. (14) can be rewritten in a non-dimensional form as:

$$\bar{f}(\bar{x}) = \bar{x} - \mathrm{N}\alpha(\bar{x}-\beta_i)\left(\frac{\bar{\delta}}{\sqrt{1-(\bar{x}-\beta_i)^2}} + 1\right) \qquad (15)$$

where $\bar{x} = \frac{x}{R+r}$, $\bar{f}(\bar{x}) = \frac{f(x)}{k_v(R+r)}$, $\beta_i = \frac{d_i}{(R+r)}$, $\bar{\delta} = \frac{\delta}{(R+r)}$, $\alpha = \frac{k_h}{k_v}$. Here α is the stiffness ratio between the horizontal and vertical springs.

By differentiating Eq. (15) with respect to $\bar{x}$, the non-dimensional stiffness is obtained as:

$$\bar{K}(\bar{x}) = 1 - \mathrm{N}\alpha\left(1 + \frac{(\bar{x}-\beta_i)^2\bar{\delta}}{(1-(\bar{x}-\beta_i)^2)^{3/2}} + \frac{\bar{\delta}}{\sqrt{1-(\bar{x}-\beta_i)^2}}\right) \qquad (16)$$

Let $\bar{K} = 0$ represent a static equilibrium position at the cam centre where $\bar{x} = \beta_i$. The relationship of the non-dimensional pre-compressed length of the horizontal spring and the spring stiffness ratio can be found as:

$$\mathrm{N}\alpha = \frac{1}{\bar{\delta}+1} \; Or \; \bar{\delta} = \frac{1}{\mathrm{N}\alpha} - 1 \qquad (17)$$

To achieve the QZS characteristic, the non-dimensional pre-compression of horizontal springs and the spring stiffness ratio should satisfy the relationship given by Eq. (17), as shown in Fig. 10. The pre-compression of the horizontal spring $\bar{\delta}$ is always larger than -1 for an existing contact condition of the cam and roller. When $-1 < \bar{\delta} < 0$, the initial uncompressed horizontal position of the roller is on the right side of the reference surface. In some cases of practical applications, the roller may separate from the cam to reach the ineffective zones. When $\bar{\delta} >$

0, the initial uncompressed horizontal position of the roller should be on the left side of the reference surface and the springs should be compressed in the full zone, which means the roller will always be in contact with the cam structure and there is no ineffective zone.

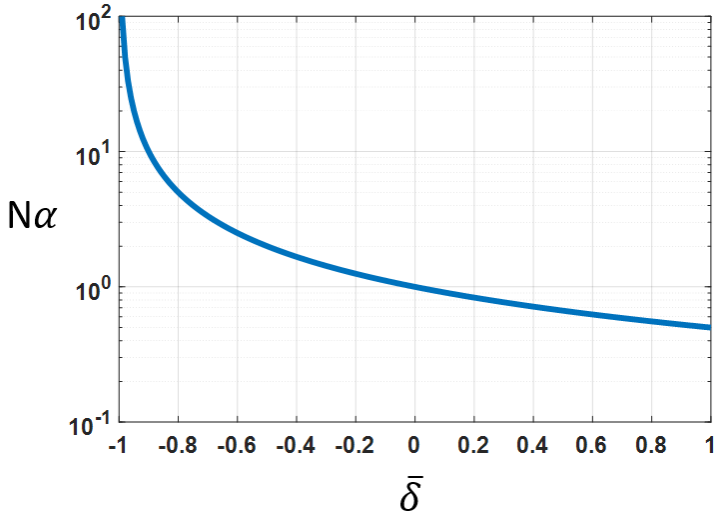

Fig. 10. Relationship of the non-dimensional pre-compression and the spring stiffness ratio.

By neglecting the third-order and higher terms in the Taylor expansion of $1/\sqrt{1-(\bar{x}-\beta_i)^2}$ at $\bar{x}=\beta_i$, Eq. (15) can be simplified as:

$$\bar{f}(\bar{x}) = \beta_i + \gamma(\bar{x}-\beta_i)^3 \qquad (18)$$

where $\gamma = \frac{-\bar{\delta}}{2(\bar{\delta}+1)}$.

When two sets of rollers and three cams are designed in an isolation vibration system with a full zone distance and the centre of the first cam is (R+r) away from the designed reference plane, the relationship of the non-dimensional force-displacement response is shown in Fig. 11. The pre-compression of the horizontal spring is determined by the stiffness ratio of the chosen springs. Only if $\bar{\delta} < 0$, the system stiffness can demonstrate the desirable zero stiffness at the designed location. When $\bar{\delta}$ approaches -1, the effective zone is small.

The detailed non-dimensional stiffness in the cam zone and the total system stiffness along the cam structure are shown in Fig. 12 and Fig. 13, respectively. It should be noticed that when $\bar{\delta}$ is close to 0, the stiffness at the edge of each effective zone is high, which may result in a stiffness “jump” when moving in or out of the effective zone and degrades isolation performance.

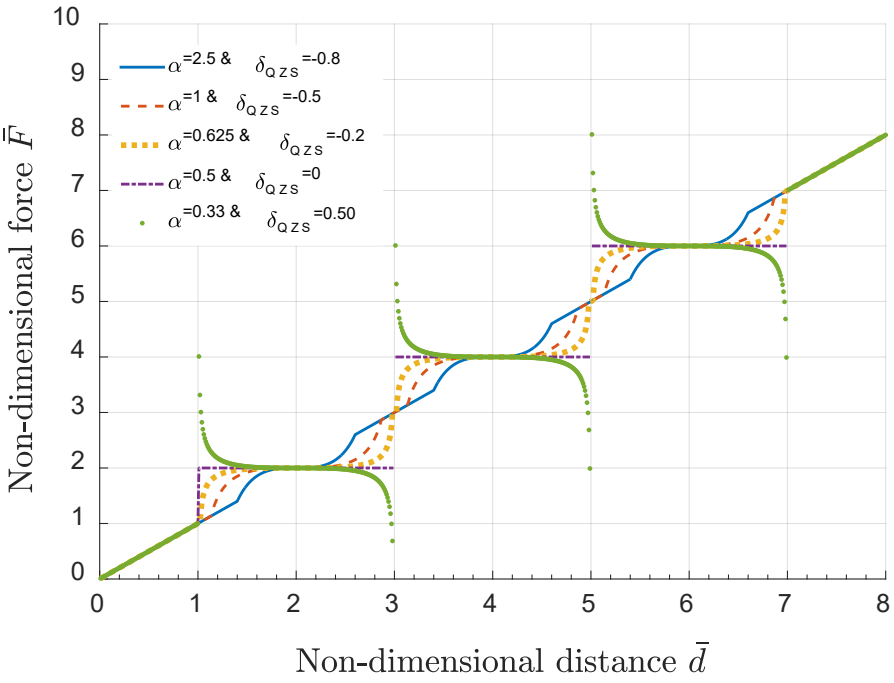

Fig. 11. Relationship of non-dimensional force and displacement response.

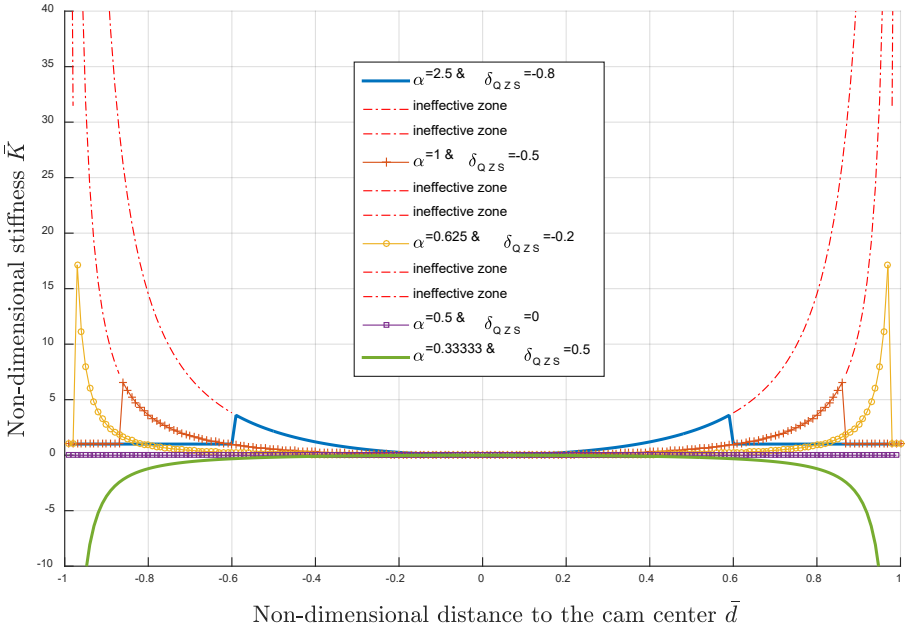

Fig. 12. Variation of the non-dimensional stiffness in the cam zone.

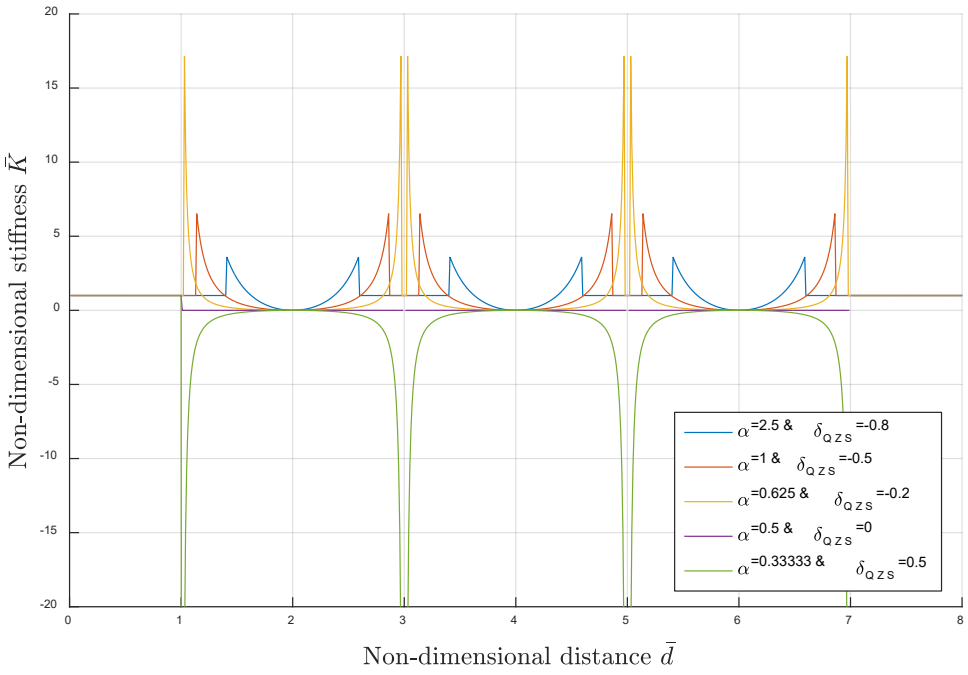

Fig. 13. Variation of the non-dimensional stiffness in the system.

3.2.2 Dynamic Response of the Multi-Cam-Roller QZS Structure

If applying an excitation from the base in the vertical direction z_e to the system (which theoretically represents the uneven road conditions), the relative displacement u can be expressed as:

$$u = z_m - z_e = y + d_i \tag{19}$$

where z_m is the absolute displacement of the supporting weight (i.e., driver's weight), y denotes the relative displacement of the roller about the cam centre and d_i is the distance of the cam centre to the reference plane(see Fig. 8).

The equation of motion of the system for a designed supported mass M with the displacement excitation can be written as [17]:

$$M\ddot{u} + C\dot{u} + f(u) = Mg - \mathrm{M}\ddot{z}_e \tag{20}$$

Substituting Eq. (18) into Eq. (20) yields

$$\ddot{u} + \frac{C}{M}(\dot{u}) + \frac{1}{M}\left(\frac{-k_v\delta}{2(\delta+(R+r))(R+r)^2}(u-d_i)^3\right) = -\ddot{z}_e \tag{21}$$

By using transformations $u = y + d_i, \dot{u} = \dot{y}$ and $\ddot{u} = \ddot{y}$, Eq. (21) becomes:

$$\ddot{y} + \frac{C}{M}(\dot{y}) + \frac{1}{M}\left(\frac{-k_v\delta}{2(\delta+(R+r))(R+r)^2}(y)^3\right) = -\ddot{z}_e \tag{22}$$

A sinusoidal excitation is assumed of the following form:

$$z_e = Z_e \cos(\omega t + \varphi) \tag{23}$$

and

$$Z_m = \sqrt{Y^2 + Z_e^2 + 2YZ_e cos\varphi} \tag{24}$$

where φ is the unknown phase between the excitation and the response. By introducing non-dimensional parameters:

$\bar{y} = \frac{y}{Z_e},\ \Omega = \frac{\omega}{\omega_n},\ \tau = \omega_n t,\ \xi = \frac{C}{2\mathrm{M}\omega_n}, \hat{y}' = \frac{\dot{\bar{y}}}{\omega_n}, \hat{y}'' = \frac{\ddot{\bar{y}}}{{\omega_n}^2}, \eta = \frac{-k_v \bar{\delta} {Z_e}^2}{2{\omega_n}^2 M(\bar{\delta}+1)(R+r)^2},$

the equation of motion is rewritten as:

$$\hat{y}'' + 2\xi\hat{y}' + \eta\hat{y}^3 = \Omega^2 \cos(\Omega\tau + \varphi) \tag{25}$$

where, $\omega_n = \sqrt{k_v/M}$ is the natural frequency of the system without the cam-roller structure.

The first-order approximate periodic solution of Eq. (25) can be written as

$$y = Ycos(\Omega\tau) \tag{26}$$

By substituting Eq. (26) into Eq. (25), we have:

$$\left(\frac{3}{4}\eta\hat{Y}^3 - \hat{Y}\Omega^2\right) cos(\Omega\tau) - 2\xi\Omega\hat{Y} sin(\Omega\tau) = \Omega^2 \cos(\varphi)\cos(\Omega\tau) - \Omega^2 \sin(\varphi)\sin(\Omega\tau) \tag{27}$$

Equating the coefficients of terms $cos(\Omega\tau)$ and $sin(\Omega\tau)$ in Eq. (27) leads to

$$\frac{3}{4}\eta\hat{Y}^3 - \hat{Y}\Omega^2 = \Omega^2 \cos(\varphi) \tag{28a}$$

$$2\xi\Omega\hat{Y} = \Omega^2 \sin(\varphi) \tag{28b}$$

By squaring both sides of Eq. (28a) and Eq. (28b) and then adding two resultant equations, the amplitude-frequency (AF) equation can be obtained as:

$$\frac{9}{16}\eta^2\hat{Y}^6 - \frac{3}{2}\eta\hat{Y}^4\Omega^2 + 4\xi^2\hat{Y}^2\Omega^2 + \hat{Y}^2\Omega^4 - \Omega^4 = 0 \tag{29}$$

When $\hat{Y}$ is solved from Eq. (29), the absolute vibration transmissibility can be found as:

$$Ta = \left|\frac{Z_m}{Z_e}\right| = \frac{\sqrt{Y^2 + Z_e^2 + 2YZ_e cos\varphi}}{Z_e} \tag{30a}$$

or

$$Ta = \sqrt{1 + \frac{3\eta\hat{Y}^4}{2\Omega^2} - \hat{Y}^2} \tag{30b}$$

For the purpose of comparison, the corresponding AF equation and transmissibility for a linear system are given by

$$\hat{Y}_{linear}{}^2 = \frac{\Omega^4}{1 - 2\Omega^2 + 4\xi^2\Omega^2 + \Omega^4};\ Ta_{linear} = \sqrt{\hat{Y}_{linear}{}^2 + 1 + \frac{2\hat{Y}_{linear}{}^2(1-\Omega^2)}{\Omega^2}} \tag{31}$$

The transmissibility due to different displacement excitations are shown in Fig.14. It is easy to note that the linear system without QZS characteristic provides vibration isolation ($Ta < 1$) only when $(\omega/\omega_n) > \sqrt{2}$. Fig.14 clearly demonstrates the advantages of the proposed nonlinear QZS isolation systems in that the transmissibility is Ta<<1 when Ω>0.2 for the cam-roller structure while Ta<1 only when $\Omega > \sqrt{2}$ for the linear system. Also, the transmissibility (Ta) of the cam-roller structure is much smaller than that of the corresponding linear structure. It also indicates that the peak value of the transmissibility at the resonance frequency for the QZS system is lower than that for the linear system. That is to say, the cam-roller QZS structure can provide a larger frequency range of vibration isolation and much better isolation performance than the corresponding linear system.

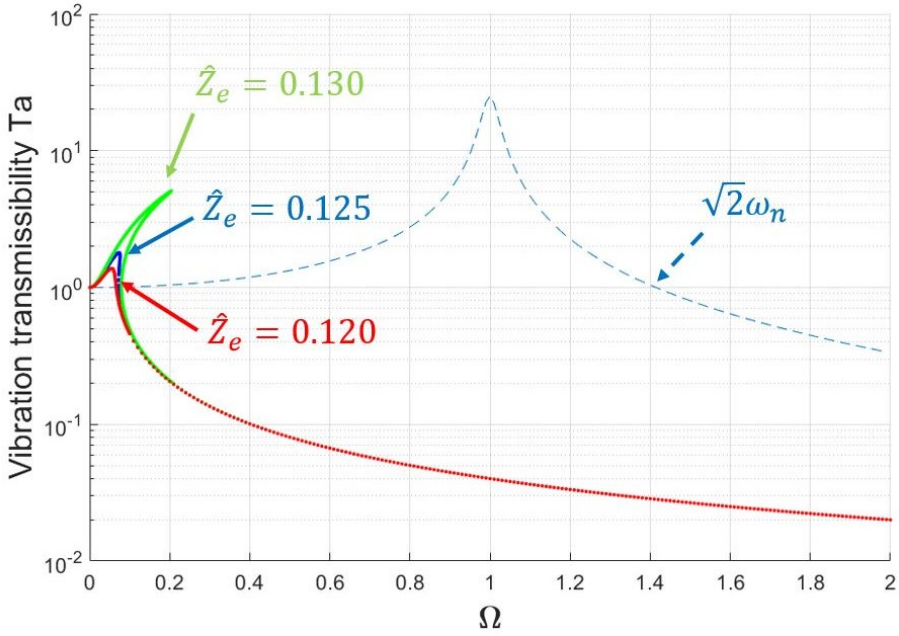

Fig. 14. Vibration transmissibility under displacement excitations (dashed line is for the corresponding linear system).

4 Proof of Concept (POC) Design, Fabrication and Test

The POC designs for both QZS systems are fabricated and tested. The fabricated metal components have the characteristics of easy assembly, adjustable frame configurations and high compatibility in case of further optimization.

4.1 Detailed Mechanical Design and Optimization

The detailed mechanical designs for each POC will be discussed in this section. The scaled POCs are used to verify the results of theoretical analysis and design innovations. Optimizations and further improvements are conducted according to the experimental results.

4.1.1 Multi-Cam-Roller QZS Structure

The POC design of the multi-cam-roller QZS structure has three components, including the cam structure, roller structure and the spring selection. The considerations for laboratory tests, including easy assembly, adjustable frame configurations, scaled load-bearing capacity, and the size of the POC prototype are taken into account.

4.1.1.1 Cam Structure Design

The cam structure plays an important role in determining the response of the supported mass (i.e., drivers). The ineffective zone for each cam would make the QZS isolation system return to a linear isolation condition. Assume that three (3) sets of roller structures are used in the system without friction and the first cam centre is away from the reference plane ($d_1 = R+r$). When imposing the QZS condition, the pre-compression of the horizontal spring can be determined by a stiffness ratio of the chosen springs. Relationships of the non-dimensional force response and system stiffness versus the displacement are shown in Fig. 15. It should be noticed that the stiffness at the edge of each effective zone is high, the stiffness “jump” may degrade the isolation performance (by causing a high vibration level).

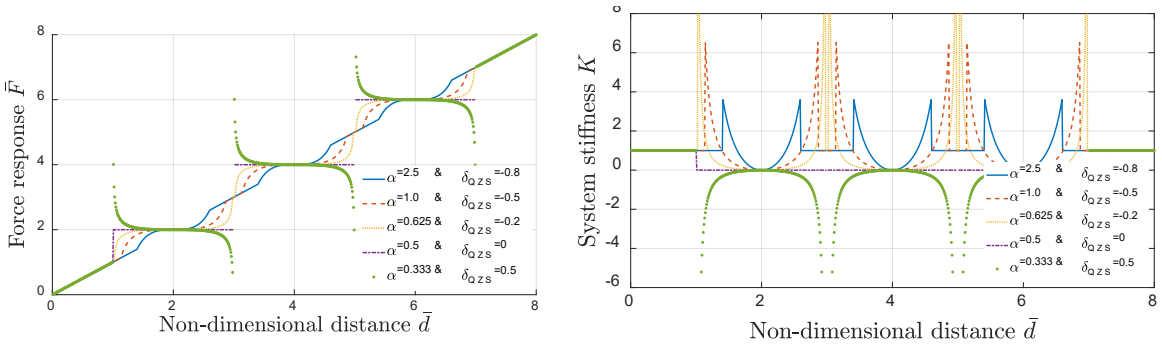

(a) (b)

Fig. 15. Non-dimensional force-displacement response and the system stiffness in full cam zone condition: (a) force-displacement curve, (b) stiffness.

In order to avoid the stiffness “jump”, the ineffective zone in each cam should be removed, and the effective zones of different cams will be joined without any gap. In this case, the system will always stay in a workable condition and the stiffness “jump” can be minimized or eliminated. Fig. 16 shows the optimal working zones of the multi-cam-roller system. It is also noticed that the QZS system has better performance near the cam centre. Shortening the design zone for each cam in the effective zone can be an option if the pre-compression is constrained by the springs. An additional benefit of removing the ineffective zone and shortening the design zone is that the accuracy of weight response can be improved. For a constant vertical spring stiffness, the perfect responded weight is determined by a distance between two cam centres. Narrowing the design zone means decreasing such a distance and thus results in more responded weight levels.

The difference of the force-displacement response between the full cam zone structure and the improved design is clearly shown in Fig. 17. The original three full cam zone structure is assumed to have a spring stiffness ratio of 1 and satisfies the QZS requirement ($\alpha = 1$ & $\bar{\delta} = -0.5$). By removing the ineffective zone and narrowing design zone to half the length of the full zone, the improved design can provide up to three (3) QZS zones than the original design.

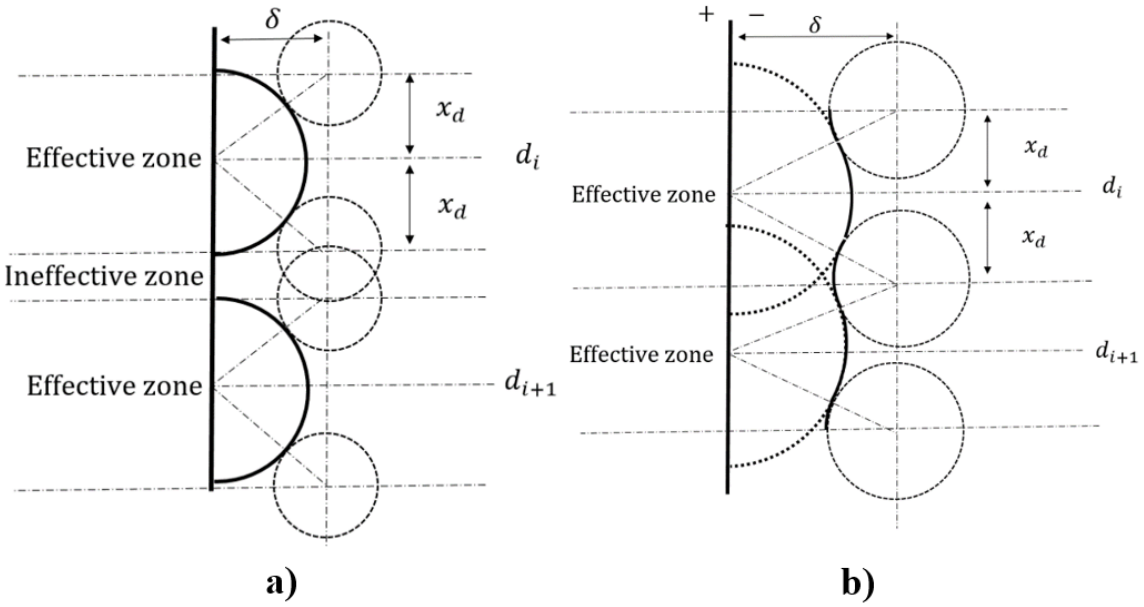

Fig. 16. Operating zones of multi-cam-roller: (a) cam-roller with ineffective zone, (b) cam-roller without ineffective zone.

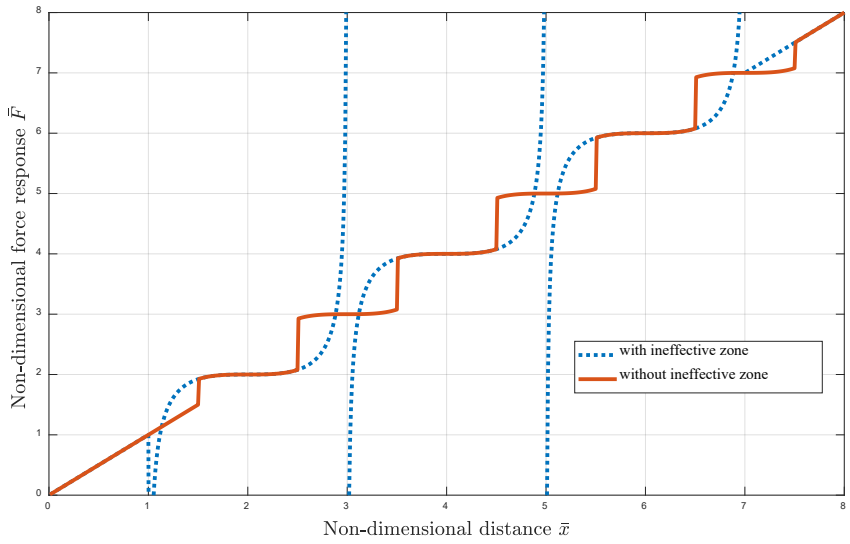

Fig. 17. Force-displacement response of the multi-cam-roller structure after removing the ineffective zone.

Three designed examples of the cam structures are shown in Fig. 18. The radius of the designed cam and roller are 8mm and 4mm, respectively. The non-dimensional pre-compression of the horizontal spring is $\bar{\delta} = -0.2, -0.5$ and -0.8. The corresponding spring set is chosen in terms of the load capacity and the stiffness ratio calculated.

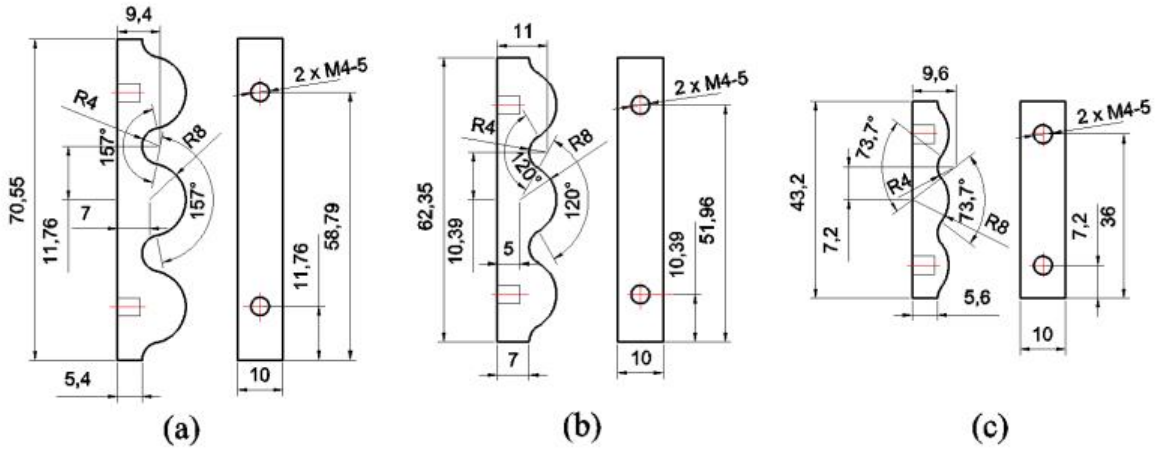

Fig. 18. Three types of cam structures: (a) $\bar{\delta} = -0.2$, (b) $\bar{\delta} = -0.5$, (c) $\bar{\delta} = -0.8$.

4.1.1.2 Roller Structure

The direct contact of the roller and cam would face a problem of the potential friction. As the vertical component of the frictional force can be upward or downward, it could affect the negative stiffness generated from the cam-roller interaction. In the proposed design, two types of roller heads are used to reduce the friction as shown in Fig. 19. The first one is the use of a hemisphere head. Although there may still exist a small dry friction, a contact area of the hemisphere head and the cam can be reduced and even becomes a line in an ideal situation. The other head is the use of bearings to replace the rolling friction by negligible sliding friction.

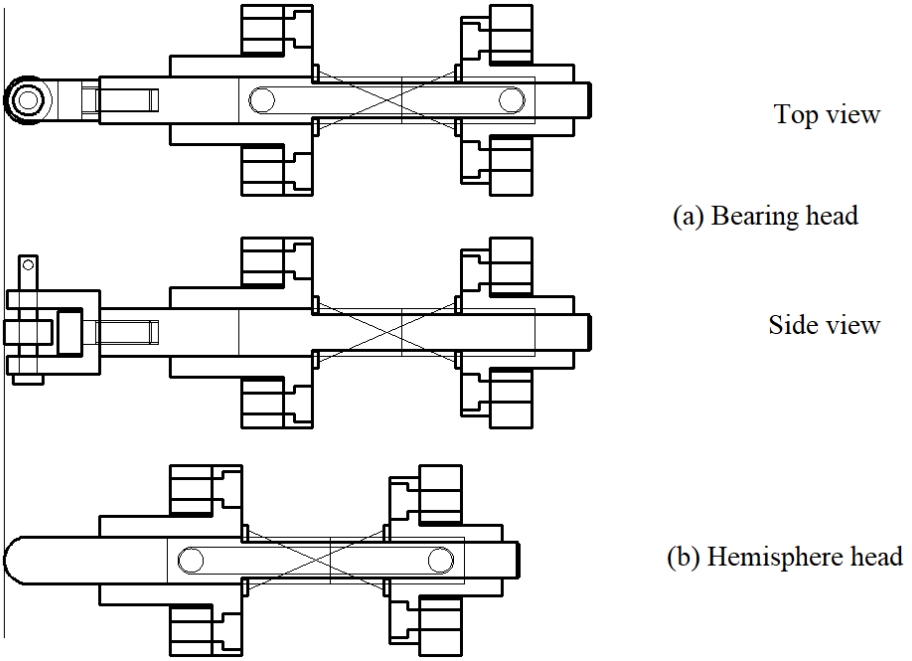

Fig. 19. Two roller head designs: (a) bearing head, (b) hemisphere head.

4.1.1.3 Spring Stiffness

The selection of spring stiffness also plays an important role in designing the cam-roller QZS isolation system. The vertical spring is mainly used for load capacity. For a prescribed structure with the constant maximum compression distance, the maximum load is limited by stiffness of the vertical spring. The vertical spring can be initially selected on the basis of the maximum load capacity. In addition, selection of the vertical spring is constrained by the stiffness of the horizontal spring. As discussed theoretically in Section 3, the pre-compression of the horizontal spring and the ratio of the total stiffness between the vertical and horizontal springs should meet the QZS requirement. In the present design, the relatively high stiffness ratio is considered so as to shorten the effective zone.

4.1.2 Limb-like Structure using Two Pairs of Oblique Springs

The parameter considerations for the limb-like QZS system using two pairs of oblique spring are mainly about the spring selection and configuration such as the lengths and inclined angles of the oblique springs. Slot design used in the frame structure can be the most efficient way for adjusting such structure parameters in the experiment. Different parameter sets can be tested to verify their performances.

4.1.2.1 Oblique Springs

In selecting oblique springs, coil springs are considered as they are cheap and easily accessible. In practical design, coil springs are assembled with a guiding rod so that the assembled structure can support load in a stable state, as shown in Fig. 20(a) where the two ends are connected with the other parts by using radial bearings as hinges.

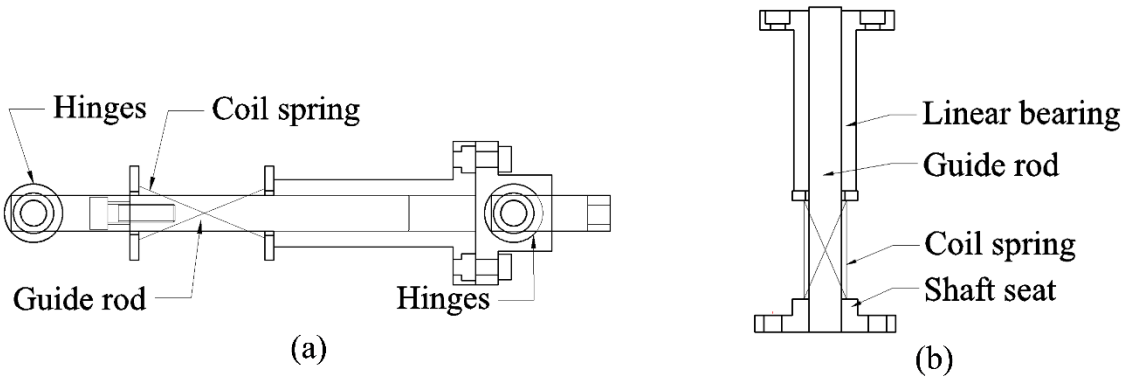

Fig. 20. Design of limb-like oblique spring system: (a) oblique spring structure, (b) vertical rod and spring structure.

4.1.2.2 Vertical Rod-Spring Structure

The design for vertical spring is the same as that of the oblique springs. The coil spring used in vertical direction can freely move along the guiding rod when it is subjected to the applied load. The guiding rod is fixed on a shaft by screw bolts, as shown in Fig. 20(b). All parts of this proposed limb-like QZS isolation system are fabricated and the whole system are assembled to experimentally validate the dynamic performance of vibration isolation under the force or displacement excitation.

4.2 Fabrication

4.2.1 Multi-Cam-Roller QZS Isolation System

The multi-cam-roller QZS structure is designed to test the mechanism of the multi-cam-roller isolation system and thus the size of the structure is not a final design for practical application. The critical design parameters such as cam radius, roller radius and the stiffness ratio are calculated for the POC design but the other parameters such as the spring stiffness, mass supported, maximum deformation and frame structure size are scaled for POC tests only.

The schematic of the POC structure is shown in Fig. 21(a), where 1 is the main spring-damper system, 2 is the main support structure, 3 is the cam structure, 4 denotes the roller head, 5 represents horizontal spring structure, 6 is the roller structure support, and 7 indicates the loaded mass or applied weight. The three dimensional (3D) model of the design is given in Fig. 21(b).

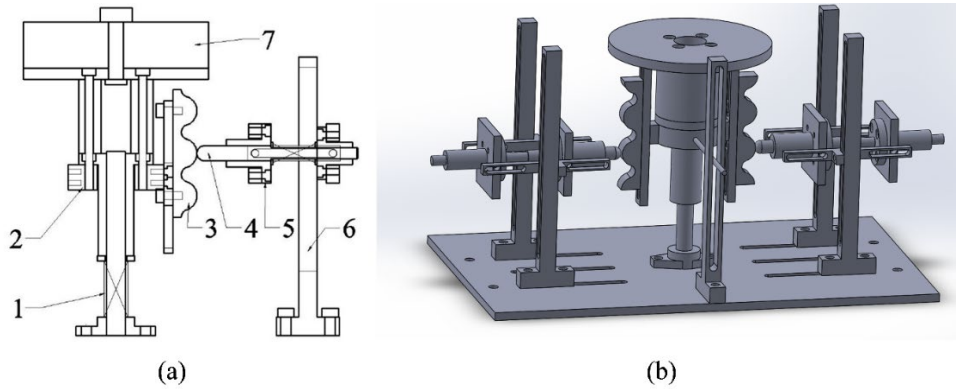

Fig. 21. The innovative cam-roller isolation system: (a) the schematic of the right half of the system, (b) 3D model.

4.2.2 Limb-like Isolation System using Oblique Springs

The limb-like oblique spring isolation system is also fabricated to test its mechanism and the design may be scaled up for practical use. The prototype of the limb-like isolation system is shown in Fig. 22(a), where 1 is the vertical rod and linear spring to support load mass, 2 denotes the supporting plate to fix one end of oblique springs and to adjust the pre-compression of the oblique spring, 3 represents the two pairs of oblique springs formed to generate negative stiffness in the vertical direction, 4 is the sleeve to install the oblique springs, 5 is the hinge, 6 is the side rod to fix the other end of oblique springs and to adjust the pre-compression of the oblique spring or the relevant parameters $\hat{a}$ and γ, and 7 represents the loaded mass. The designed 3D model is shown in Fig. 22(b).

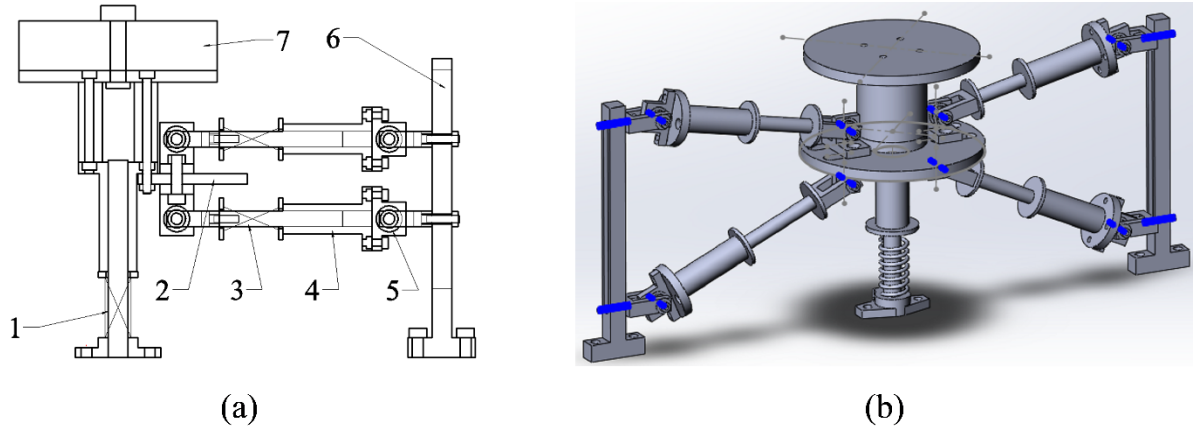

Fig. 22. The limb-like isolation system: (a) the schematic of the right half of the system, (b) 3D model.

4.3 Test Rig Set-Up and Instrument

4.3.1 Test Machine and Experimental Set-up

The INSTRON E10000 Linear-Torsion All-Electric Dynamic Test Instrument is used for both static and dynamic experiments for two POC prototypes. It is controlled by its built-in software Bluehill3 for the static test and WaveMatrix for the dynamic test. The built-in sensors include force, displacement and torque sensors. The main specifications of E10000 are the excitation frequency up to 100 Hz, linear load capacity of ±10 kN and linear stroke of ±30 mm. Both force and displacement excitations can be controlled in a linear or wave form. The experimental set-

up for the dynamic test is illustrated in Fig. 23. The experimental set-up for the static test is similar to that for the dynamic test.

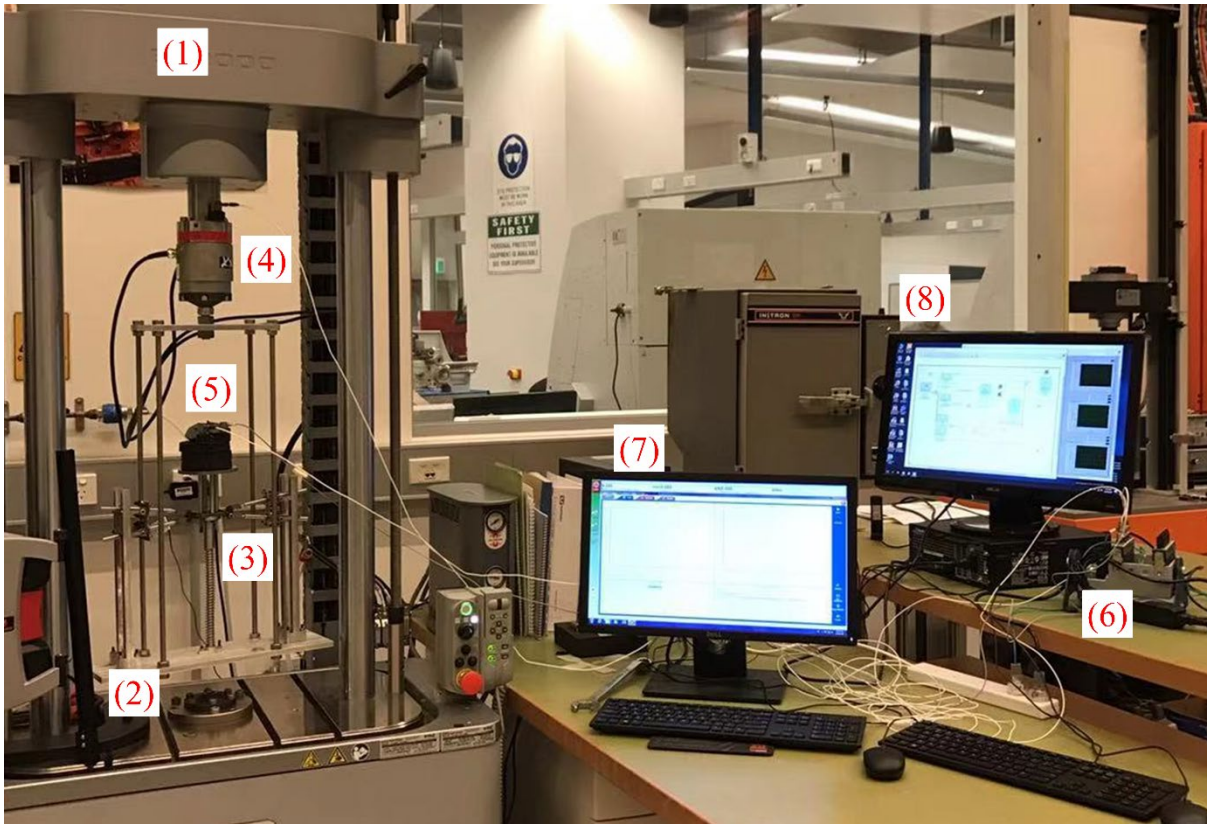

Fig. 23. Experimental set-up for the dynamic response test: (1) INSTRON E10000 machine, (2) Steel frame to hold the QZS isolation system, (3) QZS isolation system, (4) accelerometer to measure machine excitation, (5) two accelerometers to measure the response of the QZS isolation system, (6) NI cDAQ 9174/9234 data acquisition system to interface with accelerometers, (7) computer to control Instron E10000 via Bluehill3 or WaveMatrix software, (8) computer for data acquisition.

4.3.2 Equipment for Data Acquisition

Two sets of sensors are used for the data acquisition. The first set is the Instron E10000 built-in force and displacement sensors to record force-displacement relationships in the static test and the built-in displacement and time sensors to acquire displacement-time or amplitude - frequency relationships. These sensors are driven by the built-in software Bluehill3 and WaveMatrix for static and dynamic tests, respectively. The second set includes 3 digital one-DOF accelerometers driven by NI MAX via data acquisition system cDAQ NI 9174/9234 in the

dynamic test. The digital outputs from the accelerometers are recorded in series of sampling point schemes to calculate the displacement transmissibility via the Laboratory Virtual Instrument Engineering Workbench (LabVIEW) provided by National Instruments (NI).

The LabVIEW code and interface are shown in Fig. 24 and Fig. 25. A filter code is used to filter noises with frequencies lower than 0.5 Hz and higher than 20 Hz. A calibration has been made according to the sensitivity of each accelerometer and the recorded raw data are accelerations in unit *g*. The raw data of acceleration can be transformed into displacement response and the transformation between the raw data and the displacement is:

$$\mathrm{a} = \mathrm{raw\_data} * 9.81\ (\mathrm{m/s^2})$$
$$d = a/frequency^2 (\mathrm{m})$$

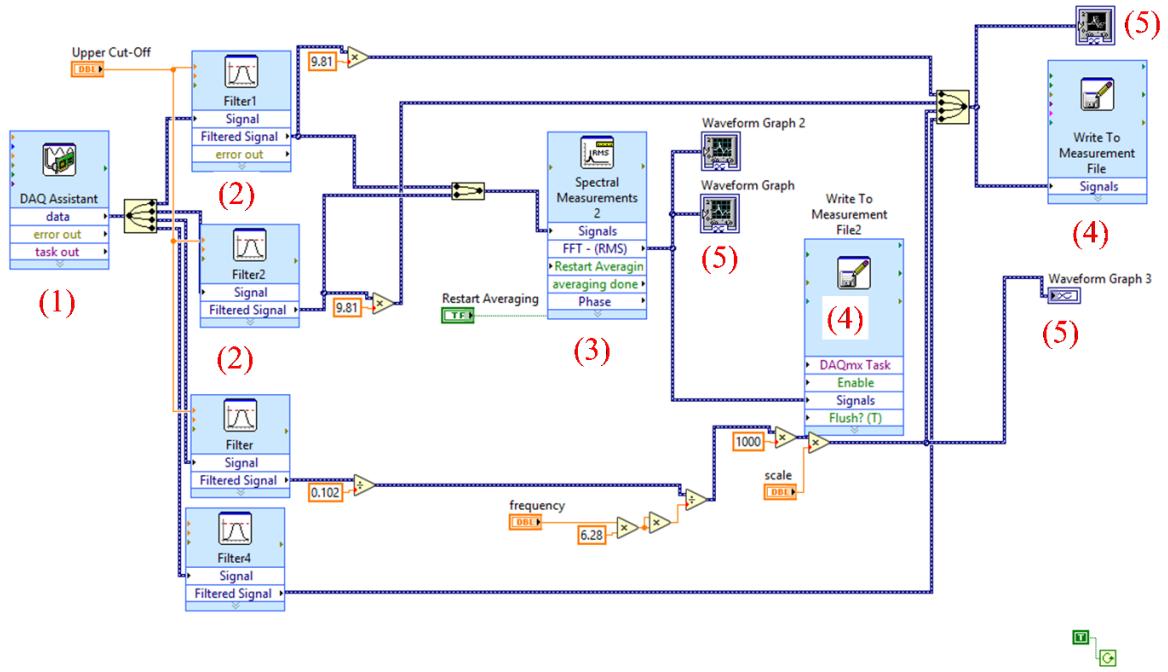

Fig. 24. Block diagram of LabVIEW program to control accelerometers and data acquisition: (1) DAQ assistant to interface with NI cDAQ 9174/9234, (2) Filter to filter noises with certain frequency range, (3) Spectral measurement for the FFT transformation, (4) Measurement file to record data in hard drive, (5) Waveform graph to display graphs in the front panel of LabVIEW platform.

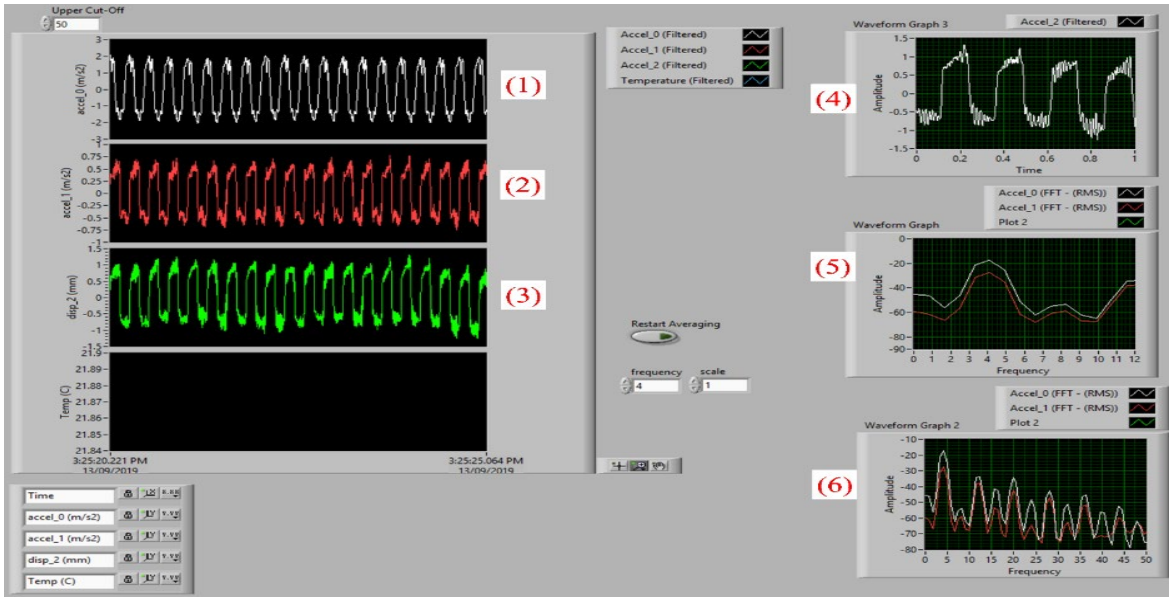

Fig. 25. Front panel of the LabVIEW code interface to real-time display excitation and response: (1) excitation acceleration, (2) acceleration response, (3) displacement response, (4) acceleration response within 1 second, (5) frequency spectrum of acceleration excitation, and (6) frequency spectrum of acceleration response.

4.3.3 Test Set-up

The test-rig set-up for investigating the static behaviour of the multi-cam-roller QZS structure is shown in Fig. 26(a) and it is also used for the static test of the limb-like QZS structure. The QZS isolation system is placed on a flat base plate with the thickness of 10 mm. The base plate is fixed at the machine platform and the vertical rod is aligned with the force rod of the machine. The displacement control mode with the loading speed of 10 mm/min is programmed using the built-in software Bluehill and the displacement is directly applied to the weight platform of the isolation system via the force rod. Both displacements and reaction forces are recorded using the Bluehill software.

Fig. 26(b) illustrates the test-rig set-up for the dynamic response test of the multi-cam-roller QZS isolation system and a similar rig is also used in the dynamic test for the limb-like QZS isolation system. A steel frame is assembled and installed to hold the QZS isolation system. Natural frequency of the frame can be calculated. It is much higher than that of the interested frequency and thus its effect can be neglected. Sinusoidal displacement excitations are applied to the QZS isolation system through the frame structure by the Instron E10000

machine and the machine is controlled by the program coded in the built-in software WaveMatrix. One accelerometer is mounted on the Instron E10000 to record the applied acceleration by the machine. Two accelerometers are mounted on the weight platform of the isolation system to record the dynamic response of the isolation system (see Fig. 23). Three accelerometers and dada acquisition are operated by the LabVIEW program via the data acquisition system NI cDAQ 9174/9234. A calibration is processed by comparing the displacements calculated using the data of the accelerometer with the excitation displacements measured from the built-in sensors of the Instron machine. The displacement transmissibility can be calculated using the recorded excitation and response data.

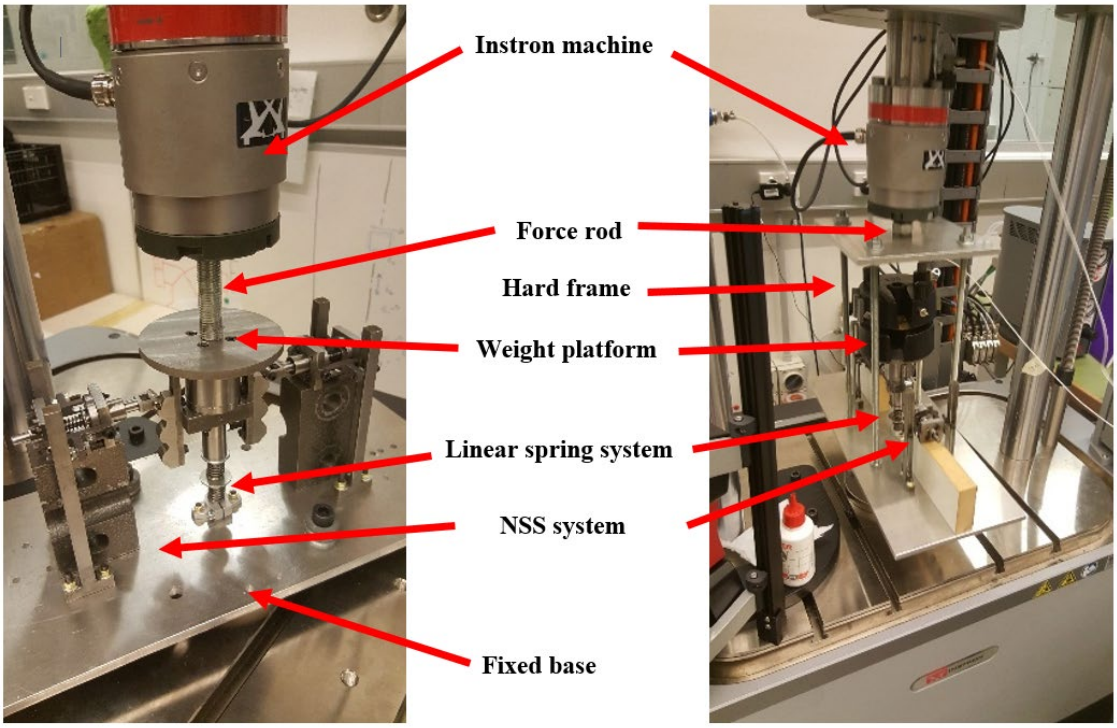

Fig. 26. POC prototype test set-ups: (a) static behaviour test, (b) dynamic response test.

4.4 POC prototype test results

4.4.1 Limb-Like QZS Structure

The POC prototype of the oblique-spring based limb-like QZS isolation system is fabricated to test its static behaviour and dynamic response. The structure parameters including stiffness ratio and pre-compression level are considered for the isolation performance.

4.4.1.1 Limb-like QZS Design and its Assembly

This bio-inspired limb-like design can significantly increase an operating zone with QZS as compared to the conventional oblique spring isolation systems. As two pairs of symmetric oblique springs produce negative stiffness in the vertical direction, the QZS condition can be obtained by combining negative stiffness with positive stiffness produced by the vertical linear spring. The limb-like QZS system comprised of two pairs of oblique springs is shown in Fig. 27, where *1* is the vertical rod and linear spring to support loaded mass, *2* is the supporting plate to fix one end of oblique springs and to adjust the pre-compression of the oblique spring, *3* presents the two pairs of oblique springs formed to generate negative stiffness in the vertical direction, *4* is the sleeve to install the oblique springs, *5* indicates the hinge, *6* represents the side rod to fix the other end of oblique springs and to adjust the pre-compression of the oblique spring or the relevant parameters, and *7* indicates the loaded mass.

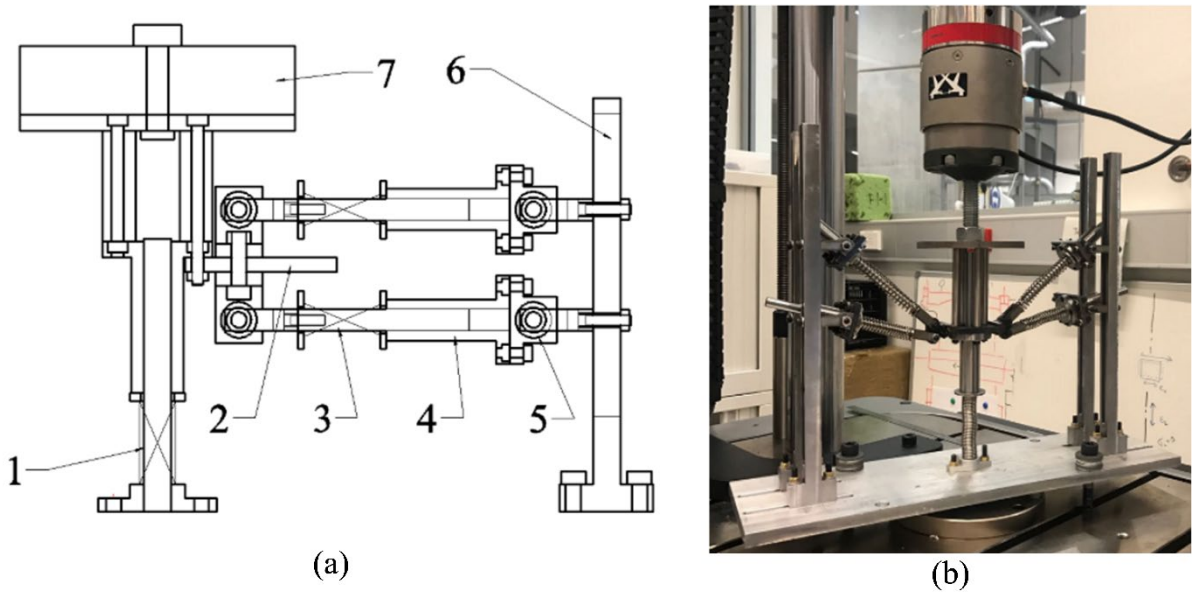

Fig. 27. POC design of the limb-like isolation system: (a) schematic of the right half of the structure, (b) physical model of the design.

4.4.1.2 Static Tests on Stiffness Characteristics

As compared to the conventional QZS structure with one pair of oblique springs, the proposed design can significantly increase the operating zone and improve isolation performance. The structure parameters measured under the QZS condition are listed in Table 3 where symbol definitions can be found in Section 3.1. Force-displacement curves of 3 tests are plotted in Fig. 28. Fig. 28(a) shows the force-displacement relationship for the QZS structure with two pairs of oblique springs to exhibit the characteristics of negative stiffness. The testing results for the vertical spring with positive stiffness are illustrated in Fig. 28(b). Repetition of the force-displacement curves in Fig. 28 indicates the testing reliability.

In Fig. 28, a starting point to measure force-displacement relationships of the vertical spring is chosen as a reference point with zero displacement. As the maximum machine stroke is 60 mm, the maximum displacement is set to be 55 mm in the experiment. The data for the negative stiffness in Fig. 28 (a) are measured in two steps and the measured data in one step for the positive stiffness are given in Fig. 28 (b). It can be seen that the measured data correlate well with those predicted by theoretical analysis.

Table 3. Key system parameters of the limb-like POC prototype

Structure parameters			Spring parameters		
h_1	a	d	δ	$k_1 = k_5$	k_2
1.5 mm	85 mm	17.5 mm	46 mm	0.71N/mm	1.47N/mm

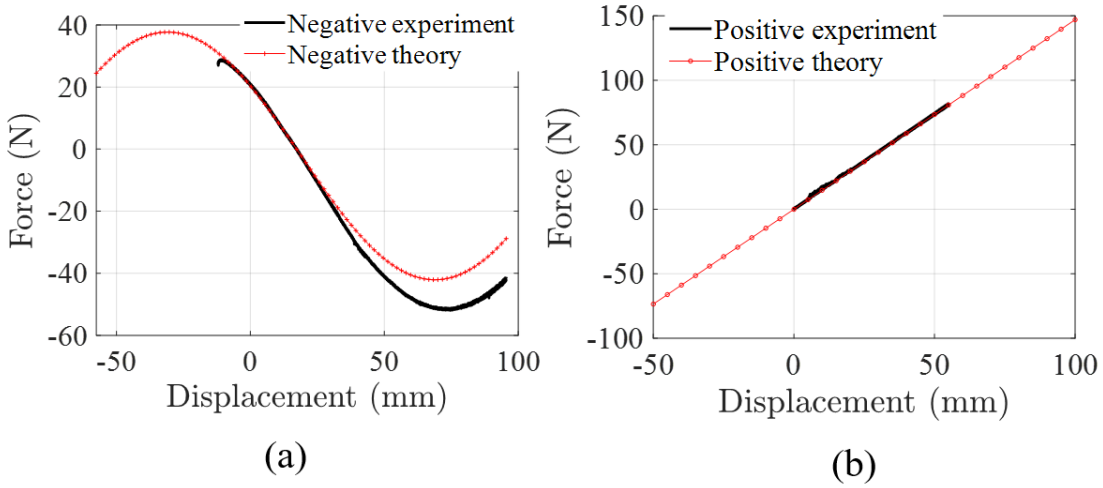

Fig. 28. Force-displacement relationship acquired by experiment: (a) negative stiffness generated by two pairs of oblique springs, (b) positive stiffness produced by the vertical spring.

Fig. 29 shows the force-displacement relationship for the limb-like QZS isolation system. It can be seen that the region of QZS is around 40 mm. Positive stiffness from the vertical spring, negative stiffness from the two pairs of oblique springs and synthesis stiffness for the QZS isolation system predicted by theoretical analysis and measured by experiment are shown in Fig. 30(b), which shows a fairly good agreement, indicating the correctness of the theoretical analysis and accuracy of the experimental results.

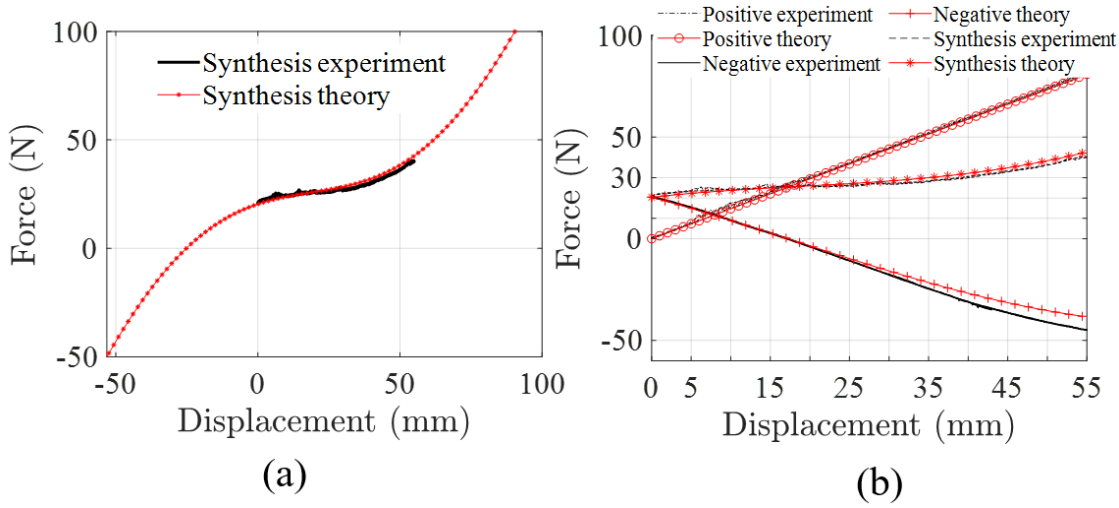

Fig. 29. Force displacement relationship acquired from experiments under QZS condition: (a) synthesis with positive and negative stiffness, (b) negative, positive and synthesis curves compared between experiments and theoretical analysis.

4.4.1.3 Dynamic Tests on Isolation Performance

The dynamic tests are conducted to verify the isolation performance of the limb-like QZS system in a frequency range of 2-10 Hz. The displacement transmissibility at each excitation frequency is calculated on the basis of the experimental results. The transmissibility of the nonlinear QZS isolation system will be compared with that of the corresponding linear isolation system to show better isolation performance of the limb-like QZS isolation system.

The limb-like QZS prototype is tested to study the dynamic response of the optimized limb-like QZS isolation system. The corresponding linear system of the present design without oblique springs is also tested for comparison. The excitations with frequencies of 2-10 Hz and an amplitude of 3 mm are used as the displacement excitations applied to the QZS system. The excitations and dynamic responses for linear and nonlinear structures for 4 and 5 Hz are

shown in Fig. 30 and Fig. 31, respectively. For clarity, only steady-state response of waveform including displacement excitation and response are provided.

It can be seen from Fig. 30(a) and Fig. 30(b) that, dynamic responses are also harmonic motions under sinusoidal excitation with frequency of 4 Hz for the linear system. The response amplitude is around 17 mm. It is almost 6 times of the excitation amplitude due to resonance. The resonant frequency of the corresponding linear system can be calculated as 3.7 Hz. For the nonlinear QZS system under the sinusoidal excitation with frequency of 4 Hz, the responses are approximately sinusoidal signals as shown in Fig. 30(c) and Fig. 31(d). Certain noises could be caused by energy dissipation in vibration attenuation. The response amplitude of the nonlinear QZS is around 1 mm and the displacement transmissibility is about 0.33.

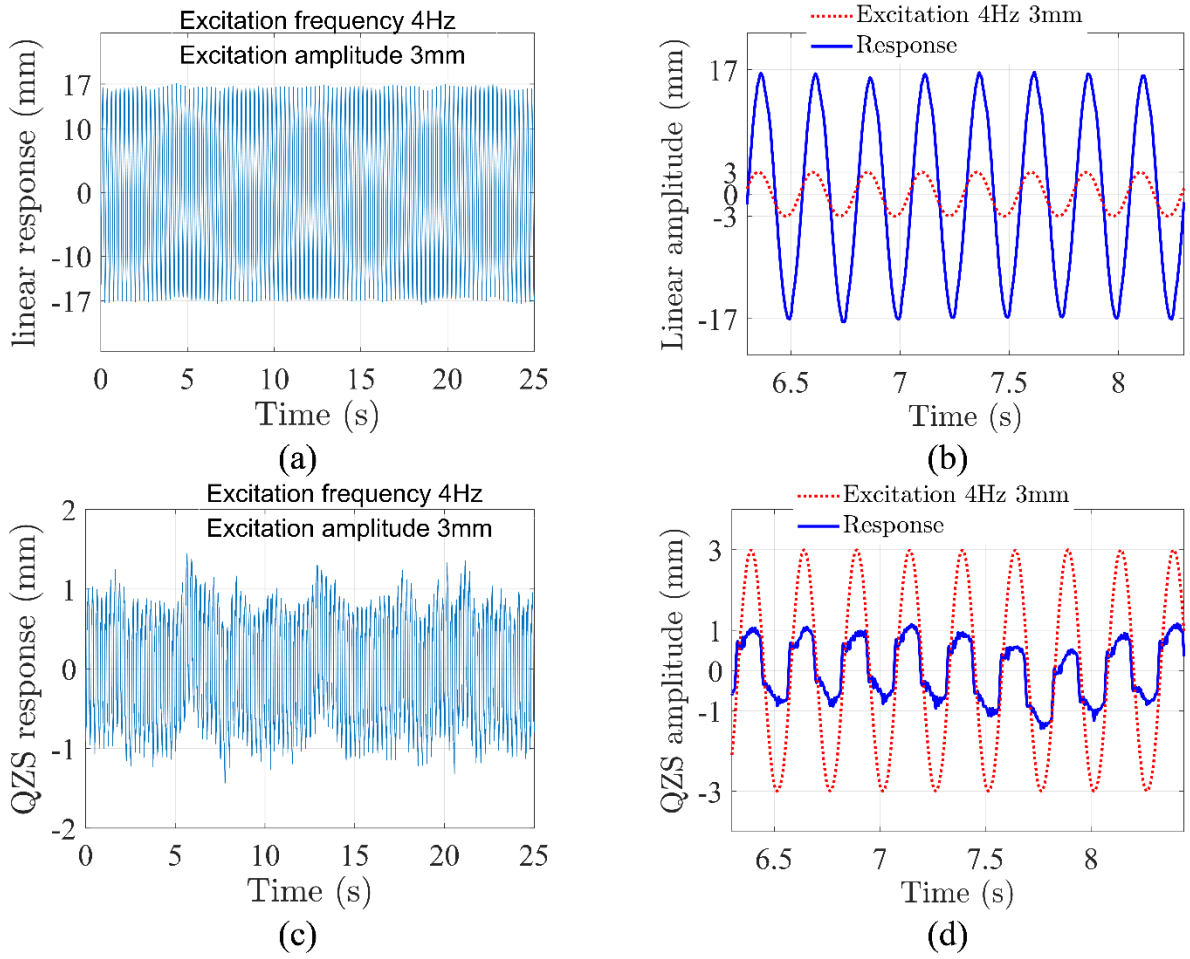

Fig. 30. Vibration response under the excitation of frequency 4Hz and amplitude 3mm: (a) linear response, (b) excitation and linear response, (c) QZS response, (d) excitation and QZS response.

Similar phenomena for the linear system under the harmonic excitation with frequency of 5 Hz to those for the 4 Hz excitation can be found in Fig. 31(a) and Fig. 31(b). The response amplitude is around 4 mm and the transmissibility is 1.33 as 5 Hz is away from the resonant frequency 3.7 Hz. Under the harmonic excitation with frequency of 5 Hz for the nonlinear QZS system, the vibration response is shown in Fig. 31(c) and Fig. 31(d). The response amplitude is further reduced to 0.75 mm with the transmissibility of 0.25. That is, the displacement excitations with frequencies of 4-5 Hz can be significantly attenuated by using the designed limb-like QZS isolation system and thus it can be used in mining equipment to considerably attenuate environmental vibrations.

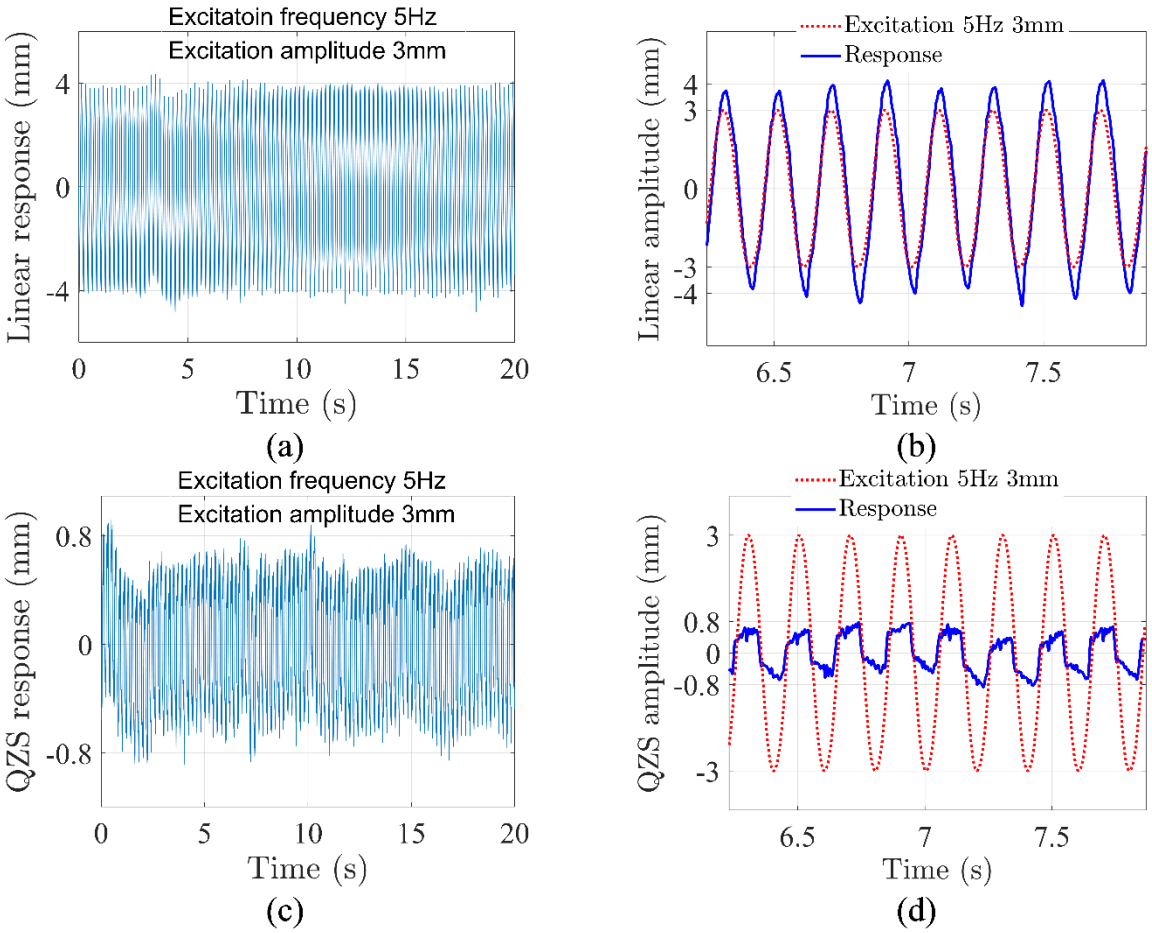

Fig. 31. Vibration response under the excitation of frequency 5Hz and amplitude 3mm: (a) linear response, (b) excitation and linear response, (c) QZS response, (d) excitation and QZS response.

The displacement transmissibility can be calculated using the measured displacements and/or accelerations of the excitations and responses via the root mean square (RMS) approach.

The obtained absolute displacement transmissibility of the corresponding linear system and that of the nonlinear QZS system is shown in Fig. 32(a). A damping ratio is found to be $\zeta = 0.16$ by using the experimental data. By using this calibrated damping ratio, the theoretical displacement excitation transmissibility can be calculated for the same structural parameters. The transmissibility calculated by theoretical analysis and also measured by experiment is illustrated in Fig. 32(b), which shows good agreement between the theoretical prediction and the experimental measurement.

The transmissibility of the QZS system is less than 1 when the excitation frequency is higher than 2 Hz, while the transmissibility of the corresponding linear system is less than 1 only when the excitation frequency is higher than 5 Hz. This indicates that the designed QZS system can isolate vibrations from the frequency of 2 Hz, and has a larger frequency range than the linear system. Fig. 32 indicates that transmissibility of the nonlinear QZS system is much less than that of the linear system, particularly in the range of 3-6 Hz.

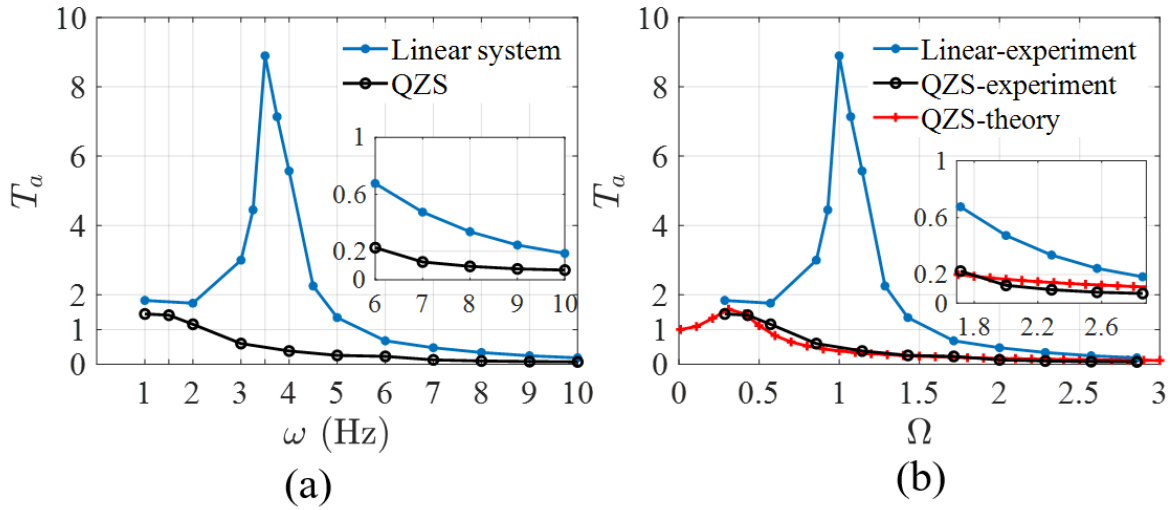

Fig. 32 Absolute displacement transmissibility: (a) comparison of the linear system and the QZS system, (b) comparison of the theoretical prediction and experimental measurement.

Overall, both static behaviour and dynamic response measured in the experiments are in excellent agreement with those of the theoretical predictions for the limb-like QZS isolation system. The designed POC is able to achieve the expected objectives: wider working zone and better isolation performance in the low frequency range.

4.4.2 Multi-Cam-Roller QZS System

In this section, the cam-roller QZS isolation system is fabricated to study its static behaviour and dynamic response experimentally. The parameters related to the QZS condition, including the friction factor, structure optimization, stiffness ratio and pre-compression level are considered and discussed.

4.4.2.1 Multi-Cam-Roller Structure and its Assembly

The schematic of the multi-cam-roller QZS structure is shown in Fig. 33(a), where *1* is the main spring-damper system; *2* is the main support structure with weight carrying platform; *3* is the cam structure; *4* indicates the roller; *5* is the horizontal spring structure; *6* represents the roller support structure and *7* indicates the loaded mass or applied weight. Two types of roller heads are used to study the effects of frictional force. One roller head is of hemisphere shape, which shows the type of sliding-friction, and the other is a bearing head, which exhibits the type of rolling-friction. The photo of the multi-cam-roller QZS system is shown in Fig. 33(b). Hard blocks (steel or wood) are placed under the horizontal spring structure to prevent bending motions.

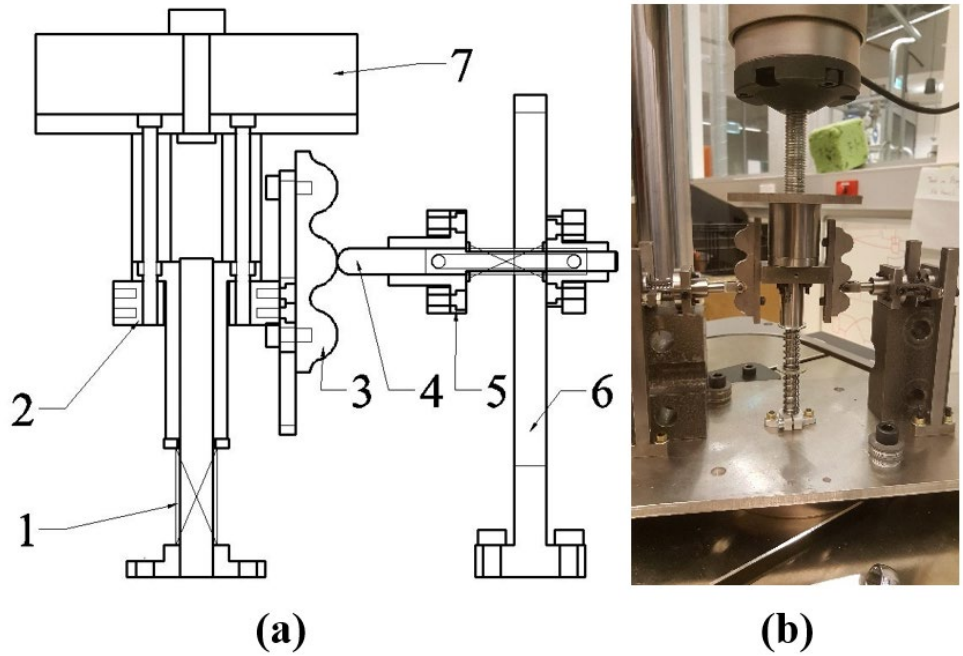

Fig. 33.The innovative multi-cam-roller QZS system: (a) the CAD drawing of the right section, (b) fabricated prototype.

4.4.2.2 Static Tests on the Multi-Cam-Roller QZS Structure

The static behaviour is tested for the multi-cam-roller QZS isolation systems with the hemispheric head and the bearing head to study the friction effects. The design configurations have been modified and calibrated according to the fabricated samples and all experimental results are compared with the simulation results considering the per-compression of the vertical spring.

4.4.2.2.1 Friction Analysis

The friction effects on the force-displacement relationships of the nonlinear cam-roller QZS system cannot be neglected in practical engineering, as there exist contact and relative motion between the cam and roller. The force-displacement relationship and the system stiffness in a full cam zone with different frictional coefficients are numerically simulated, as shown in Fig. 34 and Fig. 35, respectively. The response forces at the cam centre in the upper and lower sections are different. The reason is that, when the roller crosses the position of the metastable equilibrium at the cam centre, the frictional force changes its direction through a kinetic-static-kinetic state pattern. The difference of the response force due to the direction change is about twice the maximum static frictional force between the roller and the cam. The larger the frictional coefficient, the higher force “gap” appears at the cam centre. From Fig. 35, it can be seen that the friction effects on the stiffness are different and the friction is nonlinear in the two sections. The response force and stiffness in the upper section under the frictional forces are higher than those in the lower section.

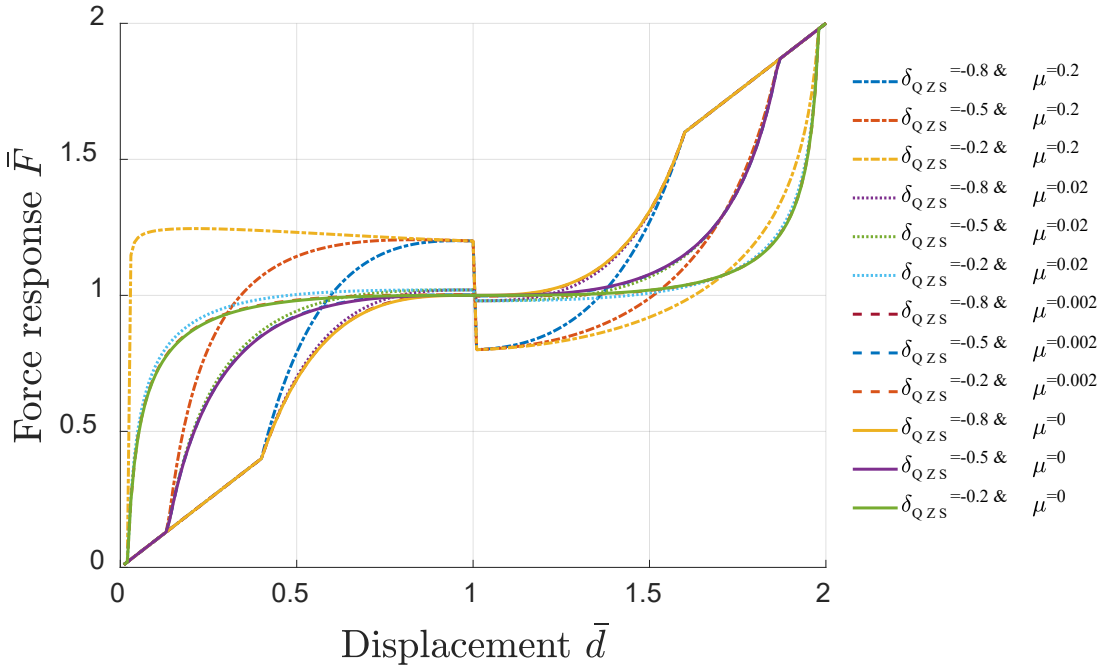

Fig. 34. Force-displacement relationship in a full cam zone with different frictional coefficients.

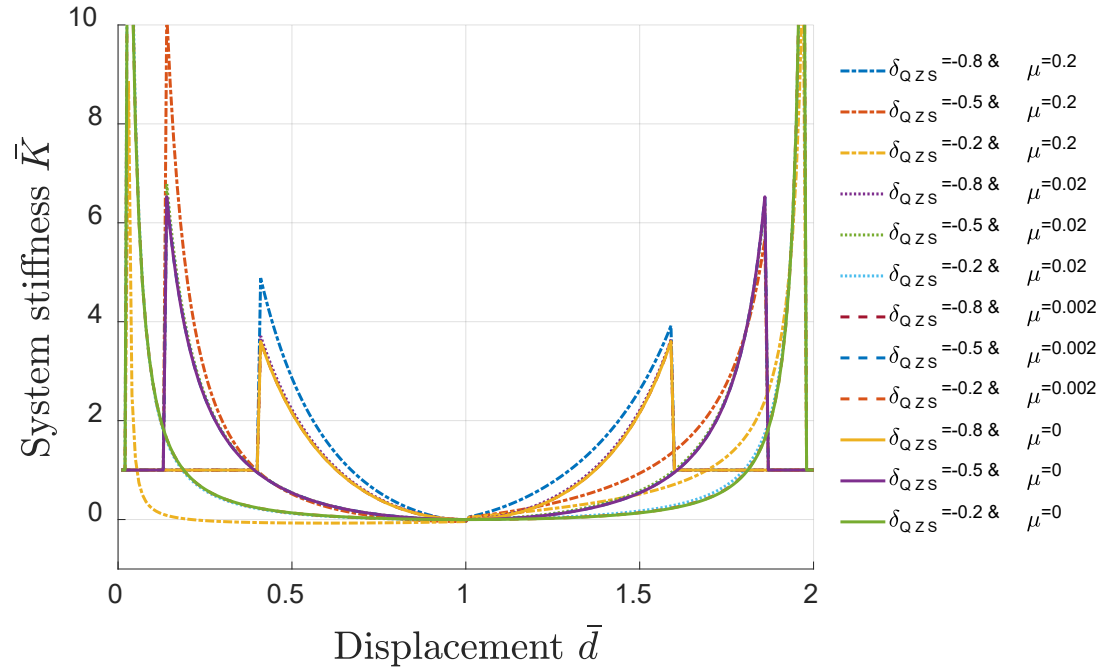

Fig. 35. System stiffness in a full cam zone with different frictional coefficients.

The prototype is tested to verify the static force-displacement relationship of the QZS system. Displacement compression is applied by the Instron machine on the weight platform and the built-in force sensor records the reaction force from the isolation system. Different QZS conditions (spring ratio α and pre-compression level $\bar{\delta}$) are considered in the experiments. The key parameters for different cases are listed in Table 4.

Table 4. Key system parameters of the cam-roller QZS prototype for different cases

Parameters	Linear**	Case 1	Case 2	Case 3
Vertical spring stiffness, K_v (N/mm)	4.98*	4.98*	4.98*	4.98*
Horizontal spring stiffness K_h (N/mm)	-	4.90*	3.152*	3.152*
Pre-compression level $\bar{\delta}$	-	-0.5	-0.8	-0.8
Cam radius, R(mm)	-	8	8	8
Roller radius, r(mm)	-	4	4	4
Roller head	-	Bearing	Bearing	Hemisphere

The experimental results of the reaction force and compression in a full cam zone of the fabricated prototype for Case 1 are shown in Fig. 36. Repeated tests are progressed with lubricating oil applied at the roller bearing heads (shown as re-test in the figure). The theoretical results are also plotted in Fig. 36 for comparison and the frictional coefficient is chosen as 0.05. With the lubricating oil applied, the force response near the cam centre location has a great improvement in reducing the friction effects.

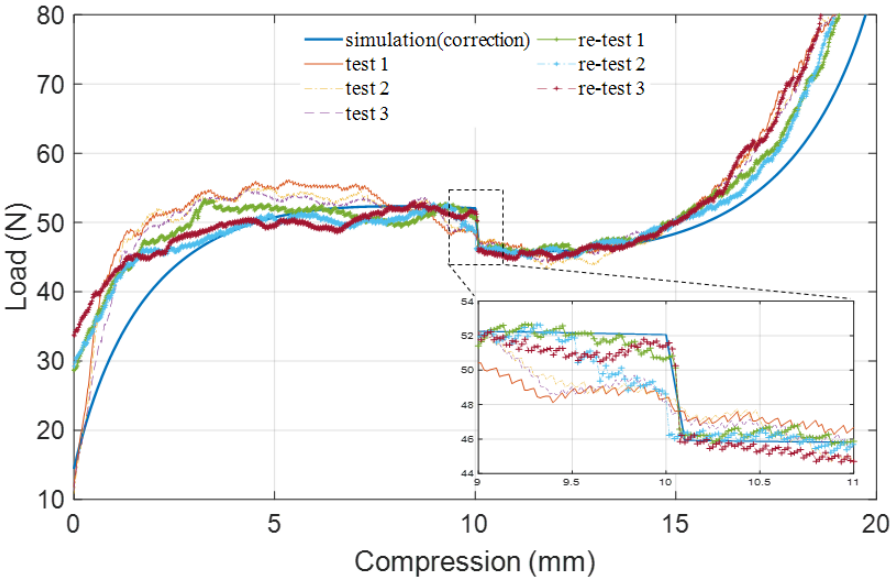

Fig. 36. Static force-displacement response of a full cam zone.

Using the hemispheric roller head would result in a sliding-friction at the contact surface. The difference of using a bearing head and a hemispheric head is shown in Fig. 37. The curve for the bearing head is much smoother than that for the hemispheric one. The different behaviours in the upper and lower sections also agree with the theoretical analysis on the friction effects.

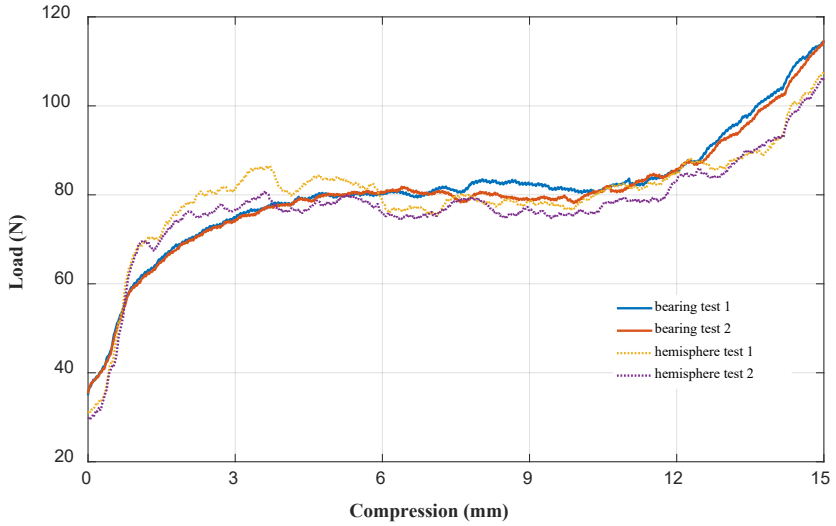

Fig. 37. Force-displacement response of using the bearing roller and the hemisphere roller with a per-compression QZS condition of $\bar{\delta} = -0.8$.

4.4.2.2.2 Optimized Structure Performance

The full range of force-displacement relationships using the multi-cam structure are measured as shown in Fig. 38, which confirms the reliability of the tests and good agreement between the theoretical and experimental results. A 2-cam zone optimized structure is fabricated to produce a spring stiffness ratio of 1 and the QZS requirement is imposed in the design ($\alpha = 1$ & $\bar{\delta} = -0.5$). The results indicate that the designed QZS response forces are 345N and 440N. The effective QZS range for each weight responded is about 19.8 mm. Further narrowing the effective zone from half the size of the full cam zone (Narrowed zone ratio of 0.5) to 0.2, the force-displacement relationship can be seen in Fig. 39. The designed QZS response forces are 80N and 160N. The effective QZS range for responded weights is about 10 mm. By neglecting the pre-compression of the vertical spring, it can be calculated that the weight response has been improved from 0.95 kg (95N) to 0.8 kg (80N). However, the effective zone for each cam zone is reduced from 19.80 mm to 10 mm, which may affect its dynamic performance.

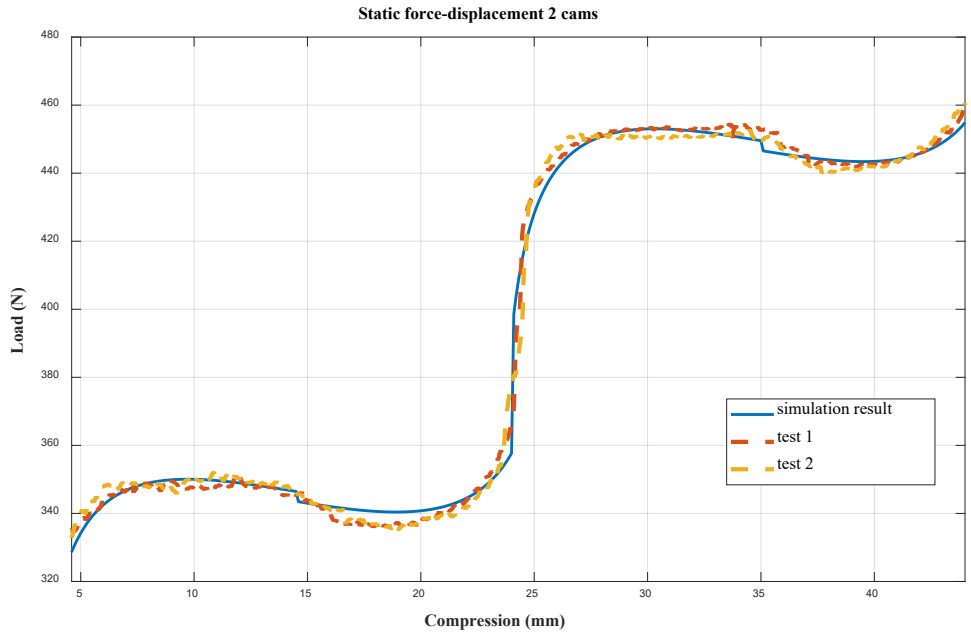

Fig. 38. Full range of force-displacement response of the multi-cam QZS system for Case 1 with optimized structure.

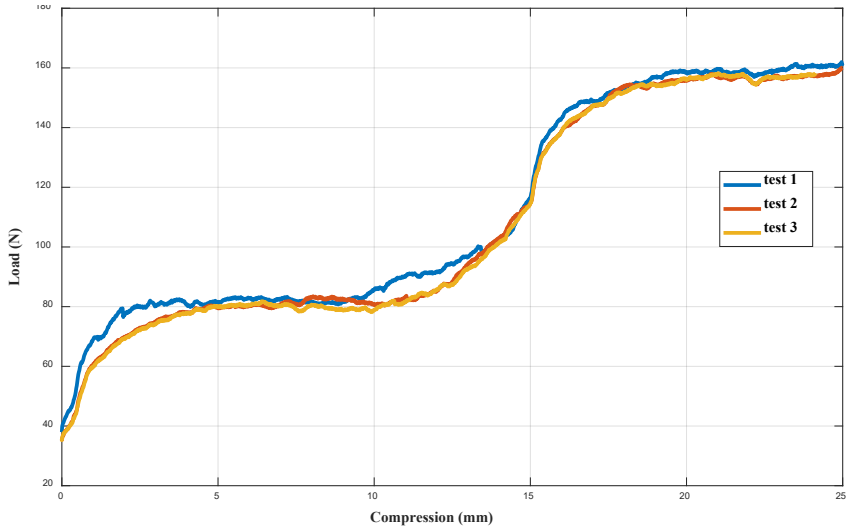

Fig. 39. Full range of force-displacement response of the multi-cam QZS system for Case 2 with optimized structure.

4.4.2.3 Dynamic Tests on Multi-Cam-Roller QZS Structure

The dynamic tests are performed to verify the isolation performance of the QZS system in a frequency range of 2-10 Hz. The displacement transmissibility can be calculated for different excitation frequencies.

Dynamic responses of the corresponding linear isolation system and the nonlinear QZS system are evaluated by laboratory tests. According to the theoretical calculation, a frequency increment of 0.5 Hz in the low frequency range of 2-4 Hz and the increment of 1 Hz in the range of 4-10 Hz are applied in the tests. The sinusoidal displacement excitations, including the peak amplitude and frequency are shown in Table 5.

Table 5. Parameters of the sinusoidal displacement excitations

Excitation sets	Amplitude (mm)	Natural frequency (Hz)	Frequency range (Hz)	
			Overall range	With a small increment
Set A (for linear system)	1.5	4.6	1-10	4-5
Set B (for QZS system Case 1)	1.5	3.5	1-10	2.5-4.5
Set C (for QZS system Case 1)	2.0	2.5	1-10	2-3

For an applied weight of 5.76 kg, the natural frequency of the linear condition can be calculated as 4.64 Hz. However, the resonance response of the corresponding linear system at 4.6 Hz exceeds the limitation of the test rig and may cause damage. Thus, experiments can only be performed in the neighbourhood of the natural frequency. Acceleration and displacement of time-history response at 4 Hz and 5 Hz are shown in Fig. 40. The root mean square (RMS) of both accelerations and displacements is calculated and the displacement transmissibility is obtained as the ratio of the weight response over the base excitation. The experimental results for the corresponding linear system are shown in Fig. 41. For the given weight, the resonance happens at the frequency below 5 Hz (close to 4.6 Hz) and vibration isolation is effective for the corresponding linear system starting from the frequency of 6.5 Hz ($\sqrt{2} \times 4.6\ Hz = 6.5\ Hz$).

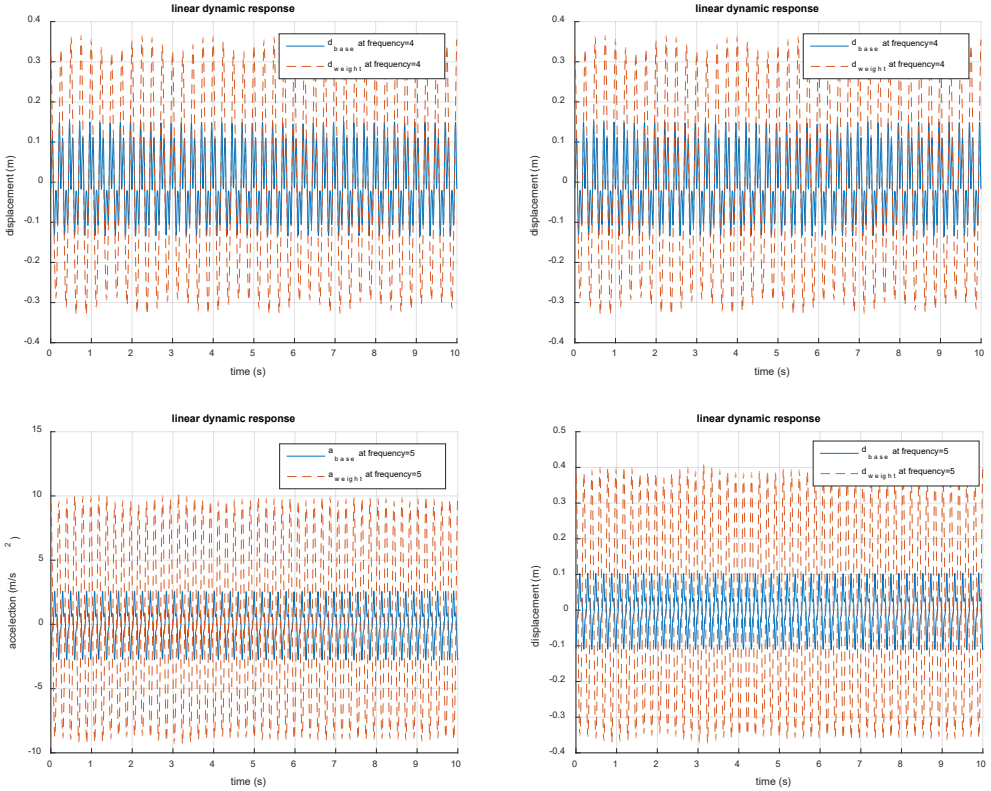

Fig. 40. Acceleration and displacement of time history response of the corresponding linear system at 4 Hz and 5 Hz.

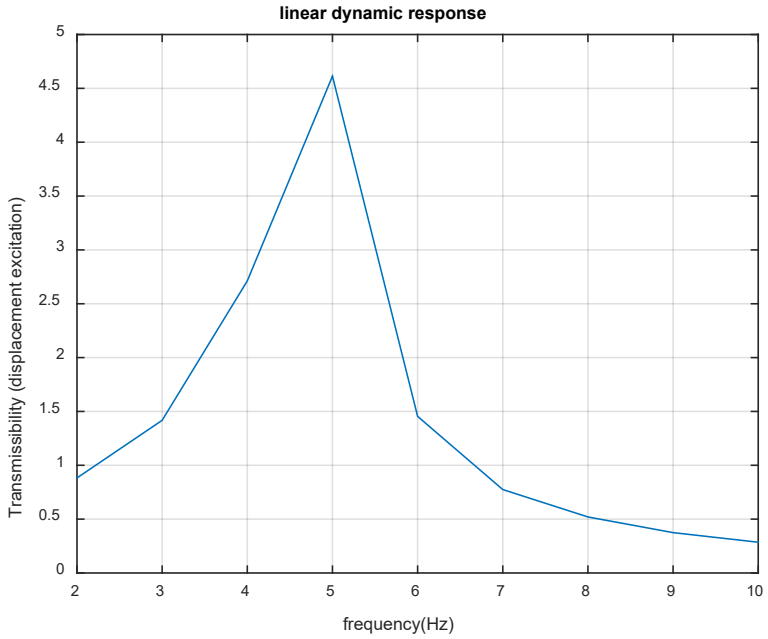

Fig. 41. Displacement transmissibility of the corresponding linear isolation system.

After attaching the cam-roller QZS structure to the supported weight, the acceleration and displacement of time-history response at 4 Hz are shown in Fig. 42. The comparison of time-history response of the corresponding linear system and the QZS system is shown in Fig. 43. The weight response has been greatly reduced after using the QZS system. It indicates that the isolation has been significantly improved by the QZS system at the chosen frequency. Comparison of the displacement transmissibility of both systems is also shown in Fig. 44. The designed QZS system, for a given weight with QZS condition under displacement excitation, can have different amplitude-frequency response curves. The experimental results are summarized in Table 6.

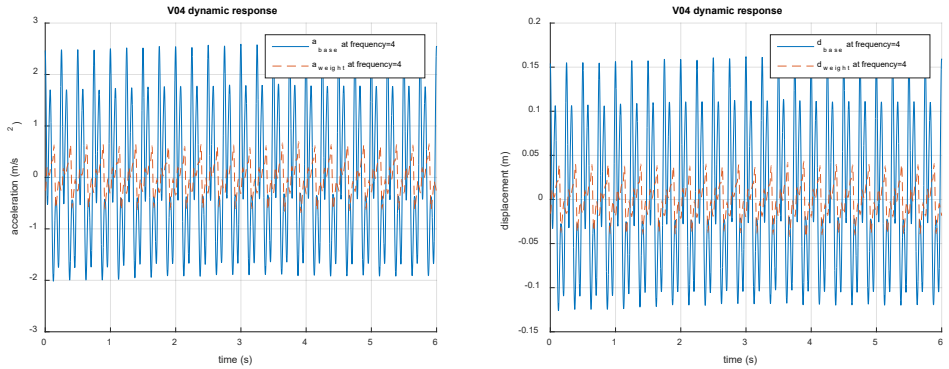

Fig. 42. Acceleration and displacement of time-history response of the QZS system at 4 Hz.

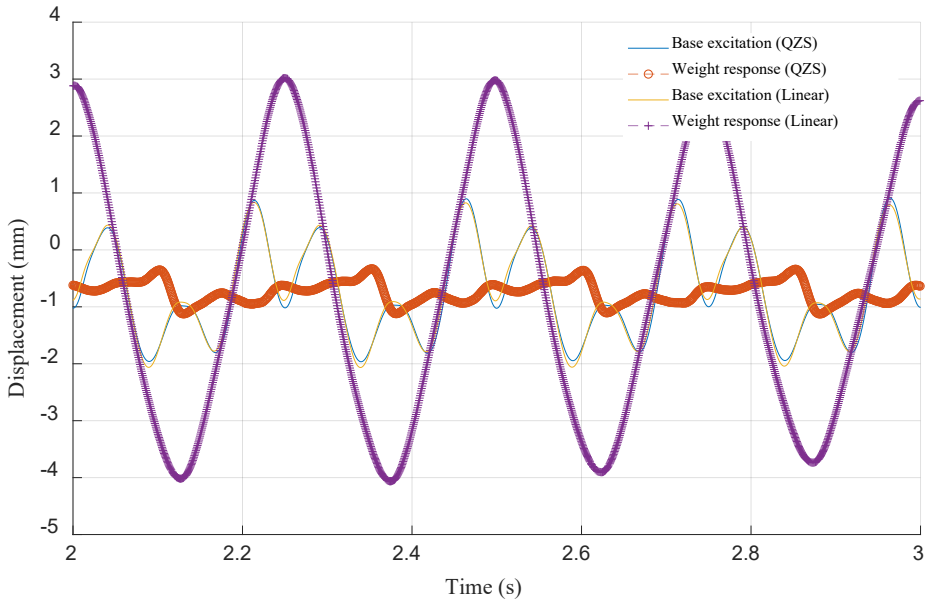

Fig. 43. Comparison of the time-history of the linear system and the QZS system at 4 Hz.

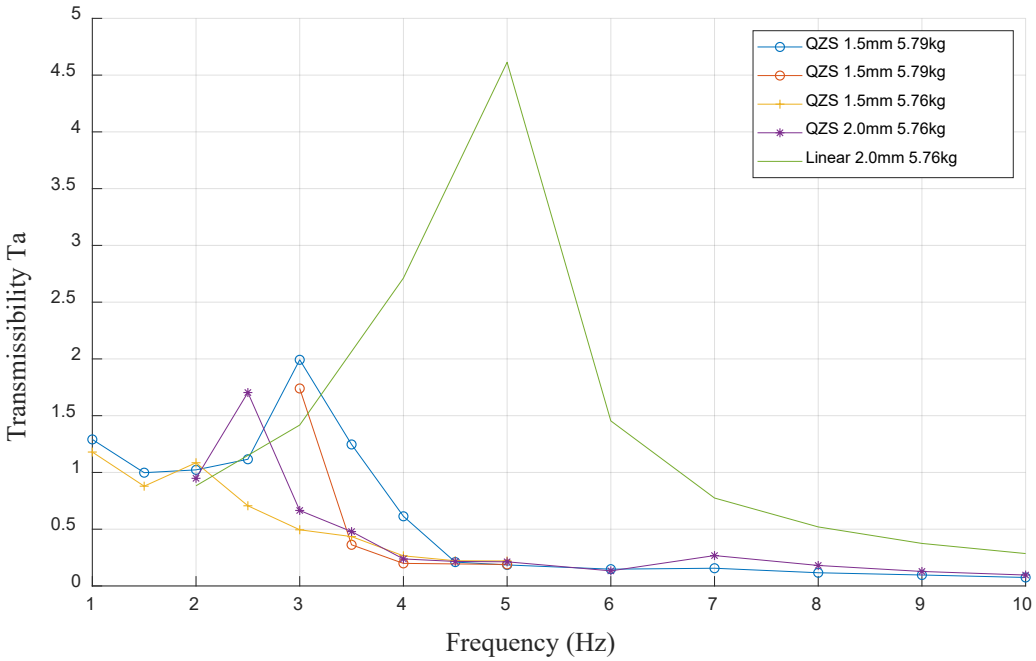

Fig. 44. Displacement transmissibility of the linear system and the QZS system.

Table 6. Summary of the vibration transmissibility

Test number	Weight (kg)	System condition	Displacement excitation(mm)	Resonance frequency(Hz)	Isolation frequency starting from (Hz)
1	5.79	Linear system	2.0	4.6	6.5
2	5.79	QZS $\bar{\delta} = -0.5$	1.5	3	3.6
3	5.76		1.5	Under 2.0	2.0
4	5.76		2.0	2.5	2.7

Overall, both static behaviour and dynamic response measured in the experiments are in excellent agreement with those of our innovative theoretical design for the multi-cam-roller QZS isolation system. The designed prototype is able to accomplish the two anticipated objectives: high isolation performance in the targeted frequency range and the ability to respond to multiple weight levels. The POC prototype can be extended to a large size prototype targeting the driver's seat applications, by considering the restrictions and constraints of space, safety and manufacturing issues.

5 Prototype Design, Fabrication and Test

By comparing the advantages and disadvantages of the two proposed systems, the multi-cam-roller design shows its benefit for real engineering application. Thus, only the multi-cam-roller QZS structure is processed into a prototype for practical applications.

5.1 Prototype Design

According to the POC prototype design and its performance shown in Section 4, a large size prototype using the multi-cam-roller mechanism is designed for isolating the vibrations in the vertical direction. The other consideration as a vehicle seat, such as comfort level, suspension system and dynamic performance of the prototype in rotation, is beyond the scope of this project.

5.1.1 Main Springs

The main spring design for the large-size prototype is a set of four linear springs. The spring specifications are shown in Appendix 8.1. The total equivalent vertical spring stiffness is 4 times the stiffness of a spring. In order to reduce the potential rotation due to the possible eccentricity of the load, the location of the four main springs is designed as far as possible away from the loading centre. If using the main springs only to perform a linear system, the theoretical calculated natural frequency of the system under the loading of 70kg weight is approximately 1.6Hz.

5.1.2 Horizontal Spring Set and Adjustment

Four horizontal springs are also designed for the roller structure. The equivalent horizontal stiffness of the roller structure is 4 times the stiffness of a horizontal spring. To achieve the QZS characteristic, the non-dimensional pre-compression of the horizontal spring and the spring stiffness ratio should satisfy the relationship given by Eq. (17), as shown in Section 3.2.1. By considering the practical applications, it is better to release the springs under non-working condition. Thus the pre-compression of the horizontal springs is designed to be 0 when no load is applied.

According to Figure 10 and Eq. (17), the total horizontal stiffness is required to be equal to the total vertical stiffness, and then a zero stiffness can be achieved. Meanwhile if cutting off the cam effective zone and adjusting the roller head position as shown in Fig. 45, a QZS stiffness

can be achieved. Using an adjustable roller set structure is able to manually achieve the desired QZS condition with different system stiffness.

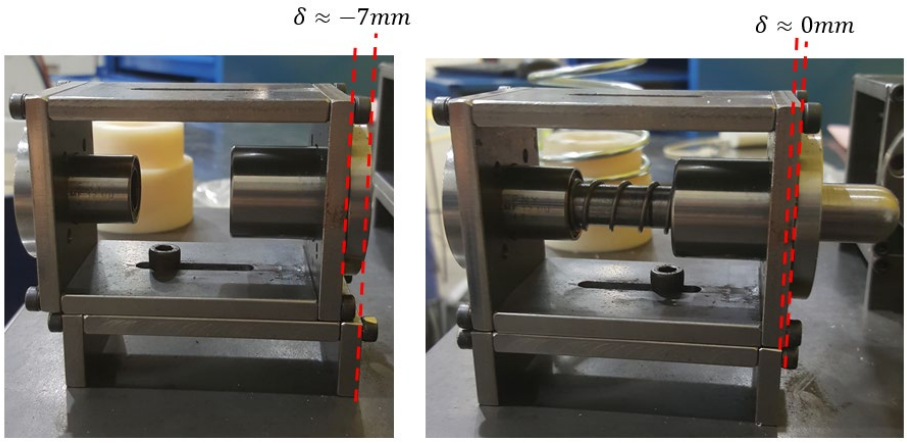

Fig. 45. Horizontal roller set with different pre-compression conditions: (a) QZS condition with δ≈-7mm, (b) designed zero stiffness condition with δ≈0mm.

5.1.3 Design of Multiple Cams

In this prototype, three cam zones are designed. Each cam zone is 12mm in width. Under a zero stiffness condition, this design can respond to three loads, and the three responded loads can be increased according to the horizontal spring pre-compression conditions. Fig. 46 presents the mechanical design and the photo of a fabricated part of the cam structure. The selected length of the cam part plays an important role in the weight applied and has been carefully designed.

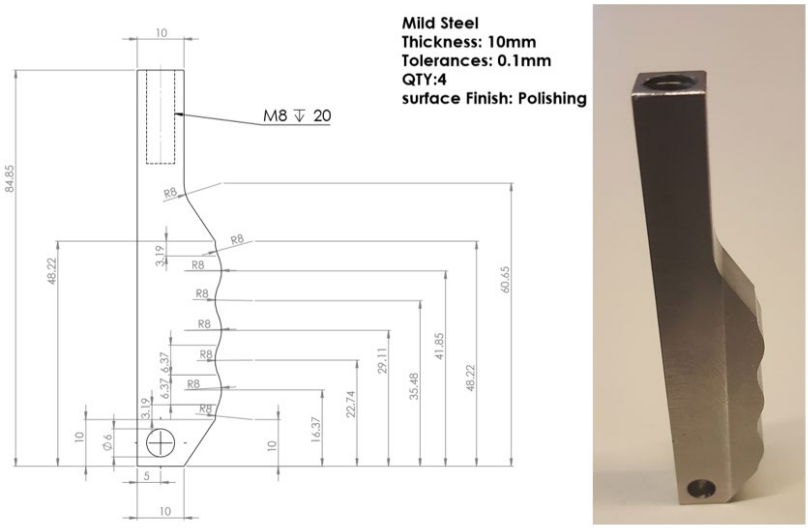

Fig. 46: The mechanical design and the photo of a fabricated part of the cam structure.

5.1.4 Prototype Assembly

The vertical spring configurations, cam structure and roller position have complicated relationships to optimally determine the targeted weights. In this prototype, the structure's own weight and a 60kg, 70kg or 80kg human weight are considered to be applied to the QZS system under a working condition. By considering some constraints imposed on the isolation system in practical applications, the structure configurations are designed to minimise the size of the prototype. Guide rods are used to restrict the motion of the loading platform in the vertical direction only (perpendicular to the ground/base).

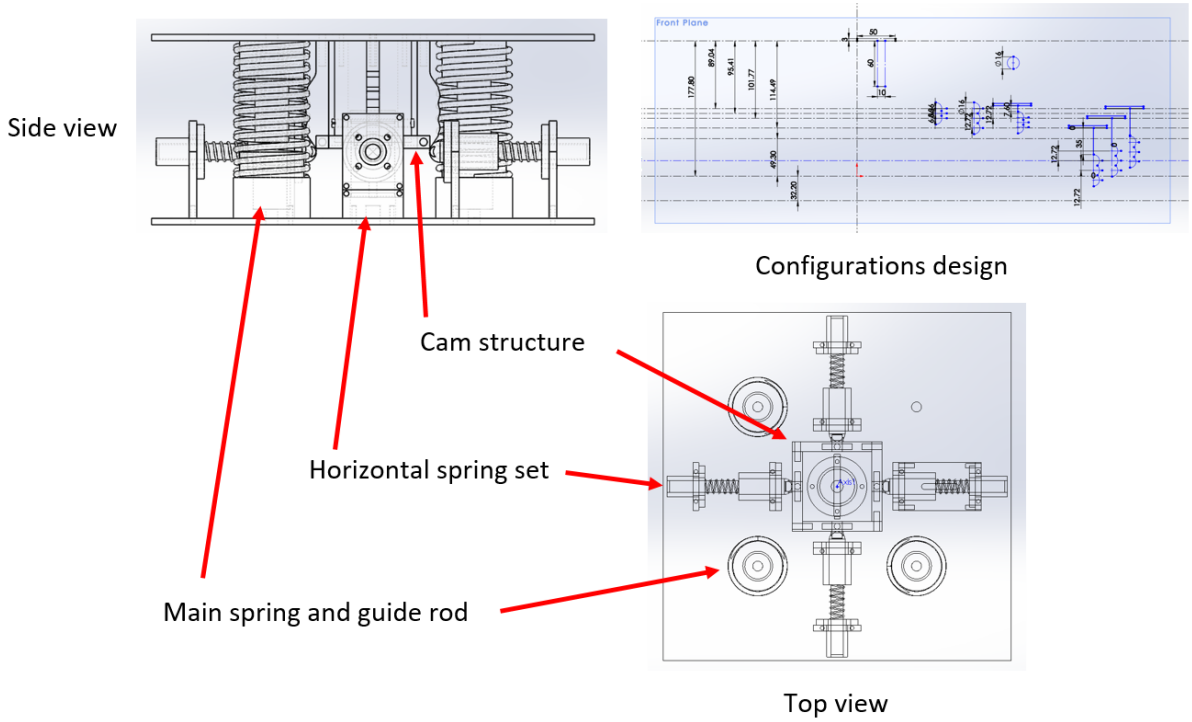

Fig. 47. Configuration design of the prototype.

5.2 Test Instrument

5.2.1 Static Test Machine

The SHIMADZU Precision Universal Testing Machines AGX50 is used for the static test to evaluate the fabricated prototype's configuration and its static performance. The AGX50 has a maximum capacity of 50kN and maximum compression of 1210mm. Its built-in software can automatically record the compression and force response. Slow compression rates of 10-15

mm/min are applied to the prototype so that the friction effect can be neglected in the static tests. Repeated tests are conducted to ensure the isolation performance and the responded weights.

5.2.2 Dynamic Test Machine

The Multi-Axial Simulation Table (MAST) is used for the dynamic test, which is a high-performance platform with six (6) degrees of freedom (multi-axial) and is controlled with an advanced control system to ensure high quality and flexible signal reproduction. This state-of-the-art shaker table is capable of producing the effects of earthquakes, ambient vibrations, wind loading and vehicle vibrations. A payload of a few tonne is achievable on the 2.2m square table, with the acceleration of up to 5g at full capacity, the frequency of up to 200Hz and the displacement of up to +/-200mm.

Fig. 48. MAST and data acquisition system for prototype test at UTS TechLab.

5.2.3 Equipment for Data Acquisition

Two sets of sensors are used for the data acquisition. The first set is the MAST built-in sensors to acquire and monitor the displacement and acceleration of its platform. These sensors are driven by its built-in software (469D Digital Seismic Table Controller). The second set includes 4 digital one-DOF accelerometers driven by the data acquisition system NI PXIe-1073. The digital outputs from the accelerometers are recorded in series of continuing sampling point schemes via the Laboratory Virtual Instrument Engineering Workbench (LabVIEW). A calibration has also been made according to the sensitivity of each accelerometer and the recorded raw data are accelerations. The raw data are then analysed through MATLAB to calculate the system transmissibility for dynamic test. A filter code is applied to the raw data to filter the noises with the frequencies over 12Hz. The raw data of acceleration can be transformed into displacement response, and can also be compared directly to show the dynamic performance of the isolation system.

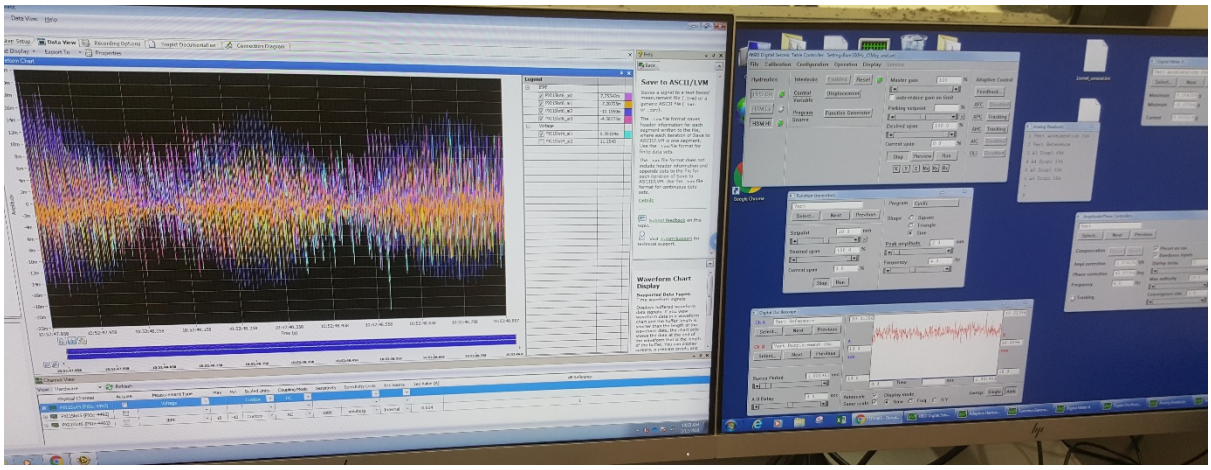

Fig. 49. Interface of the controller and data acquisition system.

5.3 Test Set-up

The static performance is evaluated before the dynamic tests to ensure the prototype's configuration. For the dynamic test, the prototype is fixed on the platform of MAST and is applied with loads (to simulate the driver's weight). The initial dynamic tests are performed with weight only. Then a vehicle seat with weight is assembled on the MAST platform to simulate the driver. For safety issue, test with a human driver is not conducted at this stage.

The digital accelerometers are located on four corners of the loading platform of the prototype, as shown in Fig. 50. The difference among the accelerometers could identify the system's rotation during the dynamic test. Since only the vertical excitations are considered in this test, an average value of the 4 sensors is used to present the vibration response of the system in the vertical direction when rotation is negligible.

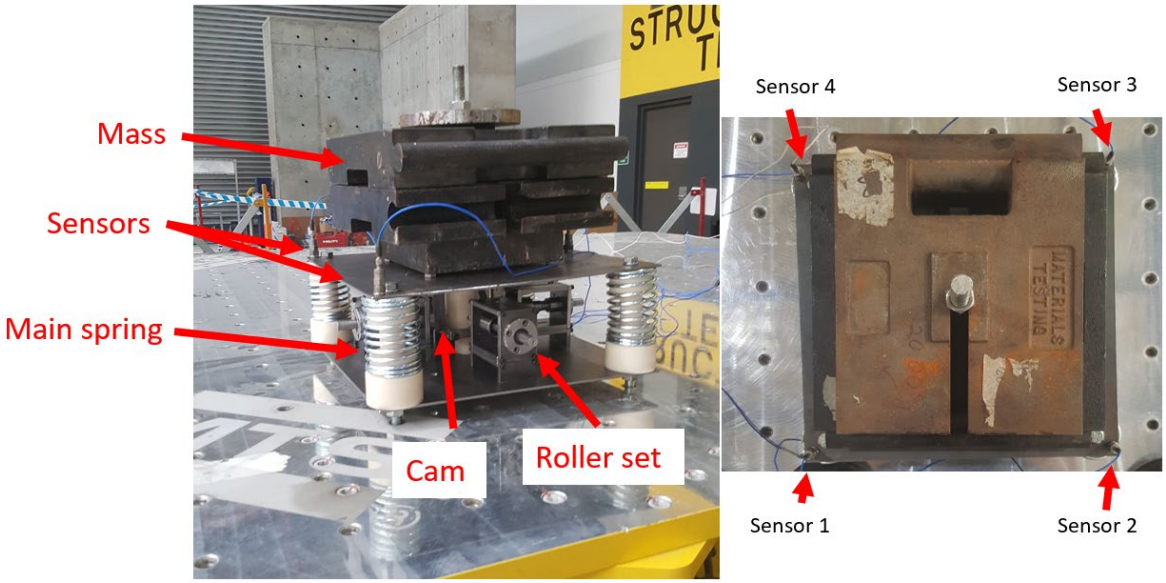

Fig. 50. The location of the sensors.

Sinusoidal excitation using a displacement controller is applied to the base of the prototype for the dynamic test. Generally, for a displacement excitation, the higher the excitation frequency, the higher the acceleration will be received. In the low frequency range from 4 to 10Hz, a $\pm$2mm sinusoidal wave displacement excitation on the MAST platform can result in a minimum 2 m/s^2 acceleration to the object fixed on it. In this report, the $\pm$2mm sinusoidal displacement excitation is used. The frequencies of the excitation are tested from 1Hz to 10Hz with an increase step of 0.5 Hz. Each single frequency excitation is set to last for 10s to ensure that the system reaches its steady state.

Different weights are applied to confirm the system performances as shown in Fig. 50 (with weight only) and Fig. 51 (Seat with weight). The detailed weight levels and their equivalent forces applied on the QZS system are listed in Table 7.

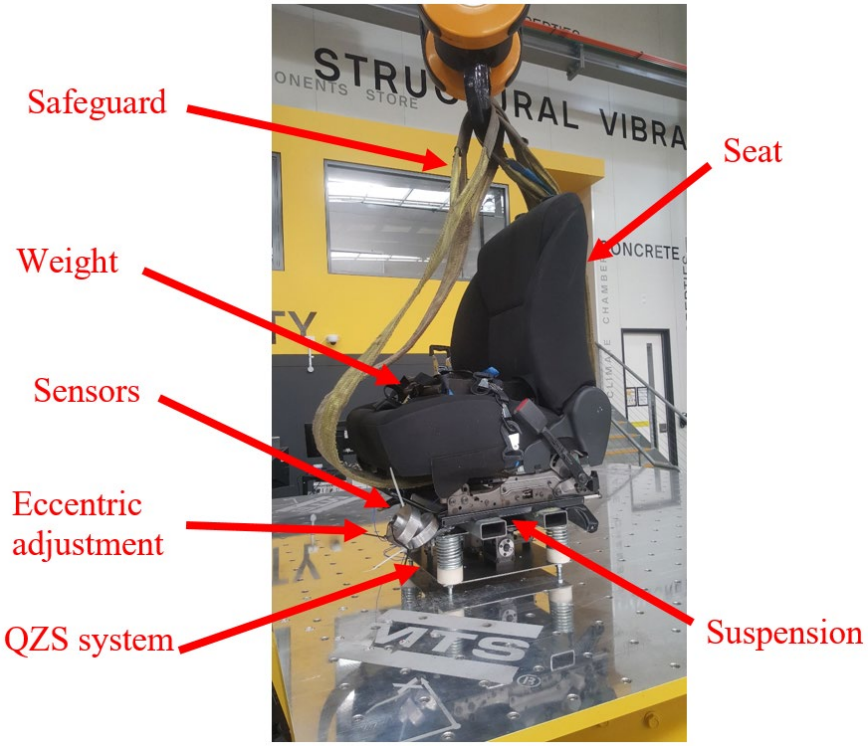

Fig. 51. Dynamic test of vehicle seat with weight (simulating the driver's weight).

Table 7. Detailed weight levels and their equivalent forces applied on the system

Mass number	Weight (kg)	Equivalent force applied (N)
Mass 74 (Mass only)	74.26	727.75
Mass 75 (Mass only)	76.59	750.58
Seat 51 (Seat+Mass)	79.65	780.57
Seat 52 (Seat+Mass)	80.71	790.96

5.4 Prototype Test Results

5.4.1 Static Tests

For a zero stiffness configuration with $\delta \approx 0mm$, the force-compression relationship is shown in Fig. 52, where the repeated tests are indicated by V01, V02 and V03. For the fabricated prototype, the supporting loads are 640N, 760N and 880N, respectively. The weight increase between cam zones is about 120N. The designed amount of this increase (about 100N for 10kg) is dependent on the main spring stiffness.

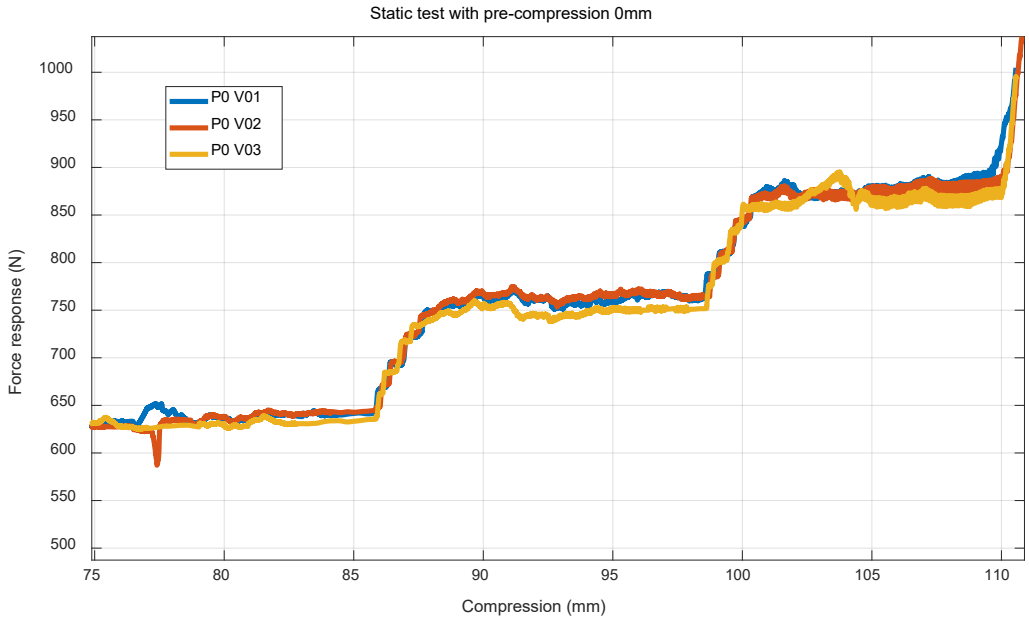

Fig. 52. Force-compression response in static test with pre-compression $\delta \approx 0mm$.

By adjusting the roller set positions, as shown in Fig. 45, the pre-compression of the horizontal springs can be selected. The new force-compression relationship is shown in Fig. 53. It can be easily observed that in the working zones, QZS characteristics can be achieved. When $\delta \approx$-3.5mm or 7mm, the system dynamic stiffness is increased from 0 to a relatively low value, and the supporting loads are extended to a range around the perfect supporting load. Using the middle cam zone as an example, when $\delta \approx$0 mm, the responding load is about 760N. When $\delta \approx$-3.5mm, the supporting load of the middle cam zone is 730±30N and when $\delta \approx$-7mm, the load of the middle cam zone is 750±60N. Under the QZS conditions, each cam zone can respond to a large range of the loading for vibration isolation.

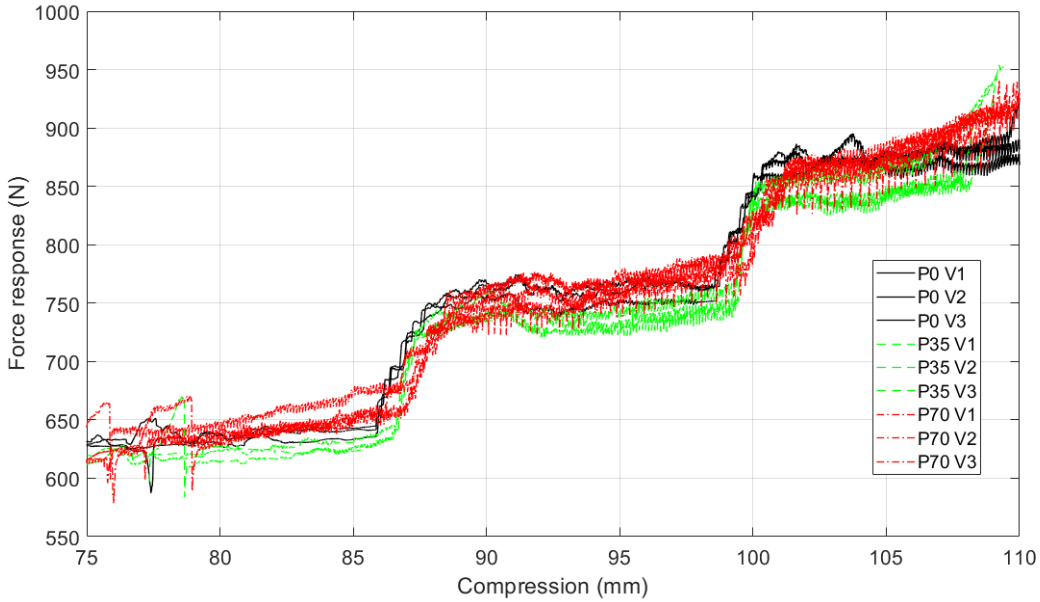

Fig. 53. Force-compression response in static test with different pre-compressions.

In short, the fabricated prototype can respond to at least 3 weight ranges, near 64kg, 76kg and 88kg. The system stiffness can be selected according to the pre-compression condition of the horizontal springs. The dynamic performances will be confirmed in Section 5.4.2.

As the pre-compression of the main spring does not affect the static performance of the QZS system (quasi-zero stiffness in workable zones), the cam structure can be improved to become an adjustable structure, and then the workable zones can be moved with the linear compression in the vertical direction. Simply by adding washers at the current cam structure root can shift the workable zones to less loadings. The tests running with 1 and 2 sets of washer (thickness 2mm for each washer) are compared with the proposed prototype without washer, as shown in Fig. 55. Then the supporting loads under QZS condition are reduced from 757N to 729N and 698N (middle cam zone as an example), respectively. In other words, every 2mm downward movement of the cam structure from the loading platform, as shown in Fig. 54(b), could result in a 30N reduction of the loading, or 2mm upward movement (cutting off the total length of the cam structure) for a 30N increase.

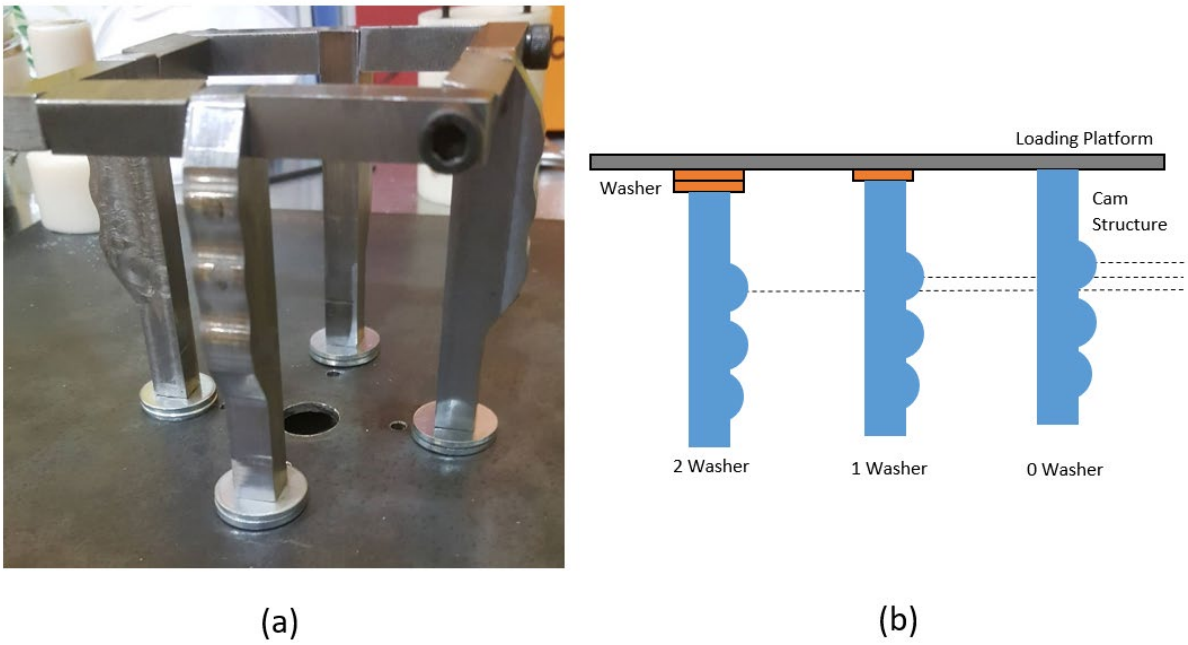

Fig. 54. Cam structure: (a) with 2 sets of washers, (b) with 0, 1 or 2 sets of washers.

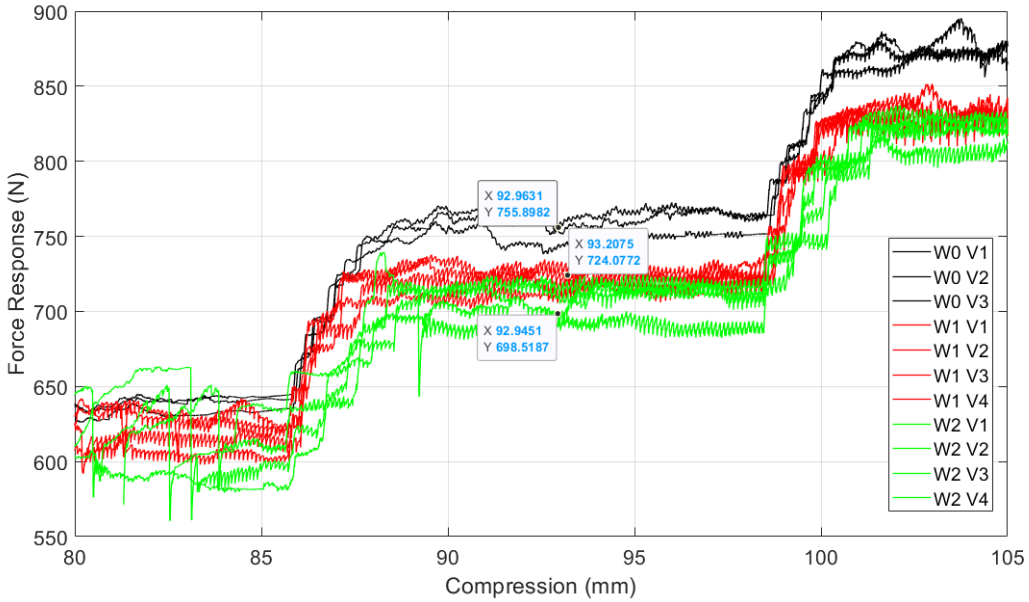

Fig. 55. Static performance of the QZS system with 0 (black lines), 1 (red lines) and 2 (green lines) sets of washer under QZS conditions (V1-V4 indicate the repeated tests).

5.4.2 Dynamic Tests

5.4.2.1 Linear system with vertical springs only

The raw data from the dynamic test of the linear system with a mass of 74 kg is shown in Fig. 56. The filter code is applied in MATLAB to remove the signals with frequency higher than 12Hz. Examples of the filtered data of Sensor 1 and the excitation (MAST platform) are given in Fig. 57 and Fig. 58, respectively.

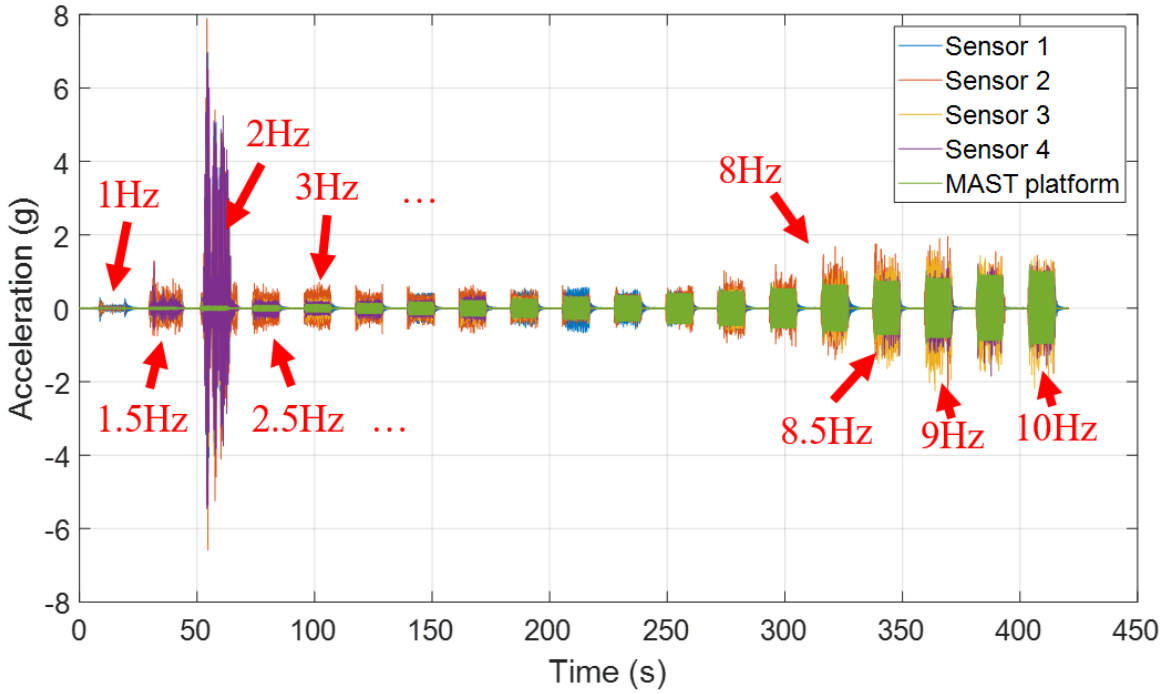

Fig. 56. Raw test data of the corresponding linear system with a mass of 74 kg.

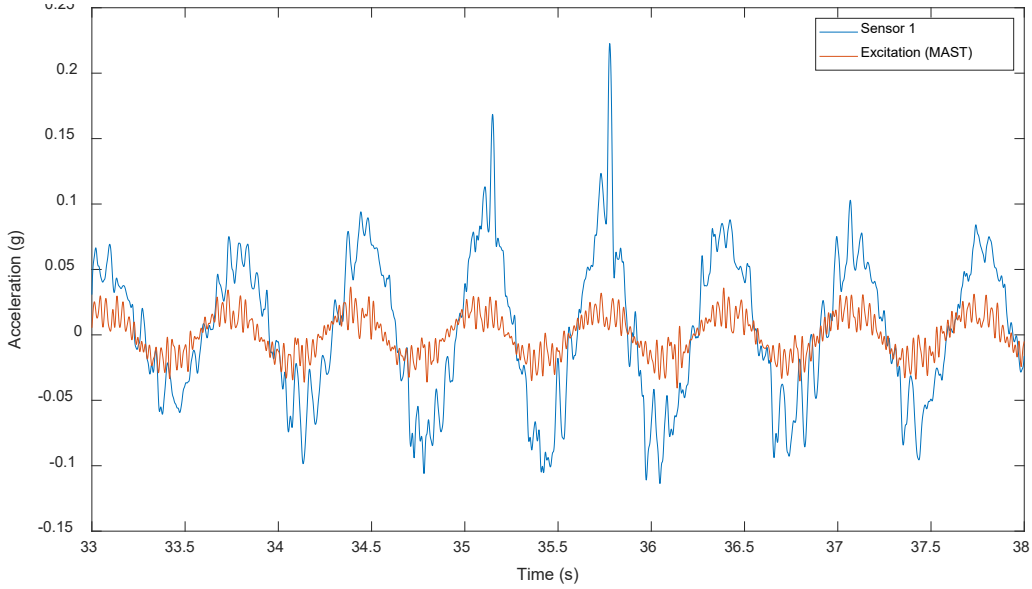

Fig. 57. Time-history of the response (Sensor 1) and the excitation (MAST platform) at 1.5Hz.

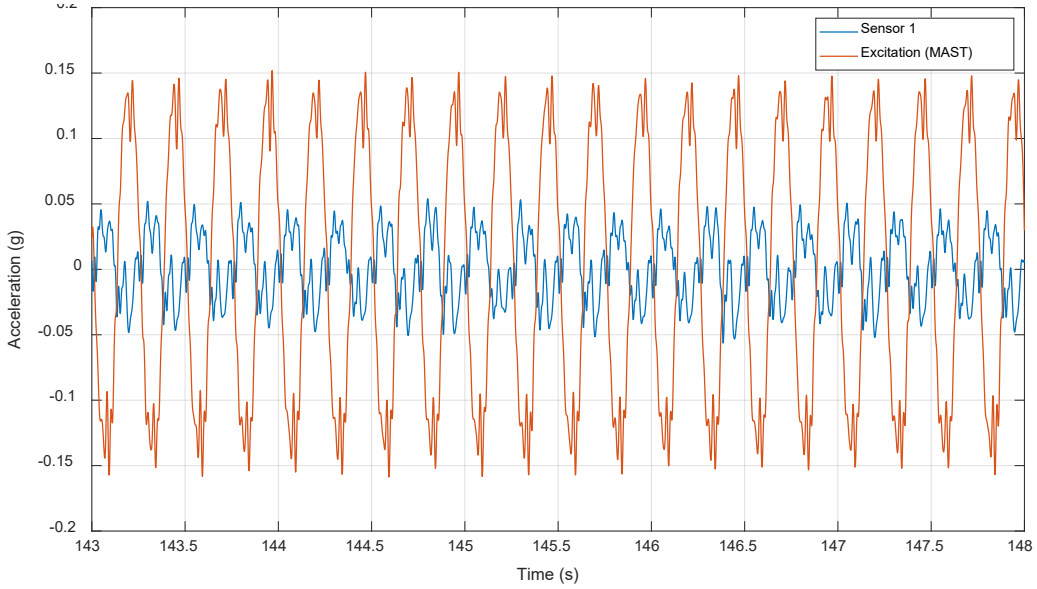

Fig. 58. Time-history of the response (Sensor 1) and the excitation (MAST platform) at 4Hz.

The root mean square (RMS) of all accelerations is calculated and the transmissibility can be obtained as the ratio of the sensor response over the base excitation. The transmissibility of the corresponding linear system is shown in Fig. 59. The natural frequency of the linear system

is at 2 Hz (for a mass of 74 kg), which is in good agreement with its theoretically calculated result. 4 Sensors give nearly same result.

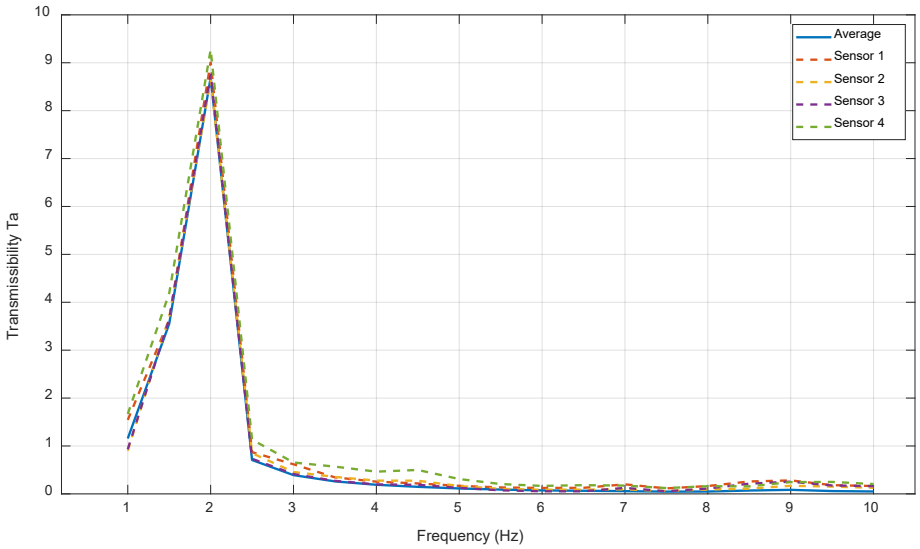

Fig. 59. Transmissibility of the linear system with a mass of 74 kg.

5.4.2.2 The QZS system

The raw data for the dynamic tests of the QZS system with different weight conditions are very similar to those for the corresponding linear system. One example of the response is given in Fig. 60, in comparison with the corresponding linear system under the same excitation.The excitations from the MAST when doing the linear test (black line) and QZS test (purple line) matched very well. While the QZS system has better performance (green line) than the linear system (red line). More raw data for different weight conditions are shown in the Appendix 8.2. After filtering the high frequency signal and calculating the RMS for each acceleration response, the transmissibility of the QZS system with different weight conditions, compared to the corresponding linear system is shown in Fig. 61.

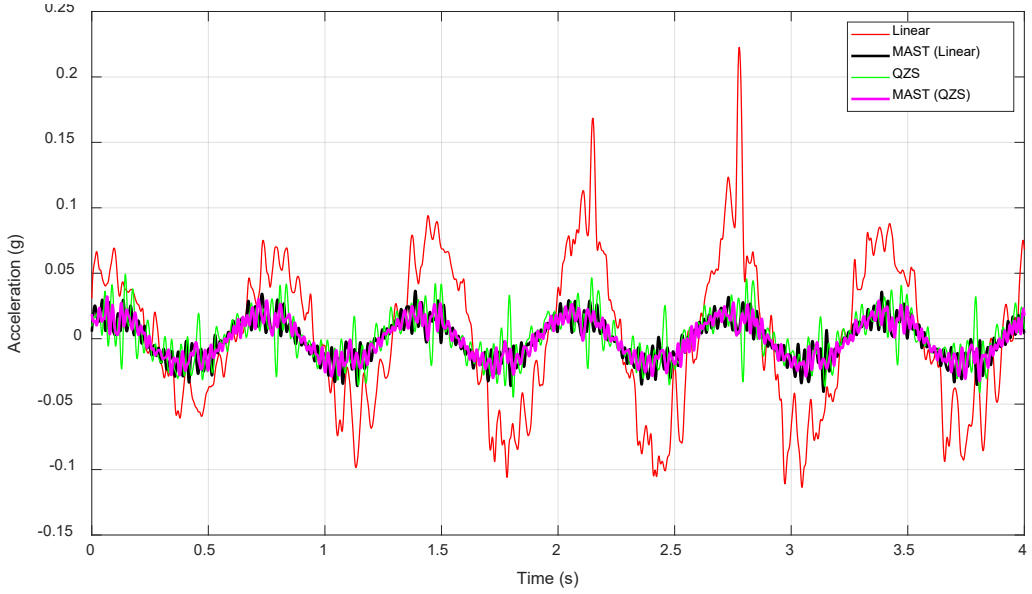

Fig. 60. Time-history response of the linear system and QZS system under 1.5Hz excitation.

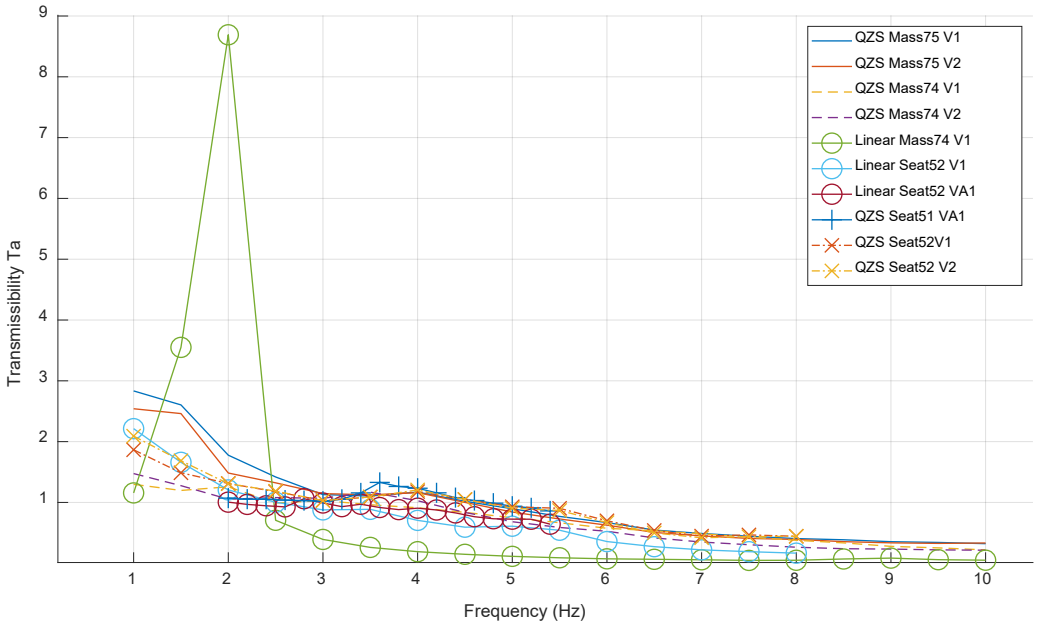

Fig. 61. Transmissibility of the linear system and QZS system under different weight conditions.

5.5 Result Analysis and Discussion

5.5.1 Excitation and Response Analysis

The Fast Fourier Transform (FFT) is used to analyse the signal for both excitation and response signals.

From the FFT analysis of the excitation signal, the excitation applied to the prototype can be determined, for example, as shown in Fig. 62. From this figure, it is confirmed that the excitations applied to the prototype agrees well with the controller output. It should be mentioned that there exist odd number (3rd, 5th and 7th) harmonic excitations due to the MAST system, which have resulted in a non-smooth signal output in the time-history response, as shown in Fig. 57, Fig. 58 and Fig. 60.

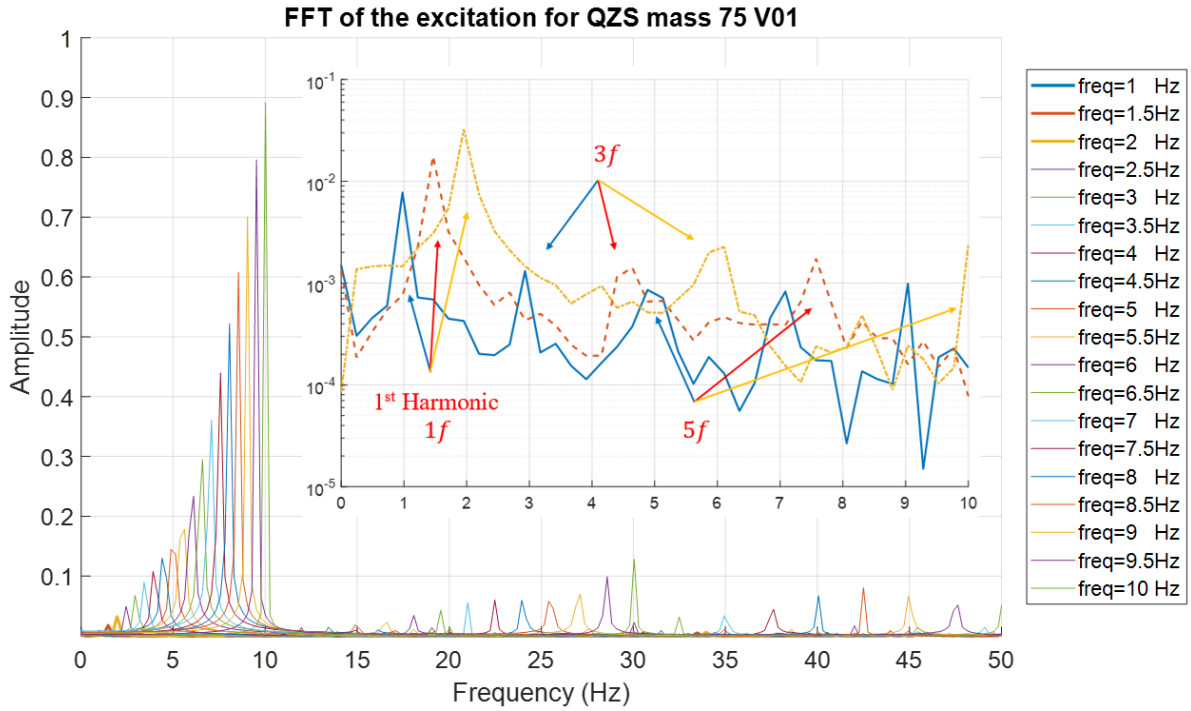

Fig. 62. FFT of the excitation for QZS system with a mass of 75 kg (1-10Hz and enlarged 1-2Hz).

From the FFT analysis for Sensor 1 response signal, as shown in Fig. 63, there are noticed peaks around 4Hz when high frequency excitations are applied (from 6Hz to 10Hz). These peaks are very close to the half of the excitation frequency, which may be due to the friction effect during the dynamic test. The response FFT diagram is given as an example for the mass of 75 kg only. Similar response can be found in other test results.

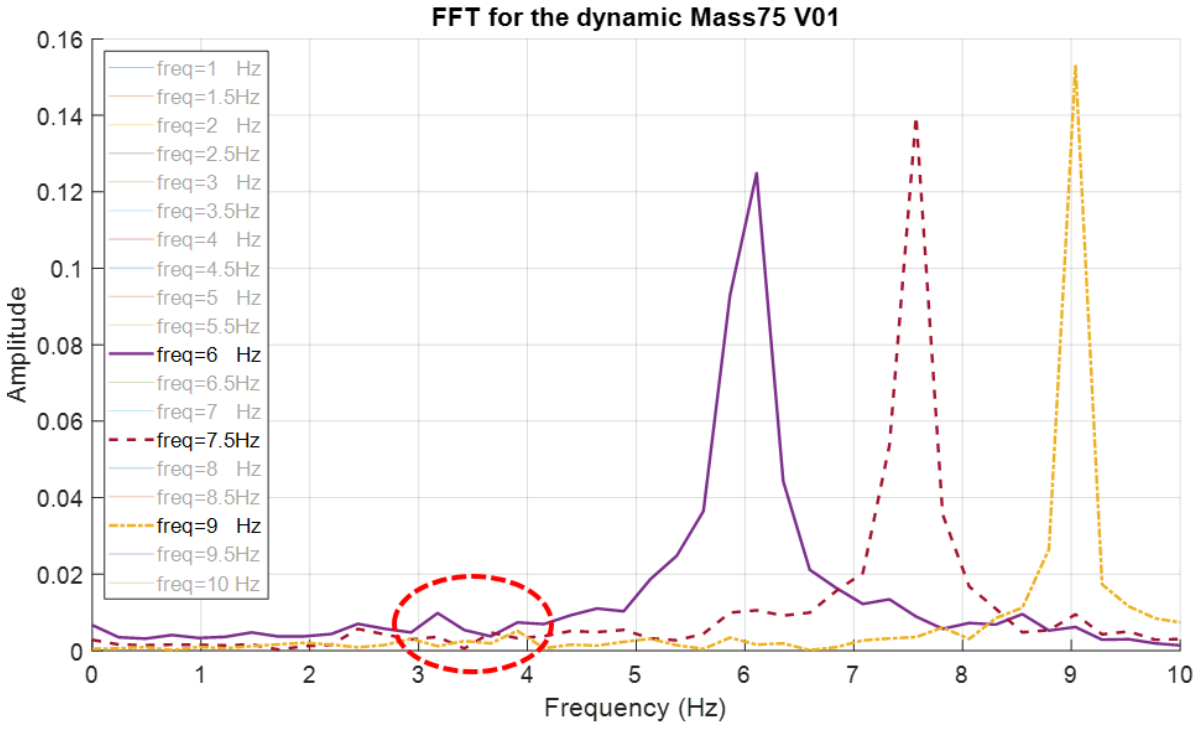

Fig. 63. FFT of Sensor 1 response for QZS system with a mass of 75 kg (at 6, 7.5 and 9 Hz).

5.5.2 The corresponding linear System

For the corresponding linear system with the mass only, the resonance frequency can be easily found at 2 Hz from Fig. 59. For the linear system assembled with the vehicle seat and the mass, the total loading is increased from 74.26kg to 80.71kg, thus the resonance frequency should be reduced to 1.5Hz. However, it is hard to be observed from Fig. 64. From the 4 sensors' response, as shown in Fig. 65, there are two small resonance peaks (lower than 1 Hz and around 2.7Hz in the enlarged figure zone), from calculation using the 3rd harmonic frequency, the resonance frequency of the linear system with Seat52 is around 0.9Hz (2.7Hz/3). High friction and damping ratio degrade the dynamic performance in the frequency range (4-10Hz).

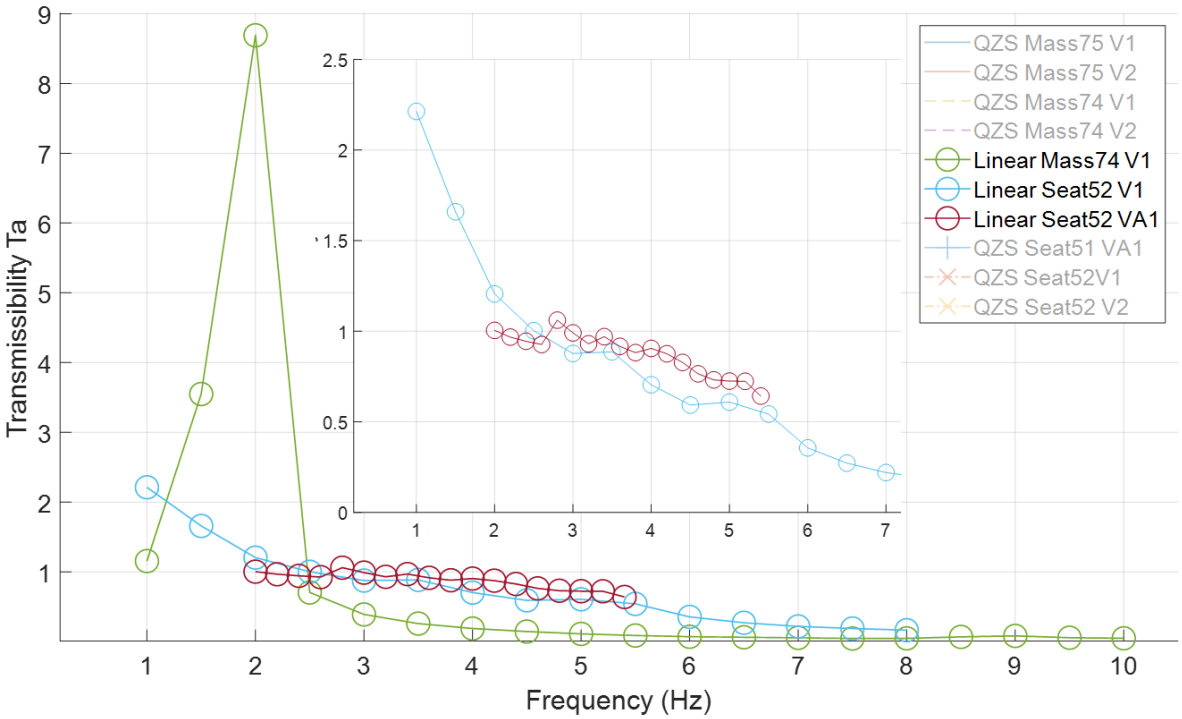

Fig. 64. Transmissibility of the corresponding linear system with different weight conditions.

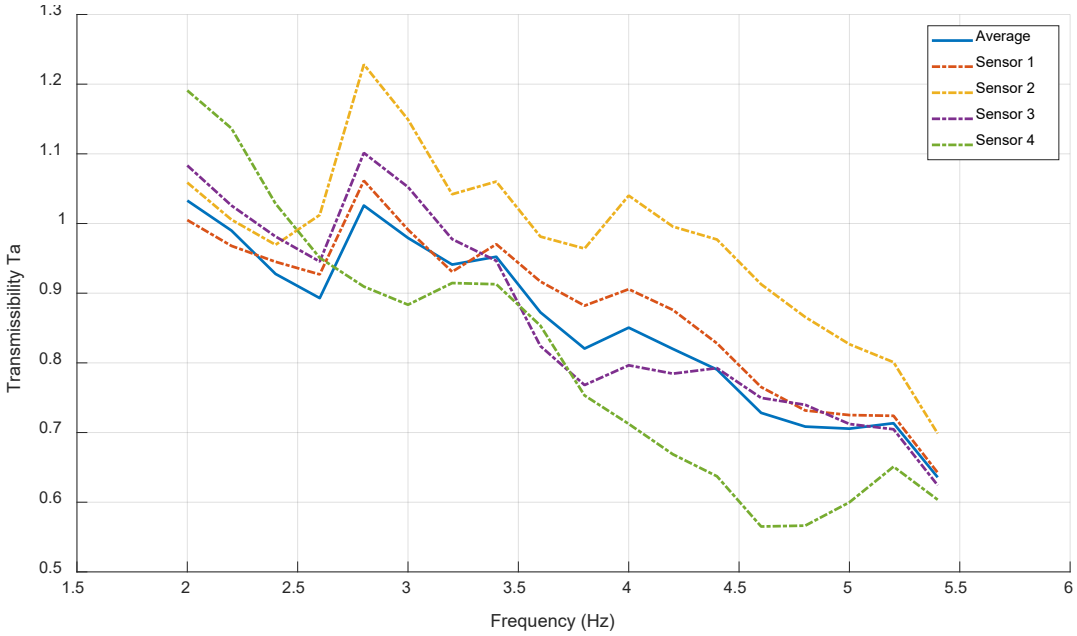

Fig. 65. Transmissibility of sensors for the corresponding linear system with Seat 52 VA1 (with a 0.2 Hz increase of the frequency from 2Hz to 5.4Hz).

5.5.3 The QZS System

In comparing with the linear system response, the resonance frequency of the QZS system is lower than 1Hz. The other peak frequency around 4Hz could be due to the 3rd harmonic mode of the system and possible friction during the dynamic test. When the overall loading is increased from a mass of 74kg , to 75 kg, and Seat52 (74.26kg to 80.71kg), the 3rd harmonic frequency is reduced from 4Hz to 3.8Hz and 3.6Hz from Fig. 66. Thus the 1st harmonic frequency should be around 1.2Hz.

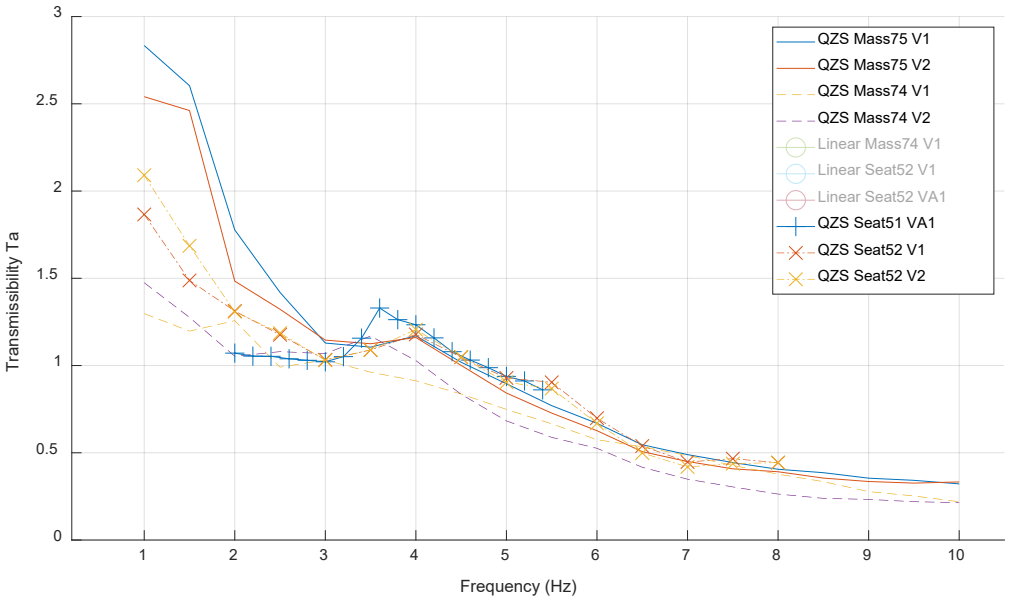

Fig. 66. Transmissibility of the QZS system with different weight conditions.

Overall the QZS system has good isolation performances in the low frequency range, and the proposed multi-cam-roller QZS system is able to provide good isolation to account for multi-weight (of the drivers) issue. For an engineering application as a vehicle seat, further improvements on the prototype are required by considering physical constraints.

5.6 The Improved Design for Practical Applications

5.6.1 Cam Structure for Accurate Weight Response

As experimentally verified in Section 5.4.1, the QZS workable zone can be independently from the per-compression state of the vertical springs. Manually or automatically adjustable

structure can be further applied on the cam structure to achieve a full range weight response. The proposed structure based on the current prototype is shown in Fig. 67. From the calculation based on the test results, if the adjustable cam structure can reach a maximum 8 mm movement (+-4mm from the current design), the supporting weight level (from 50-100kg) can be responded accurately under the QZS condition. The supporting weight only depends on the vertical spring stiffness.

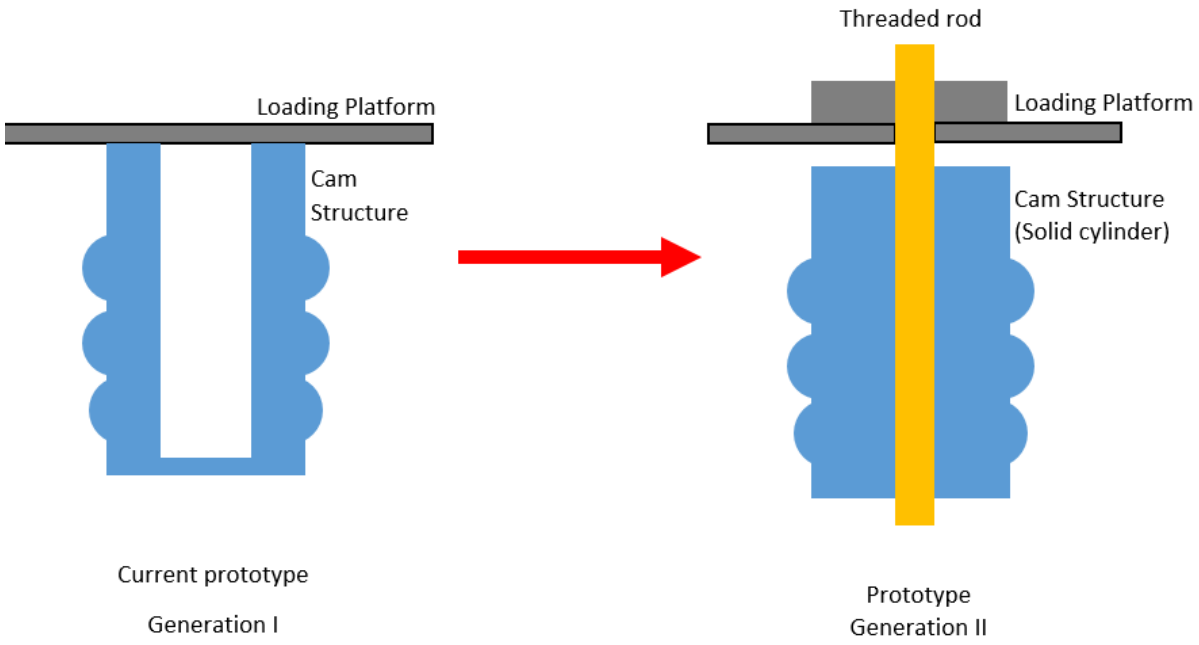

Fig. 67. The improved cam structure.

5.6.2 Friction (Damping) and Rotation Issue

From the dynamic tests, it is noted that the damping ratio of the QZS system is much higher than the corresponding linear system, which is mainly due to the frictions on the cam-roller contact surface and the guide rod contact. High damping ratio would degrade the dynamic performance of vibration isolation.

In order to minimize the friction effect and reduce the damping ratio, solid hemisphere rollers should be firstly considered to be replaced by the bearing rollers. Although the design specifications require re-planning and the cost would be increased, the overall performance can be significantly improved.

Another improvement can be on the frictions due to the guide-rod contact. Current prototype uses 5 guide rods to restrict the motion in rotation. The eccentricity of the loading would cause an unbalanced position of the loading platform and direct contact of the guide rods. The unwanted unbalanced position and frictions can be avoided or reduced with additional guide designs, such as slide pathway enhancement or with seat ergonomics consideration.

5.6.3 Integration with a Standard Vehicle Seat

The integration of the QZS system and the vehicle seat should focus on the center of gravity (CG) allocation. Current design has placed the QZS system under the suspension system, so the CG of the seat can be adjusted to the loading center of the QZS system. However, in order for the suspension system workable on comfort adjustment (height or location of the seat), it would be a good option to insert the QZS system between the seat and its suspension system and align the CG of the seat with loads to the loading center of the QZS system. By doing this, the rotation issue can be reduced.

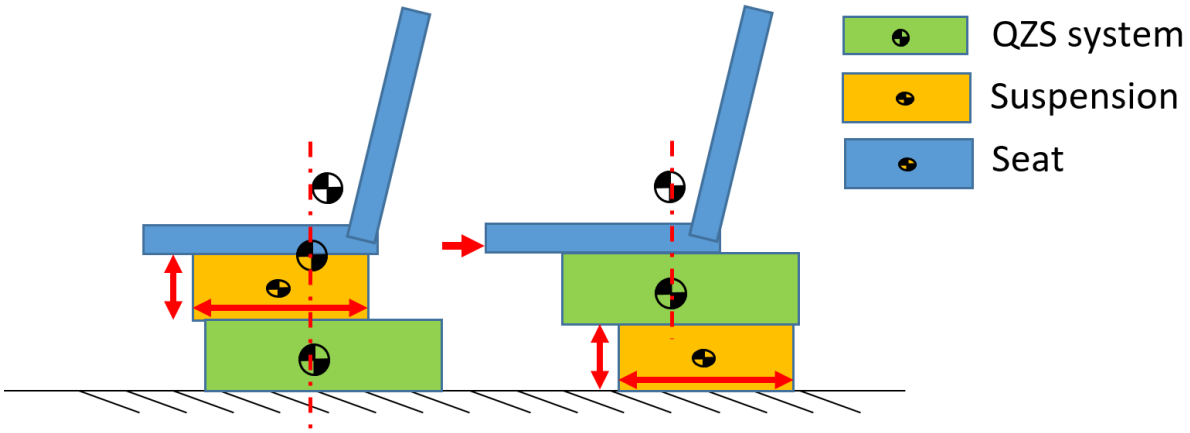

Fig. 68. Integration with a vehicle seat.

6 Conclusion and the Further Work beyond this Project

This project has been progressing very well and been successfully completed with the anticipated outcomes. Two novel quasi-zero stiffness (QZS) vibration isolation systems have been designed and validated. The corresponding theoretical and experimental results have been documented in two technical papers which have been submitted to highly-respected international journals. Furthermore, the designed multi-cam-roller QZS vibration isolation

system has been implemented into a driver's seat to isolate the ground vibrations. Preliminary laboratory tests on the driver's seat at UTS TechLab have confirmed the effectiveness of the proposed QZS system, which paves a way to extend its application to other mobile mining equipment to reduce the vibration-induced health problems for those working with the mining equipment.

6.1 Concluding Remarks

This report has included dynamic modelling, theoretical analysis, proof of concept designs, prototype fabrication, and extensive laboratory tests for the development of innovative QZS vibration isolation systems for attenuating low-frequency vibrations in mining operation environments. The project has been executed in a three-stage work progress in line with the planned research tasks. Two types of QZS vibration isolation systems based on multi-cam-roller and limb-like oblique springs were proposed, theoretically analysed, and numerically studied for vibration isolation in Stage 1 (from 1st Jan to 30th June 2019). Then two QZS vibration isolation systems were proof of concept designed, fabricated and tested to validate the theoretical predictions and vibration isolation performance in Stage 2 (from 1st July to 30th September 2019). It was confirmed that the proposed cam-roller isolation system has the capability to account for different driver's weights. The developed limb-like oblique spring isolation system has a large operating region of quasi-zero stiffness for isolation performance. In Stage 3 (from 1st October to 20th December 2019), a practical multi-cam-roller QZS isolation system with a loading capacity of 60~100 kilograms was designed, manufactured and tested. This multi-cam-roller QZS isolation system was tested on the Multi-Axial Simulation Table (MAST) to evaluate its isolation performance. It was found that the designed prototype is able to isolate the vibrations transferred from the platform (ground). Then the designed multi-cam-roller QZS isolation system (structure) was incorporated into a car seat as a supporting frame to form an integrated driver's seat with QZS isolation structure. The isolation performance of the integrated driver's seat was tested again on the MAST which provides a ground vibration from 1.0 to 10 Hz. The initial testing results indicated that the integrated driver's seat can reduce the vibrations transferred from the ground. In the meantime, the laboratory tests also provided some suggestions for the designed prototype to be improved.

6.2 Tangible Outputs of this Project

Successful completion of this project has advanced the QZS vibration isolation theory (generated two papers), provided two designs of the QZS systems, and opened wide applications of the QZS isolation system to mobile mining equipment to reduce the harmful effects of hazardous vibrations on the mining workers. Specifically:

1) Two technical papers have been submitted to two international prestigious journals (and of course, we have acknowledged the financial support from the *CSHST* in the section of Acknowledgement of these papers). One paper is entitled “Increase of quasi-zero stiffness region using two pairs of oblique springs” and submitted to journal *Mechanical Systems and Signal Processing*. The other paper is entitled “Design of a quasi-zero stiffness isolation system for supporting different loads” and submitted to *Journal of Sound and Vibration*. These two journals are widely recognized on the top 10% of journals in the area of mechanical engineering. This implies that our two designs are innovative and novel.

2) Design principles, theoretical analysis, and extensive laboratory evaluation of two QZS innovative vibration systems can be readily adopted for practical applications of the vibration isolation systems. The novel design of multi-cam-roller isolation system can be potentially applied for a patent. At this stage, the intention of the patent application is dampened due to the paperwork preparation and the resource limitations. Should this happens later, we will first seek for the approval from the *CSHST* Trust.

3) The designed multi-cam-roller isolation system has been integrated into a car seat to verify the proof-of-concept design. Preliminary laboratory tests indicated that the designed isolation system can be effectively incorporated into the design of the driver’s seat structure. This potentially leads to a novel design of car seat based on the QZS isolation theory, a passive vibration isolation structure.

6.3 Further Work beyond this Project

If funding available, further design towards to product development will be finalised by first targeting at the driver’s seat of heavy truck or at mining operating platform. Then field testing will be conducted to examine the isolation performance. At this stage, a further funding opportunity is being sought, with the ultimate goals of implementing the proposed QZS systems into mobile mining equipment to reduce the vibration-induced health problems for those working with the mining equipment. The present project has proposed, designed and validated two novel QZS vibration systems. Practical implementation of these two novel vibration systems still requires the work to be done on optimization, improvement and

specifications for the application situations. Different applications have different requirements and limitations, which have to be considered in the product designs.

The designed prototype of the multi-cam-roller QZS isolation system has been extended to a large size prototype targeting the driver's seat applications. The laboratory tests have proved the effectiveness of the fabricated prototype. For the product structure design, further structural optimization towards to application is required to be finalised, by considering the restrictions and constraints of space, safety and manufacturing issues. Then field testing will be conducted to examine the isolation performance under different operating conditions (the amplitudes and frequencies of vibration excitations). Following the extensive field testing, further optimization and improvement of the proposed designs based on the testing results will be carried out with an ultimate goal of product development. After implementing the QZS vibration isolation system on the driver's seat of heavy truck, the novel QZS vibration isolation system will be targeted at mining operating platform.

In line with the planned tasks, the current project has conducted a preliminary evaluation of the QZS isolation system incorporated into a car seat, and confirmed that the designed QZS system can be integrated into the design of a car seat for practical application. At this stage, a further funding opportunity is being sought to continue the current research to fully develop an industry-ready product to reduce the vibration-induced health problems for those working with the mining equipment. It is anticipated that an innovative product for heavy-duty truck seat would be developed with a further funding of one year.

7 References

[1] Carrella A., Brennan M. J., and Waters T. P. (2007) "Static analysis of a passive vibration isolator with quasi-zero-stiffness characteristic," *Journal of Sound and Vibration*, 301(3-5), pp. 678-689.

[2] Valeev, A., & Kharisov, S. (2016). "Application of vibration isolators with a low stiffness for the strongly vibrating equipment." *Procedia Engineering*, *150*, pp.641-646.

[3] Lee C. M., Goverdovskiy V. N., and Temnikov A. I. (2007) "Design of springs with "negative" stiffness to improve vehicle driver vibration isolation," *Journal of Sound and Vibration*, 302(4-5), pp. 865-874.

[4] Kovacic I., Brennan M. J., and Waters T. P. (2008) "A study of a nonlinear vibration isolator with a quasi-zero stiffness characteristic," *Journal of Sound and Vibration*, 315(3), pp. 700-711.

[5] Carrella A., Brennan M. J., Waters T. P., and Lopes Jr V. (2012) "Force and displacement transmissibility of a nonlinear isolation system with high-static-low-dynamic-stiffness," *International Journal of Mechanical Sciences,* 55(1), pp. 22-29.

[6] Klatt, T., & Haberman, M. R. (2013). "A nonlinear negative stiffness metamaterial unit cell and small-on-large multiscale material model." *Journal of Applied Physics*, *114*(3), p. 033503.

[7] Xu D., Yu Q., Zhou J., and Bishop S. R. (2013) "Theoretical and experimental analyses of a nonlinear magnetic vibration isolator with quasi-zero-stiffness characteristic," *Journal of Sound and Vibration*, 332(14), pp. 3377-3389.

[8] Liu, Y., Xu, L., Song, C., Gu, H., & Ji, W. (2019). "Dynamic characteristics of a quasi-zero stiffness vibration isolator with nonlinear stiffness and damping." *Archive of Applied Mechanics*, pp. 1-17.

[9] Carrella A., Brennan M. J., Kovacic I., and Waters T. P. (2009) "On the force transmissibility of a vibration isolator with quasi-zero-stiffness," *Journal of Sound and Vibration*, 322(4-5), pp. 707-717.

[10] Huang X., Liu X., Sun J., Zhang Z., and Hua H. (2014) "Vibration isolation characteristics of a nonlinear isolation system using euler buckled beam as negative stiffness corrector: A theoretical and experimental study," *Journal of Sound and Vibration*, 333(4), pp. 1132-1148.

[11] Ding, H., & Chen, L. Q. (2019). "Nonlinear vibration of a slightly curved beam with quasi-zero-stiffness isolators." *Nonlinear Dynamics*, *95*(3), pp. 2367-2382.

[12] Robertson W. S., Kidner M. R. F., Cazzolato B. S., and Zander A. C. (2009) "Theoretical design parameters for a quasi-zero stiffness magnetic spring for vibration isolation," *Journal of Sound and Vibration*, 326(1-2), pp. 88-103.

[13] Zhou J., Wang X., Xu D., and Bishop S. (2015) "Nonlinear dynamic characteristics of a quasi-zero stiffness vibration isolator with cam-roller-spring mechanisms," *Journal of Sound and Vibration*, 346(1), pp. 53-69.

[14] Lan C. C., Yang S. A., and Wu Y. S. (2014) "Design and experiment of a compact quasi-zero-stiffness isolator capable of a wide range of loads," *Journal of Sound and Vibration*, 333(20), pp. 4843-4858.

[15] Magid E. B., and Coermann R. (1960) "The reaction of the human body to extreme vibrations," *Proceedings of the Institute of Environmental Science*, 37, p. 135.

[16] Gallagher S., and Mayton A. (2007) "Back injury control measures for manual lifting and seat design," CDC Report 8579-DS1.

[17] Sun X., Xu J., Jing X., and Cheng L. (2014) "Beneficial performance of a quasi-zero-stiffness vibration isolator with time-delayed active control," *International Journal of Mechanical Sciences*, 82, pp. 32-40.

[18] Bluehill3, https://www.instron.us/en-us/service-and-support/resources/manuals?dt=Manual &q=bluehill.

[19] WaveMatrix, https://www.instron.us/products/materials-testing-software/wavematrix

[20] LabVIEW 2019, https://www.ni.com/en-au/shop/labview/labview-details.html

[21] MatLab 2019b, https://au.mathworks.com/products/matlab/whatsnew.html

[22] cDAQ-9174 CompactDAQ Chassis, http://www.ni.com/en-au/support/model.cdaq-9174.html.

[23] NI-9234 C Series Sound and Vibration Input Module, https://www.ni.com/en-au/support/model.ni-9234.html.

8 Appendix

8.1 Prototype Springs

	Horizontal spring(3488)	Main spring(71733S)
Free length(mm)	31.8	177.8
Inner diameter (mm)	12.75	51.28
Material	Stainless Steel-SST	Spring Steel-SPR
Outer diameter (mm)	15.24	59.51
Stiffness (N/mm)	1.926	1.926
Total coils	5.88	11.00
Wire diameter (mm)	1.24	4.11

Outside the QZS workable zone, the system performance is similar to a linear system as shown. The total vertical stiffness is about 7.38N/mm.

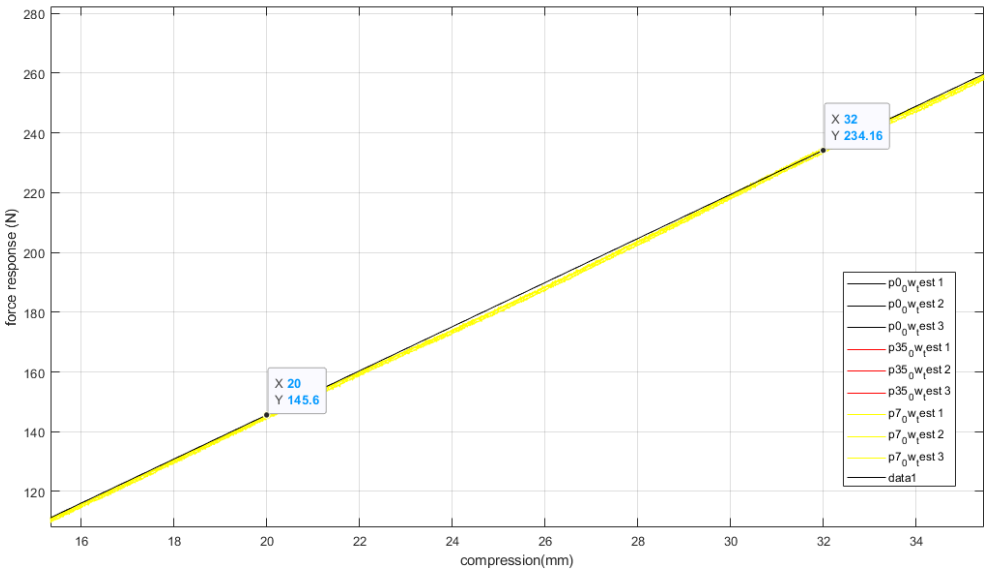

8.2 Raw Data of the Dynamic Tests

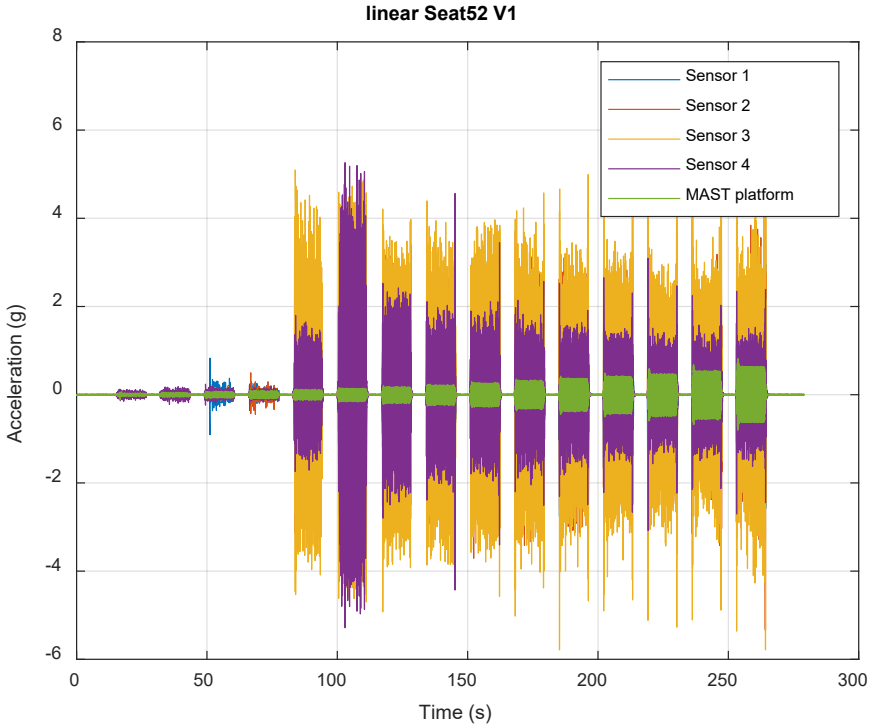

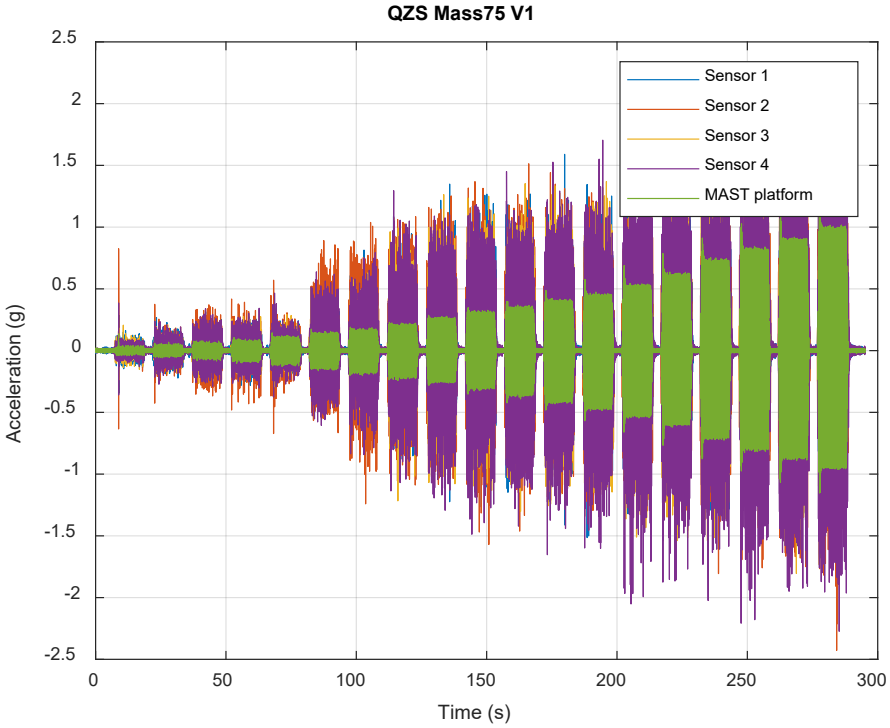

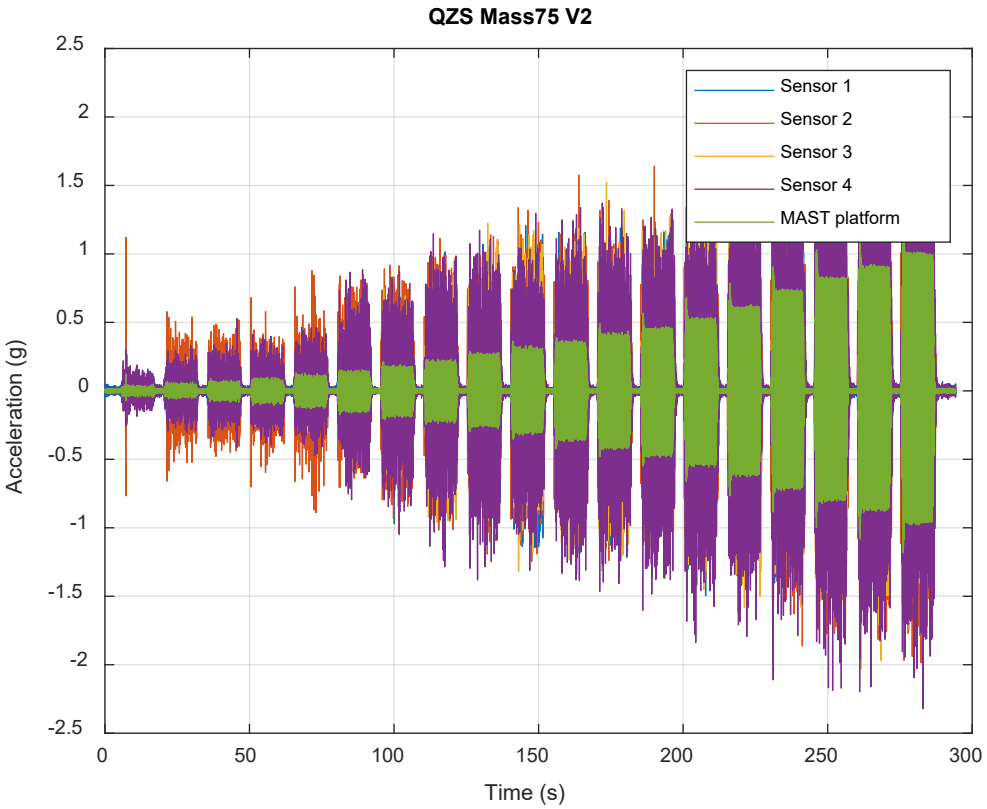
QZS Mass75 V2
Sensor 1
Sensor 2
Sensor 3
Sensor 4
MAST platform
Acceleration (g)
Time (s)
2.5
2
1.5
1
0.5
0
-0.5
-1
-1.5
-2
-2.5
0
50
100
150
200
250
300

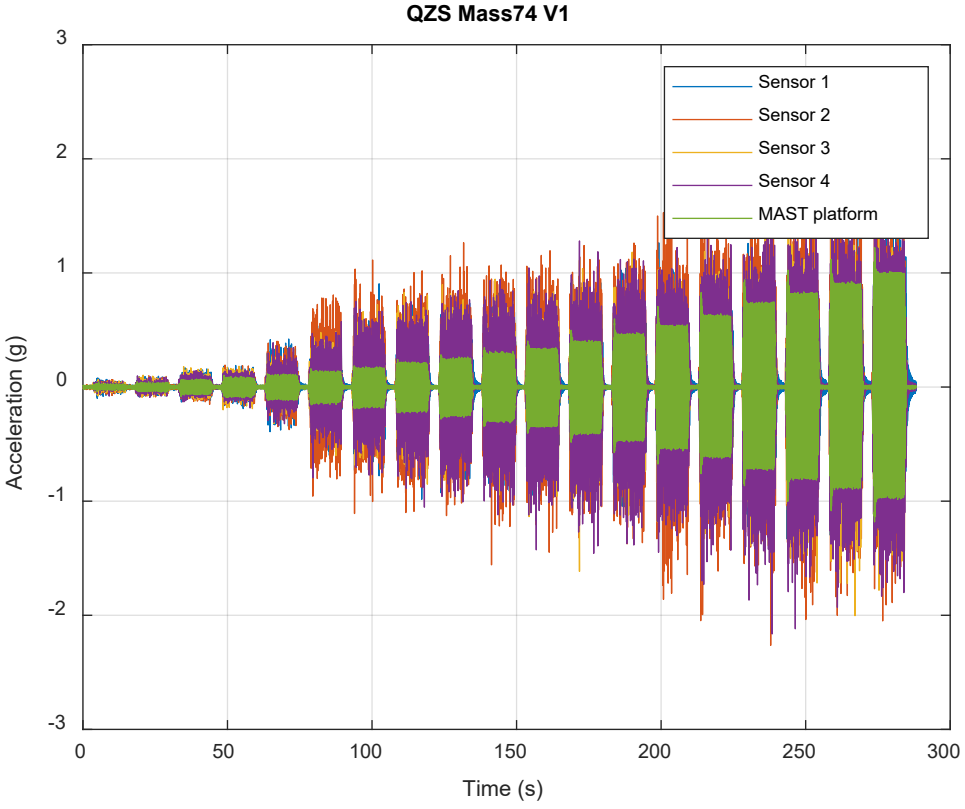
QZS Mass74 V1
Sensor 1
Sensor 2
Sensor 3
Sensor 4
MAST platform
Acceleration (g)
Time (s)
3
2
1
0
-1
-2
-3
0
50
100
150
200
250
300

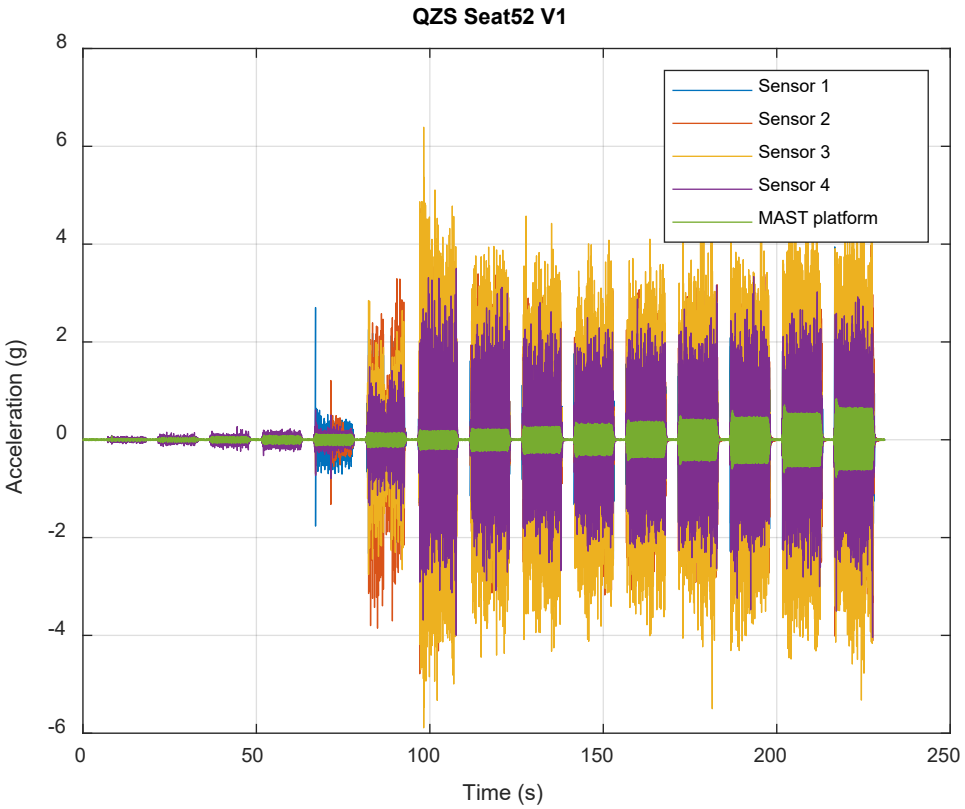

===== *End of the Final Report* =====